STATIC PENETRATION RESISTANCE OF SOILS

CENTRE FOR NEWFOUNDLAND STUDIES

TOTAL OF 10 PAGES ONLY
MAY BE XEROXED

(Without Author's Permission)

SAMEH MOHAMED
ABDEL-GAWAD

00025
CENTRE FOR NFLD. STUDIES
JAN 1981
MEMORIAL UNIVERSITY
OF NEWFOUNDLAND

National Library of Canada

Cataloguing Branch
Canadian Theses Division

Ottawa, Canada
K1A 0N4

Bibliothèque nationale du Canada

Direction du catalogage
Division des thèses canadiennes

NOTICE

The quality of this microfiche is heavily dependent upon the quality of the original thesis submitted for microfilming. Every effort has been made to ensure the highest quality of reproduction possible.

If pages are missing, contact the university which granted the degree.

Some pages may have indistinct print especially if the original pages were typed with a poor typewriter ribbon or if the university sent us a poor photocopy.

Previously copyrighted materials (journal articles, published tests, etc.) are not filmed.

Reproduction in full or in part of this film is governed by the Canadian Copyright Act, R.S.C. 1970, c. C-30. Please read the authorization forms which accompany this thesis.

THIS DISSERTATION
HAS BEEN MICROFILMED
EXACTLY AS RECEIVED

AVIS

La qualité de cette microfiche dépend grandement de la qualité de la thèse soumise au microfilmage. Nous avons tout fait pour assurer une qualité supérieure de reproduction.

S'il manque des pages, veuillez communiquer avec l'université qui a conféré le grade.

La qualité d'impression de certaines pages peut laisser à désirer, surtout si les pages originales ont été dactylographiées à l'aide d'un ruban usé ou si l'université nous a fait parvenir une photocopie de mauvaise qualité.

Les documents qui font déjà l'objet d'un droit d'auteur (articles de revue, examens publiés, etc.) ne sont pas microfilmés.

La reproduction, même partielle, de ce microfilm est soumise à la Loi canadienne sur le droit d'auteur, SRC 1970, c. C-30. Veuillez prendre connaissance des formules d'autorisation qui accompagnent cette thèse.

LA THÈSE A ÉTÉ
MICROFILMÉE TELLE QUE
NOUS L'AVONS REÇUE

NL-339 (3/77)

STATIC PENETRATION RESISTANCE OF SOILS

by

SAMEH ABDEL-GAWAD, B.Sc. (Eng) ©

A Thesis Submitted in Partial Fulfillment

of the Requirements for the Degree of

MASTER OF ENGINEERING

Faculty of Engineering and Applied Science

Memorial University of Newfoundland

July 1979

St. John's Newfoundland

STATIC PENETRATION RESISTANCE OF SOILS

TO MY DAUGHTER MYE

ABSTRACT

In-situ tests play an important role in geotechnical investigations, particularly in situations where the problems of sample recovery and the consequent sample disturbance are severe limitations.

This thesis is part of an ongoing research on penetrometers at Memorial University of Newfoundland. The results reported here are for two cone penetrometers, 35.6 mm and 76.2 mm diameter, which were used in a static mode.

Different theoretical and experimental results are available in the literature to define the failure mechanism associated with the penetration resistance of cones into soils.

Strength parameters and penetrometer interaction properties of fine sand and silty clay were determined using the conventional triaxial and direct shear tests. The results were then used as the basis for theoretical prediction of the penetration resistance after explicitly accounting for penetrometer base apex angle, penetrometer size and roughness. Comparison of unit penetration resistance values measured in controlled laboratory tests and predicted by theory subsequently permitted the suggestion of the most appropriate method for the penetration mechanism.

Methods for evaluating in-situ shear strength of soils from measured cone penetration resistance are suggested. Values of shear strength parameters (C and ϕ) are determined and compared with those of other investigators.

ACKNOWLDDGEMENTS

This dissertation was completed at the Faculty of Engineering and Applied Science, Memorial University of Newfoundland. The project was partially funded by a Natural Sciences and Engineering Research Council of Canada Grant A-3710, to Dr. T.R. Chari, the project supervisor. The writer wishes to acknowledge with thanks the receipt of a Memorial University Fellowship during the period of this study.

The writer is deeply indebted to his supervisor Dr. T.R. Chari, Associate Professor of Engineering, for his constant advice, guidance, encouragement and continuous support during the course of the research, and for his careful review of the manuscript. Thanks are due to Dean R.T. Dempster, Dean of Engineering for the facilities provided and to Dean F.A. Aldrich, Dean of the Graduate School for his constant encouragement.

Among the various individuals who contributed to this study, the writer wishes to acknowledge, in particular, Mr. A. Bursey for his assistance in the instrumentation, Mr. P. Robinson and his colleagues at the University Technical Services for their cooperation in assembling the experimental facility.

The cooperation of Mrs. Gwen Kerri in typing this thesis within a short period of time is acknowledged with thanks.

Finally, the writer wishes to specially thank his wife for her assistance in drafting the drawings and compiling this thesis. But for her continued understanding, patience and encouragement this work

would have been impossible.

TABLE OF CONTENTS

Page

LIST OF TABLES

LIST OF FIGURES

Figure		Page

NOTATIONS

The symbols listed below and used in this thesis generally confirm to those suggested by the American Society of Civil Engineers(Nomenclature for soil Mechanics, Journal of Soil Mechanics and Foundations Division, June 1962) and the Canadian Geotechnical Journal. They are also defined when they first appear in this thesis. SI units are used throughout.

I - English Letters

$\bar{A}$, A_k	- dimensionless parameters
B	- width or diameter of foundation
$\bar{B}$, B_k	- dimensionless parameters
C	- soil cohesion
$\bar{C}$	- dimensionless parameter
C_{Is}	- cone index of a standard cone
C_{Ix}	- cone index of penetration V_x with cone diameter d_x
D	- base depth of foundation
$\bar{D}$	- dimensionless parameter
D/B	- relative depth
d_c, d_γ, d_q	- depth factors for cohesion, friction and surcharge terms respectively
e	- void ratio
E	- elastic modulus
I_r	- rigidity index
I_D	- density index
K	- lateral earth pressure coefficient
K_b	- at rest earth pressure coefficient

L	- length of foundation
n_r	- degree of roughness
m	- relative depth (D/B)
M	- exponent of shear rate factor
N_c, N_γ, N_q	- Bearing capacity factors for cohesion, friction and surcharge respectively
$N_{\gamma q}$	- bearing capacity friction-surcharge factor
P	- penetration force
P_0	- surcharge
q	- ultimate pressure on the foundation
q_c	- ultimate cone resistance
q_f	- ultimate bearing capacity, or unit penetration resistance
r	- coordinate of slip line field in r-z plane
r_γ	- roughness factor
R_o	- outside radius of the penetrometer
w	- water content of soil
z	- coordinate of the slip line fields in r-z plane
Z_o	- depth to which base of cone has penetrated

II - Greek Letters

α	- base semi-apex angle
α_1, α_2, α_T	- dimensionless parameters
β, ψ, θ, θ_o	- angles which determine the shear surface associated with static penetration
$\bar{\beta}$	- complement to half the cone apex angle
γ	- soil density
$\bar{\gamma}$	- the topmost angle of plane shear zone
γ_s	- unit weight of soil

δ	- penetrometer to soil friction angle
δ/ϕ	- penetrometer roughness
ξ_c, ξ_γ, ξ_q	- shape factor for cohesion, friction and surcharge terms respectively
$\xi_{\gamma q}$	- shape factor for friction surcharge term
σ, σ_o, σ_n	- normal stress
σ_m	- mean normal stress
$\grave{\sigma}$	- effective stress
σ_r, σ_λ, σ_Z,	
$\sigma_{\lambda Z}$, τ_{rZ}, $\tau_{r\lambda}$	- stress component for axialy symmetric case
σ_1, σ_3	- major, minor principal stress
ϕ	- angle of internal friction for the soil
τ	- shear stress
τ_f	- shear strength
ν	- poisson's ratio

III - Symbols

mm	- millimeter
cm	- centimeter
m	- meter
μm	- micrometer
μ"	- microinch
kg	- kilogram
kN	- kilonewton
kPa	- kilopascal

CHAPTER I

INTRODUCTION

1.1 General

The objectives of any soil investigation are to estimate the stratigraphy including the extent, thickness and location of different layers and to determine the engineering properties of the layers such as the strength, permeability and compressibility, so as to choose the best site and the most appropriate foundation design for the chosen location. Recovery of "undisturbed" soil samples, either from trial pits or bore holes generally forms part of such site investigations. In offshore foundation studies, the presence of the water medium and its hydrostatic head, and the underconsolidation of the surficial layers make the task of sample recovery difficult. In-situ tests have thus become an indispensable component of offshore site investigation.

Among the in-situ methods, the penetrometer is now finding greater application in both terrestrial and underwater investigations. A variety of cone penetration equipment have been developed for terrestrial soils (Sanglerat 1972) and a review of the various methods and the state-of-the-art in different countries is given in ESOPT (1974). The penetrometer is basically a field instrument, the penetration resistance of which is correlated to the soil properties. These results supplement the laboratory tests on soil samples.

Cone penetrometer tests (CPT) in a static mode have been used for more than thirty years, mostly in Europe, in terrestrial geotechnical engineering. Use of this instrument in North Sea investigations has been reported to be successful. Static penetrometers require seabed rigs (De Ruiter 1975, Zuidberg 1975) to test surficial sediments and a drill string attachment (Ferguson et al 1977) for tests inside bore holes. For site-specific foundation studies, static penetration tests appear to be extremely relevant and useful.

One limitation associated with static penetration tests in the oceans is the need for suitable reaction rigs. With a view to developing a quick and economical way of testing surficial soils, the use of the standard "Fugro" penetrometer with some modifications was suggested and a laboratory free fall penetrometer was developed (Dayal 1974) at Memorial University. There were some operational and structural problems when this penetrometer was tried at sea (Jones 1976).

The modified version of the penetrometer is 76.2 mm diameter with a 60° cone and a 625 cm^2 friction sleeve. A description of the penetrometer and preliminary results from its sea trials south of Newfoundland during May 1978 are reported by Chari et al (1978, 1979).

As a part of this ongoing research on penetrometers, laboratory experiments were conducted to facilitate interpretation of the output from the 76.2 mm diameter penetrometer. The study reported here relates to static tests with the standard "Fugro" penetrometer and the 76.2 mm Memorial penetrometer. A study of the two penetrometers in a free fall mode has been made by Chaudhuri (1979).

Cone penetration **tests are prefered in geotechnical studies for a** variety of reasons:

1. it provides test data that are amenable to analytical interpretation,

2. it is applicable to a variety of soils ranging from sands to soft clay,

3. it is similar to the behaviour of pile foundations, especially in the strain or stress path caused in the soil failure, and

4. compared to other methods, the penetrometer in general is easy, quick and economical to operate.

Results reported by Meyerhof (1961a), Nowatzki and Karafiath (1972, 1978), Durgunoglu and Mitchell (1973, 1975) and Baligh and Vivatrat (1979) identify a number of variables which influence the penetration resistance. These are the penetrometer size, cone angle and roughness, soil friction angle, soil compressibility and the depth of penetration. The aim of this study is to examine the effects of these parameters and their relative influence on the two types of penetrometers.

Recent geotechnical literature contains numerous failure mechanisms for soil and different theoretical methods to predict static penetration resistance. Among these, the theories of Meyerhof (1961a), Nowatzki and Karafiath (1972) and Durgunoglu and Mitchell (1973) have been widely used. The soil failure mechanism associated with static penetration resistance is one of the aspects which will be considered in detail in this investigation in relation to these three theories.

1.2 Scope of This Work

An investigation of penetrometer-soil interaction was undertaken in order to express the static penetration resistance of soils in terms of the penetrometer base apex angle, base roughness, depth of penetration, soil cohesion and angle of shear resistance. The specific objects of this study are:

1. to delineate the failure mechanism associated with static penetration resistance,

2. to choose an appropriate analytical solution which satisfies the failure mechanism and which will predict the static penetration resistance of soils in terms of the geometry of the penetrometer and properties of the soil,

3. to evaluate the analytical method through carefully controlled laboratory penetration tests,

4. to determine the relative importance of the various parameters such as the penetrometer size, base apex angle, base roughness, angle of internal friction, compressibility of soils, saturation of soil, rate of penetration and relative depth of penetration, and

5. to illustrate how in-situ strength may be deduced from the results of cone penetration tests.

The state-of-the-art is reviewed in Chapter II. The failure mechanism associated with static penetration resistance and the theories for determining the ultimate base resistance are described. Chapter III describes the experimental program of this investigation. Analysis of the laboratory results, comparison of the measured and predicted penetration resistance, and the influence of the different variables are analyzed in Chapter IV. Finally, summary and conclusion of this investigation and recommendations for further work are presented in Chapter V.

CHAPTER II

REVIEW OF LITERATURE

2.1 General

Cone penetrometers are widely used to investigate the properties of soil deposits in-situ. They are important tools in evaluating the bearing capacity of soils. Depending on the depth of penetration in relation to its size, cone penetrometers can be treated as an equivalent shallow or deep foundation.

Early attempts to predict the bearing capacity of soil were based on earth pressure theory proposed by Rankine in the nineteenth century. For a strip footing on a granular material with internal friction, Rankine proposed the formula:

$$q_f = \gamma_s D \tan^4(\pi/4 + \phi/2) \quad [1]$$

where

q_f = ultimate pressure on the foundation,

γ_s = soil unit weight,

D = depth of burial of the foundation, and

ϕ = angle of internal friction for the soil.

Bell (1915) proposed a modification to this for clay to take into account the cohesion in clay and suggested the formula as:

$$q_f = \gamma_s D \tan^4(\pi/4 + \phi/2) + 2C \tan^3(\pi/4 + \phi/2) + 2C \tan(\pi/4 + \phi/2) \quad [2]$$

where C is the soil cohesion.

Experiments by Prandtl (1920) showed that the bearing capacity under a strip load on a rigid-plastic, incompressible and weightless material is:

$$q_f = C\,N_c \qquad [3]$$

where

$$N_c = \cot\phi\left[e^{\pi \tan\phi} \tan^2(\pi/4 + \phi/2) - 1\right] \qquad [4]$$

Reissner (1924) considered the effect of a surcharge, q, and concluded that the bearing capacity was increased by an amount qN_q where:

$$N_q = e^{\pi \tan\phi} \tan^2(\pi/4 + \phi/2) \qquad [5]$$

A widely used bearing capacity equation which considers soil cohesion, friction and surcharge was first presented by Terzaghi (1943) as:

$$q_f = C\,N_c + p_o\,N_q + 1/2\,\gamma_s\,B\,N_\gamma \qquad [6]$$

where

p_o = Overburden pressure at base level

C = soil cohesion

B = width of the foundation

γ_s = soil unit weight

N_c, N_q and N_γ are the bearing capacity factors.

The values of Bearing Capacity factors N_c, N_q and N_γ are influenced by the type of failure surface assumed. It is the determination of these factors which varies in different theories that are available. For an assumed failure mechanism and knowing the mechanical properties of the penetrometer, one can determine the bearing capacity factors in terms of C and ϕ. Hence, if q_f measured with the penetrometer, C and ϕ can be calculated.

Various bearing capacity theories currently used will be reviewed below and each one of them will be considered in the subsequent analysis to decide the most relevant one to the series of experiments conducted.

2.2 Terzaghi's Theory

In the analysis of the bearing capacity of shallow foundations, Terzaghi (1943) assumed that the slip surface ends at the base level of the foundation (Fig. 1) and the overburden was replaced with an equivalent surcharge. The zones of plastic equilibrium can be subdivided into three zones (I), (II) and (III) as shown in the figure. Zone (I) is a wedged-shaped zone located beneath the loaded strip, in which the major principal stresses are vertical. Zone (II) is the radial shear zone, emanating from the outer edges of the loaded strip, whose boundaries intersect the horizontal at angles of $(45^0 + \phi/2)$. The slip line of this radial shear zone may be closely approximated as a logarithmic spiral. Finally, zone (III) is the Rankine passive zone.

The bearing capacity of a shallow strip foundation of width B and depth D can be represented by expression [6]. Similarly for deep foundations, Fig. 2b, Terzaghi has indicated that the bearing capacity is approximately equal to that of shallow foundation [equation 6] with the shape of failure assumed same, but including the additional effects of skin friction along the foundation shaft and the shearing stress along a vertical outer boundary of the mass of soil adjacent to the foundation.

2.3 Meyerhof's Theory

Based on field observations and subsequent theoretical and laboratory analysis, Meyerhof (1951) modified Terzaghi's theory. Terzaghi's theory was generally found to be conservative and for deep foundations, the mobilization of the shear strength of the entire surcharge is doubtful.

In an attempt to overcome these limitations, Meyerhof extended the analysis of the plastic equilibrium of a surface footing to shallow and deep foundations. According to this theory, zones of plastic equilibrium increase with foundation depth to a maximum for a deep foundation (Fig. 2 a, b). Meyerhof also indicated and illustrated how the zones of failure are influenced by the shape and the roughness of the foundation.

At the ultimate bearing capacity, the region above the composite failure surface is, in general, assumed to be divided into two main zones on each side of the central zone ABC (Fig. 2a) namely, a radial shear zone BCD and a mixed shear zone BDEF in which the shear varies between the limits of radial and plane shear, depending on the depth and roughness of the foundation.

Meyerhof presented the ultimate bearing capacity in a form given by Terzaghi (1943) [Eq. 6], but the factors N_c, N_q and N_γ were different and depend on the depth, the shape, and the roughness of the base as well as the angle of internal friction ϕ. Meyerhof's analytical treatment of the bearing capacity problem was based on extension of the work of Prandtl (1920) and Reissner (1924), where the weight of the soil was neglected and the bearing capacity given as:

$$q = C N_c + p_o N_q \quad [7a]$$

and that of Ohde (1936) where the weight of the material was taken into account and an approximate bearing capacity given as:

$$q = 1/2 \gamma_s B N_\gamma \quad [7b]$$

Values for N_c, N_q and N_γ given by Meyerhof (1951) are shown in Figures 3, 4 and 5 respectively. Meyerhof (1961a) extended his investigation to the influence of base configuration on the slip line geometry in the vicinity of the base. He assumed a failure mechanism shown in Fig. 6 for shallow and deep wedge and cone shaped foundations. As shown in this figure, for a perfectly smooth wedge with a semi-angle α the region above the failure surface on each side of the centre line of the foundation is assumed to be divided into a plane shear zone ACD, a radial shear zone ADE and a mixed shear zone AFEG (shallow wedge) or a plane shear zone AEF (deep wedge). As the roughness of the wedge increases, the angle at A in zone ACD decreases. For a perfectly rough wedge, a central elastic zone ACD forms a false base in the case of a blunt wedge when the bearing capacity is identical to that of a horizontal base. For a sharp wedge this elastic zone coalesces with the wedge. The bearing capacity can be represented by equation [6] with appropriate modified values for N_c, N_q and N_γ.

For shallow foundations ($D/B \leq 1$) the stress $p_o = \gamma D$ where D is the base depth of the wedge, while for deep foundations ($D/B \geq 4$ to 10)

$$p_o = K_b \gamma D \qquad [8]$$

where K_b = earth pressure coefficient on the shaft near base, which is about 0.5 for sands and 1.0 for clays, Meyerhof (1951).

The bearing capacity factors N_c, N_q and N_γ, as suggested by Meyerhof (1961a) are given in Figs. 7, 8 and 9 for the limiting conditions of perfectly rough and perfectly smooth wedges at shallow and great depths.

The bearing capacity factors of cones are somewhat larger than those for the wedges. This is because at the ultimate bearing capacity of a cone, plastic flow of the soil induces circumferential stresses, which raise the bearing capacity above that for a corresponding wedge. The bearing capacity of cones can be obtained from empirical shape factors in conjunction with equation [6] to give the cone resistance. Values of the cone bearing capacity factors N_{cr}, N_{qr} and $N_{\gamma r}$ are also presented in Figs. 7, 8 and 9 respectively.

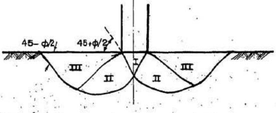

FIG. 1 FAILURE MECHANISM ASSUMED BY TERZAGHI

(Terzaghi 1943)

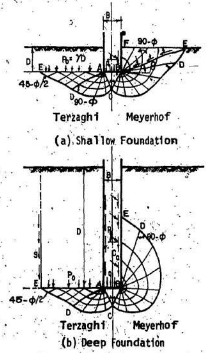

FIG. 2 PLASTIC ZONES NEAR ROUGH STRIP FOOTINGS

(Meyerhof 1951)

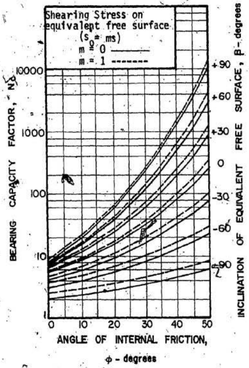

FIG. 3 GENERAL BEARING CAPACITY FACTOR N_c FOR STRIP FOOTINGS

(Meyerhof 1951)

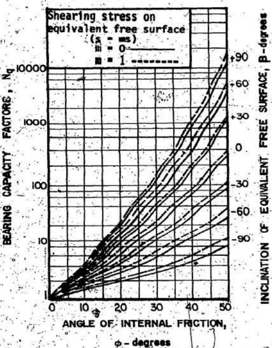

FIG. 4 GENERAL BEARING CAPACITY FACTOR N_q FOR STRIP FOOTINGS

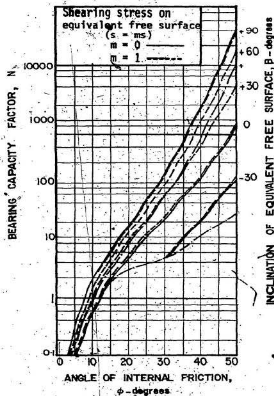

FIG. 5 GENERAL BEARING CAPACITY FACTOR N_γ FOR STRIP FOOTINGS

(Meyerhof 1951)

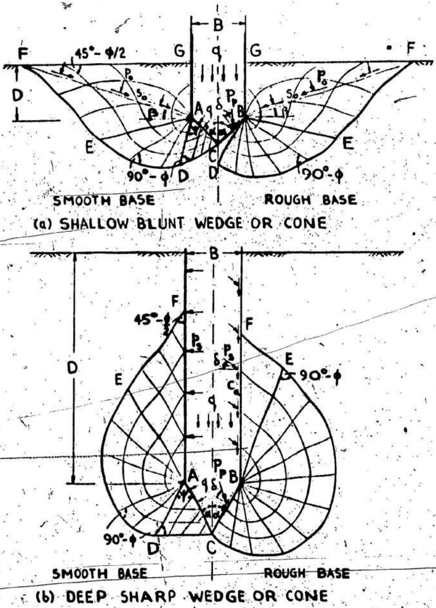

FIG. 6 FAILURE MECHANISM ASSUMED BY MEYERHOF

(Meyerhof 1961a)

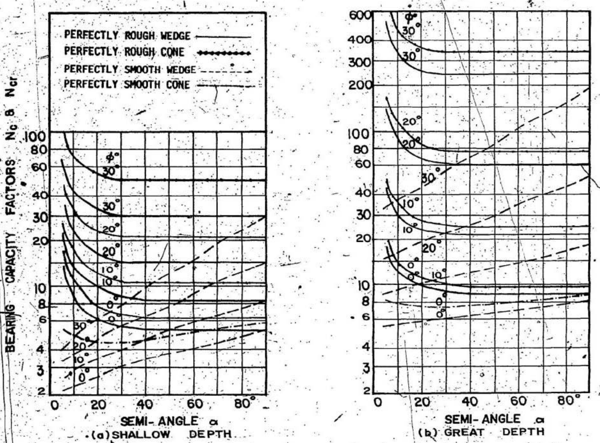

FIG. 7 BEARING CAPACITY FACTORS N_c AND N_{cr}

(Meyerhof 1961a)

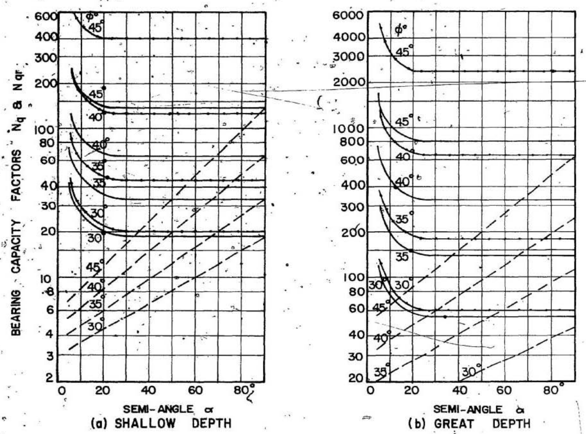

FIG. 8 BEARING CAPACITY FACTORS N_q and N_{qr}

(Meyerhof 1961a)

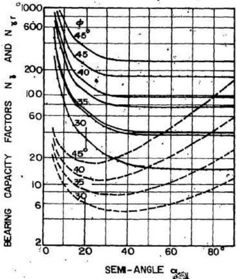

FIG. 9 BEARING CAPACITY FACTORS N_γ AND $N_{\gamma r}$

(Meyerhof 1961a)

2.4 Theory of Berezantzev, Khristoforovand and Golubkov

Based on the limit equilibrium theory and experimental investigation on load bearing capacity of single piles in dense sand, Berezantzev et al (1961) suggested the failure mechanism shown in Figure 10. The radial slip surface in this mechanism was assumed to end prior to reaching the base of the foundation. They suggested the following formula for the average value of ultimate bearing capacity:

$$q_f = A_k \gamma_s B + B_k \alpha_T \gamma_s D \qquad [9]$$

where the coefficient "α_T" is a function of the ratio D/B and of the angle ϕ and is given in Table 1. The factors A_k and B_k are equivalent to the bearing capacity factors in formula [6] and these are given in Figure 11.

Berezantzev et al (1961) justified the formula [9] by model tests carried out at Leningrad Institute of Railway Engineers.

2.5 Theory of Biarez, Burel and Wach

Biarez et al (1961), reported the results of tests on several scale model foundations using thin metal cylinders in the form of piles. Comparisons were made with calculations using the plastic theory. Observation of the failure mode in the soil at various test stages revealed a rigid wedge beneath the foundation, with a half angle at its apex of about 50° for a shallow foundation. This angle was reported to decrease with increasing depth of foundation. For relatively great depths, the radial shear zone of the failure surface reaches a vertical tangency as shown in Fig. 12.

TABLE I

COEFFICIENT "α_T" AS A FUNCTION OF (D/B) AND (ϕ)

D/B \ ϕ	26^o	30^o	34^o	37^o	40^o
5	0.75	0.77	0.81	0.83	0.85
10	0.62	0.67	0.73	0.76	0.79
15	0.55	0.61	0.68	0.73	0.77
20	0.49	0.57	0.65	0.71	0.75
25	0.44	0.53	0.63	0.70	0.74

(Berezantzev et al 1961)

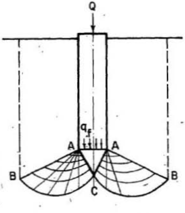

FIG. 10 FAILURE MECHANISM ASSUMED BY BEREZANTZEV ET AL

(Berezantzev et al 1961)

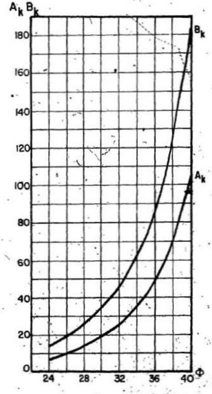

FIG. 11 COEFFICIENTS FOR BEREZANTZEV'S THEORY

(Berezantzev et al 1961)

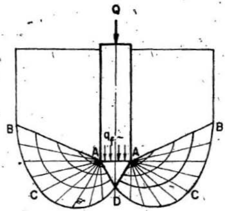

FIG. 12 FAILURE MECHANISM OF BIAREZ, BUREL AND WACH

(Biarez et al 1961)

Values for N_q and N_γ were derived based on the above failure mechanism. The experimental values at shallow depths were found to be less than the computed values, while for great depths they were very close to the theoretical values.

2.6 Vesic's Theory

To provide information on the factors which influence the bearing capacity of deep foundations in sand, Vesic (1963) conducted large-scale model experiments at Georgia Institute of Technology. Cylindrical and prismatic foundations of various sizes resting at different depths in homogeneous sand masses of different relative densities were loaded statically to failure. Additional tests with colored sand, laid in layers were made to study the mechanism of shear failure in the soil mass. The results showed that irrespective of the relative density of sand, for deep foundation punching shear failure occurs.

The general bearing capacity for deep foundation in sand was given as:

$$q_f = p_o N_q^* \xi_q \qquad [10]$$

where

q_f = ultimate bearing capacity,

p_o = overburden pressure,

N_q = bearing capacity factor for surcharge term, and

ξ_q = shape factor.

To evaluate the bearing capacity factor N_q for a long rectangular foundation, a shear pattern based on observations of tests on colored sand was considered (Fig. 13). The failure mode consists of an elastic zone ACD with two adjoining plastic zones CDF and ADE. The extent of development of these zones is determined by the angle θ at the apex. This angle may be represented empirically by:

$$\theta = 1.9\phi \qquad [11]$$

where ϕ is the angle of internal friction of the sand.

On the basis of observations, Vesic suggested the following expression for N_q:

$$N_q = e^{3.8\phi \tan\phi} \tan^2(45 + \phi/2) \qquad [12]$$

A comparison of the bearing capacity factor N_q for local and general shear failure is shown in Fig. 14.

2.7 Hu's Theory

Hu (1965) assumed the failure mechanism shown in Fig. 15 in which the radial slip surface reaches a vertical tangency. The logarithmic spiral surface CE meets the vertical tangential plane passing through the general surface at F, and a continuity of the slip surface is thus maintained. The configuration OACEFGHO consists of a lower part, the failure mechanism proper OACEO, in which the stress at every point reaches the state of plastic equilibrium and an upper part, the overburden OEFGHO, in which the stress is in a state of mixed shear. The interface OE is seen as an internal failure surface across which full shear mobilization takes place. For $\phi = 0$ or C-soils, however, shear mobilization across the interface is not assumed. This is because the point of vertical tangency E is now moved to the base level as a

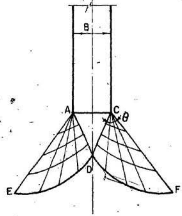

FIG. 13 FAILURE MODE FOR LOCAL SHEAR (Vesic 1963)

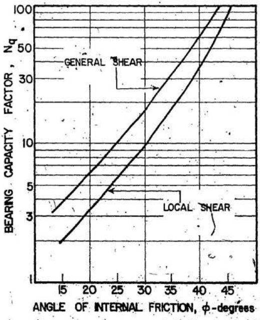

FIG. 14 COMPARISON OF BEARING FACTOR N_q FOR LOCAL AND GENERAL SHEAR

result of the logarithmic spiral being replaced by a circular arc. Under this condition, the vertically upward plastic flow of the foundation soil at failure does not permit shear strength to be developed across the horizontal base plane, resulting in $s_o = 0$. This in turn requires that E must stop short of the base plane to allow the edge angle a full value of 45^o under the passive Rankine state. The failure mechanism therefore resembles that suggested by Terzaghi, shown in Fig. 2 after substituting a circular arc for the logarithmic spiral.

Based on the above failure mechanism, Hu derived the following equation for the total base bearing capacity:

$$q_f = C N_c + \gamma_s B N_{\gamma q} \qquad [13]$$

where $N_{\gamma q}$ is the bearing capacity factor for surcharge-friction term. Hu justified his theoretical values by comparing them with the measured bearing capacity of sands in various states of compaction and at different depths.

2.8 Cavity Expansion Theory

Another approach to the problem of base bearing capacity originated in the work by Bishop, Hill and Mott (1945), who considered the problem of expansion of a spherical or cylindrical cavity inside an infinite mass of an ideal solid. In such a case there exist around the cavity a highly stressed zone where the material, by assumption, behaves as a rigid-plastic solid. Outside that zone it behaves as an ideal elastic (or linearly deformable) solid. Vesic (1972) used this concept and assumed that advancement of the penetrometer takes place by the expansion of a spherical cavity.

Fig. 16 illustrates the problem of expansion of a spherical cavity as viewed by Vesic. A spherical cavity of initial radius R_i is expanded by uniformly distributed internal pressure P. When this pressure is increased, a zone around the cavity will pass into a state of plastic equilibrium. This plastic zone will expand until the pressure reaches a maximum value, P_u, at which point the cavity will have a radius R_u. The plastic zone around the cavity will have a radius, R_p. Beyond R_p, the rest of the mass remains in a state of elastic equilibrium.

General solutions of the problem of spherical and cylindrical cavities in an ideal soil, possessing both cohesion and friction in the Mohr-Coulomb sense, are presented by Vesic (1972) and numerically evaluated in the form of tables and graphs suitable for application to Engineering practice.

The concept of expansion of cavities has recently been extended by Baligh (1976) who suggested that the point resistance in cone penetration tests in cohesionless soils is usually quite high and that a realistic analysis of the bearing capacity of deep foundations in sand must therefore be based on the behaviour of the soil at high stresses. The soil response was found to differ from the common behaviour at normal stress levels in two important aspects: (1) the decrease of the angle of internal friction with the mean normal stress, i.e., the Mohr-Coulomb failure envelope is not straight but is actually convex; and (2) the significant decrease in volume which took place upon shearing even in dense granular media. Baligh considered the effect of a curved Mohr-Coulomb failure envelope on the bearing capacity

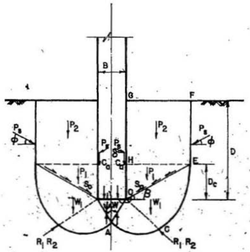

FIG. 15 FAILURE MECHANISM ASSUMED BY HU
(Hu 1965)

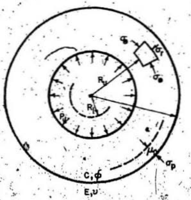

FIG. 16 EXPANSION OF CAVITY
(Vesic 1972)

of deep foundations in sands by obtaining the solutions to problems of cavity expansion. An analytical expression for a curved envelope is introduced, compared with experimental results, and then incorparated in a computer program to evaluate the expansion pressure for cylindrical and spherical cavities, taking into account both the envelope curvature as well as the compressibility of the soil.

2.9 Numerical Technique

The finite difference approximation based on the method of characteristics is widely used in the numerical analysis of differential equations of the type applicable to the bearing capacity problems. Lundgren and Mortensen (1953) used this method to obtain a solution of the strip footing bearing capacity problem. The same method was used for the axially symmetric circular footing problem by Cox et al (1961). Numerical technique has been also applied to deep foundations. Strip loading conditions were analyzed by Graham (1968) and solutions were provided for axisymmetric circular foundations by Nowatzki and Karafiath (1972, 1978).

Nowatzki and Karafiath (1972, 1978) presented a theoretical 3-dimensional analysis of cone penetration using plasticity theory and the Coulomb failure criterion. The differential equations of plastic equilibrium were solved numerically, using finite difference technique, for an ideal uniform dry sand to show the variation of slip-line field geometry with changes in the apex angle of the cone. In this analysis an assumption of the slip lines is required. Nowatzki and Karafiath assumed that the slip surface ends at the base level of the penetrometer (Fig. 17) which is equivalent to neglecting the shear

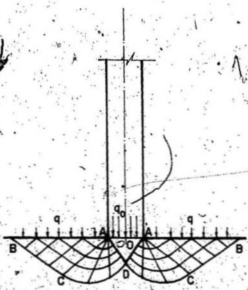

FIG. 17 SLIP LINE SURFACES ASSUMED BY NOWATZKI AND KARAFIATH

(Nowatzki and Karafiath 1972)

strength of the overburden as was done by Terzaghi (1943). The results indicate that, with increasing apex angle, less soil volume is affected. Both theoretical and laboratory results showed that the value of cone index (penetration resistance/area of cone base) increases with increasing apex angle. A series of laboratory experiments supported the validity of the theory in dense sand and demonstrated that the soil compressibility affects the cone index to the extent that it no longer serves as a measure of frictional strength. For very loose soils, differences in cone angle have little effect on cone index, all other conditions being equal.

Finally they correlated the theoretical and experimental results to show how the theory may be used for any soil to predict the angle of internal friction.

2.10 Theory of Durgunoglu and Mitchell

Durgunoglu and Mitchell (1973, 1975) have suggested the failure mechanism associated with the static penetration resistance of cohesionless and low-cohesion soils as shown in Fig. 18a, b. They performed model tests to establish a rational basis for the theoretical development taking into account the effects of penetrometer configuration, penetrometer to soil friction, soil relative density and the relative depth of the failure mechanism. The failure surface as shown represents closely the actual failure surface obtained in experiments with wedge shaped penetrometers. The rupture pattern is very similar to that assumed by Hu (1965) for the analysis of pile foundation. Examining Figure 18 it can be seen that a plane shear zone exists adjacent to the base of the penetrometer. The slip surface of the radial shear zone can be approximated by a logarithmic spiral which either intersects

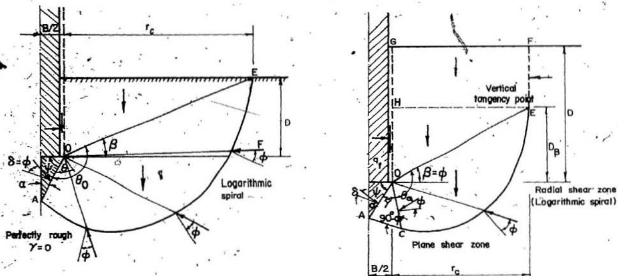

(a). Small Relative Depths

(b) Large Relative Depths

FIG. 18 PROPOSED FAILURE MECHANISM ASSOCIATED WITH WEDGE PENETRATION INTO SOIL

(Durgunoglu and Mitchell 1973)

the ground surface at point E (Fig. 18a) or becomes vertically tangent to line EF (Fig. 18b) depending on the relative depth of the foundation.

The geometric configuration of the plane shear zone adjacent to the wedge (Fig. 18b) is determined by the known wedge or cone semi-apex angle α, the topmost angle $\bar{\gamma}$, and the included angle ACO which is equal to $(90^{\circ} - \phi)$. As the roughness δ/ϕ of the cone increases, the angle at point O decreases and vanishes for a perfectly rough cone ($\delta = \phi$). Methods for calculating this angle have been presented in detail by Durgunoglu and Mitchell (1973).

Based upon the above failure mechanism, Durgunoglu and Mitchell arrived at the following equation for penetration resistance:

$$q_f = C\, N_c\, \xi_c + \gamma_s\, B\, N_{\gamma q}\, \xi_{\gamma q} \qquad [14]$$

where all the terms were previously defined.

Equilibrium analysis of the failure zone shown in the free body diagram (Fig. 19a) yields the following expression for the value of N_c:

$$N_c = \frac{1 + \sin\phi \, \sin(2\bar{\gamma} - \phi)}{\sin\phi \, \cos\phi} \, e^{2\theta_o \tan\phi} - \frac{1}{\tan\phi} + \frac{\cos(2\bar{\gamma} - \phi)\tan\psi}{\cos\phi} \, e^{2\theta_o \tan\phi} \qquad [14a]$$

where

N_c = bearing capacity factor,

ϕ = soil friction angle,

$\bar{\gamma}$ = the topmost angle of the plane shear zone,

$\psi = 90^{\circ} - \alpha$ (α = semiapex angle)

$\theta_o = 180^{\circ} - (\psi + \tilde{\gamma}) + \beta$

Similarly, from this static equilibrium analysis of the body OCEFG (Fig. 19b) the following expression for $N_{\gamma q}$ was derived by Durgunoglu and Mitchell:

$$N_{\gamma q} = \frac{\cos(\psi - \delta)}{\cos\delta} \frac{(1 + \sin\phi \sin(2\tilde{\gamma} - \phi))}{\cos\phi \cos(\tilde{\gamma} - \phi)} \left\{ \frac{\cos^2(\tilde{\gamma} - \phi)}{4\cos^2\psi \cos^2\phi} I_{\theta} + \frac{3 \cos(\tilde{\gamma} - \phi) \cos^2\beta}{4 \cos\psi \cos\phi} e^{2\theta_o} \tan\phi \,(m - 2/3\, \tilde{m}) - K_o \frac{\cos\psi \cos\phi}{\cos(\tilde{\gamma} - \phi)} \cdot (m - \tilde{m})^2 \cdot (m + 2\tilde{m}) + K \frac{\cos\psi \cos\phi}{\cos(\tilde{\gamma} - \phi)} m^3 \right\} - \frac{\tan\psi}{4} \qquad [14b]$$

where

$N_{\gamma q}$ = bearing capacity factor for friction-surcharge,

ϕ = angle of internal friction of soil,

ψ = $90^{\circ} - \alpha$ (α = semiapex angle),

δ = base to soil friction angle,

$\tilde{\gamma}$ = the topmost angle of the plane shear zone,

θ_o = $180^{\circ} - (\psi + \gamma) + \beta$,

K = lateral earth pressure coefficient,

m = relative depth,

$\tilde{m}$ = D_{β}/B

D_{β} = the vertical distance of point E on the failure surface above base level (a function of β)

$$\bar{m} = 1/2 \; \frac{\sin\beta \cos(\bar{\gamma} - \phi)}{\cos\psi \cos\phi} \; e^{\theta_o \tan\phi}$$

and
$$I_\theta = 1/\left[1 + 9 \tan^2\phi \left\{3 \tan\phi \left[e^{3\theta_o \tan\phi} \cos\beta - \cos(\theta_o - \beta)\right] + \left[\left(e^{3\theta_o \tan\phi} \sin\beta + \sin(\theta_o - \beta)\right]\right\}\right] \qquad [14c]$$

In order to calculate the bearing capacity factors N_c and $N_{\gamma q}$ from Equations [14], the value of the angle β must be known. For relative depths equal to or greater than the critical depth (The depth at which the vertical tangency point coincides with the ground surface) the angle β is equal to the angle of internal friction ϕ of the soil. For relative depths less than the critical relative depth, the failure surface will intersect the ground surface before reaching vertical tangency. In this case, β will be smaller than ϕ and must be calculated by interactive procedures. Values of N_c and $N_{\gamma q}$ calculated from Equations [14] are valid only for wedge shaped foundations. For cone shaped foundations, Durgunoglu and Mitchell suggested the following shape factors:

$$\xi_{\gamma q} = (1.0 - 0.4 \; B/L) + \frac{1.5}{B/D + \dfrac{1.5}{(0.6 + \tan^6\phi) \; B/L}} \qquad [15a]$$

$$\xi_c = 1.0 + (0.2 + \tan^6\phi) \; B/L$$

where $\xi_{\gamma q}$ is the cone factor for friction-surcharge term and ξ_c is the cone factor for the cohesion term.

2.11 Other Factors Affecting Bearing Capacity

2.11.1 Depth

For deep foundation, the effect of the overburden pressure on bearing capacity is introduced as a depth factors d_c, d_γ and d_q by

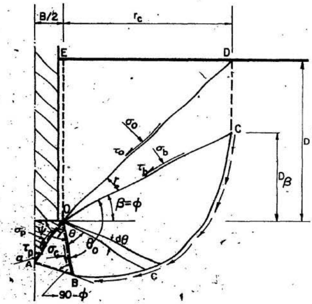

FIG. 19a FREE BODY DIAGRAM FOR DETERMINATION OF BEARING CAPACITY FACTOR (N_c)

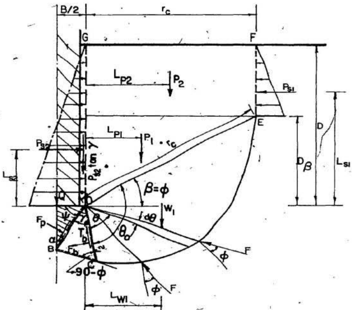

FIG. 19b FREE BODY DIAGRAM FOR DETERMINATION OF BEARING CAPACITY FACTOR ($N_{\gamma q}$)

(Durgunoglu and Mitchell 1973)

most investigators. These factors are dimensionless parameters depending on the ratio D/B and the angle of internal friction. Vesic (1975) considered these parameters as an increase in the individual bearing capacity factors due to the shearing strength of the overburden. Skempton (1951) proposed a depth factor for the cohesion term as:

$$d_c = 1.0 + 0.2\,(D/B) \qquad [16]$$

Brinch Hansen (1961) has proposed the following generalized and semi-emprical equation for the depth factors:

$$d_c = 1.0 + \frac{0.35}{(B/D) + (0.6/(1 + 7\tan^4\phi))} \qquad [17a]$$

$$d_\gamma = 1.0 \qquad [17b]$$

$$d_q = d_c - (d_c - 1)/N_q \qquad [17c]$$

Meyerhof (1963) proposed the following equations for depth factors:

$$d_c = 1.0 + 0.2(D/B)\tan(\pi/4 + \phi/2) \qquad [18a]$$

for $\phi = 0.0^o$:

$$d_q = d_\gamma = 1.0 \qquad [18b]$$

for $\phi \geq 10^o$ and $D/B < 1.0$:

$$d_q = d_\gamma = 1.0 + 0.1(D/B)\tan(\pi/4 + \phi/2) \qquad [18c]$$

De Beer (1967) suggested the following depth factors:

$$d_q^q = 1.0 + (\tan^2(45^o - \phi/2)\ e^{\pi\tan\phi} - 1)\ e^{-\pi\tan(B/D)} \qquad [19a]$$

$$d_\gamma = 1.0 \qquad [19b]$$

Brinch Hansen (1970) has also proposed the following approximate formulae:

for $D/B \leq 1.0$:

$$d_q = 1.0 + 2\tan\phi(1 - \sin\phi)^2\ (D/B) \qquad [20a]$$

$$d_\gamma = 1.0 \qquad [20b]$$

$$d_c = d_q - (1 - N_q)/N_c \tan\phi \qquad [20c]$$

and for $\phi = 0.0^0$:

$$d_c = 1.0 + 0.4\ D/B \qquad [20d]$$

for $D/B > 1.0$:

$$d_q = 1.0 + 2\tan\phi(1 - \sin\phi)^2 \tan^{-1}(D/B) \qquad [21a]$$

$$d_\gamma = 1.0 \qquad [21b]$$

$$d_c = d_q - (1 - d_q)/N_c \tan\phi \qquad [21c]$$

and for $\phi = 0.0^o$:

$$d_c = 1.0 + 0.4\tan^{-1}(D/B) \qquad [21d]$$

Thus it is seen that in case of deep foundations, appropriate correction factors are to be introduced to account for the overburden beyond the zone of soil shear.

2.11.2 Shape

Most of the bearing capacity theories have been formulated for infinitely long footings. For foundation shapes which are not long and rectangular, the difficulties in obtaining mathematical solutions for bearing capacity are considerable. To account for the effect of foundation shape, dimensionless parameters called the shape factors are introduced. These parameters are a function of (B/L), (D/B) and (ϕ). Early suggestions by Terzaghi (1943) and Skempton (1951) for the shape factors are:

for circular areas:

$$\xi_c = 1.3 \qquad [22a]$$

$$\xi_\gamma = 0.6 \qquad [22b]$$

for rectangular areas:

$$\xi_c = 1.0 + 0.2\ (B/L) \qquad [23a]$$

$$\xi_\gamma = 1.0 - 0.2\ (B/L) \qquad [23b]$$

Brinch Hansen (1961) developed the following semi-empirical shape factor equation:

$$\xi_c = 1.0 + (0.2 \tan^6\phi)\ (B/D) \qquad [24a]$$

$$\xi_q = d_c - d_c - 1/\ N_q \qquad [24b]$$

$$\xi_\gamma = 1 - 1/2\ (0.2 + \tan^6\phi)\ (B/L) \qquad [24c]$$

Meyerhof (1961b, 1963) also proposed similar empirical expression:

$$\xi_c = 1.0 + 0.2 \tan^2(45^\circ + \phi/2)\ (B/L) \qquad [25a]$$

$$\xi_q = \xi_\gamma = 1.0 \qquad \text{for } \phi = 0.0^\circ \qquad [25b]$$

$$\xi_q = \xi_\gamma = 1.0 + 0.1\ \tan^2(45^\circ + \phi/2)\ (B/L) \quad \text{for } \phi = 10^\circ \qquad [25c]$$

Expressions for shape factors were recommended by De Beer (1967) based primarily on extensive experiments and subsequently modified by Vesic (1975) as:

for rectangular base:

$$\xi_c = 1.0 + (B/L)\ (N_q/N_c) \qquad [26a]$$

$$\xi_q = 1.0 + (B/L)\ \tan\phi \qquad [26b]$$

$$\xi_\gamma = 1.0 - 0.4(B/L) \qquad [26c]$$

for circular base:

$$\xi_c = 1.0 + (N_q/N_c) \qquad [27a]$$

$$\xi_q = 1.0\ \tan\phi \qquad [27b]$$

$$\xi_\gamma = 0.6 \qquad [27c]$$

2.11.3 Soil Compressibility

Soil compressibility is generally not an influencing factor in bearing capacity equations as the rupture is assumed to be a general shear failure surface. Consequently no corrections are made for soil compressibility. Vesic (1963) has suggested that, for compressible soils, local or punching shear failure, rather than general shear failure occurs. Based on the shear pattern shown in Fig. 13, an expression for N_q (Equation 12) was developed. This equation is plotted and compared to the classic Reissner equation for N_q for general shear in Fig. 14. It may be seen in Fig. 13 and 14 that for compressible soils (local shear conditions), the bearing capacity factor N_q is much lower than for incompressible soils (general shear conditions).

Vesic (1972) has also suggested that the relative compressibility of a sand mass may be expressed in terms of its rigidity index, I_r, defined as:

$$I_r' = E/(1+\nu)\ (C+q\tan\phi) \qquad [30]$$

where

E = elastic modulus,

C = soil cohesion,

ϕ = soil friction angle,

q = overburden pressure, and

ν = Poission's ratio.

Bearing capacity factors calculated by Vesic (1972) using the assumption that the ultimate pressure on the soil under a foundation is equal to the ultimate pressure needed to expand a spherical cavity inside the same soil mass are given in Fig. 20.

Durgunoglu and Mitchell (1973) have also made a reference to soil compressibility and suggested caution in the use of their method. For compressible soils, their method is clearly recognized to cause overestimation of the penetration resistance as a result of the invalidity of the failure mechanism assumed. They also report that, due to soil compressibility, the shear surface is restricted to a smaller zone around the penetrometer tip as suggested by Vesic (1963).

2.12 Summary

It is seen from the literature reviewed that the basic form of

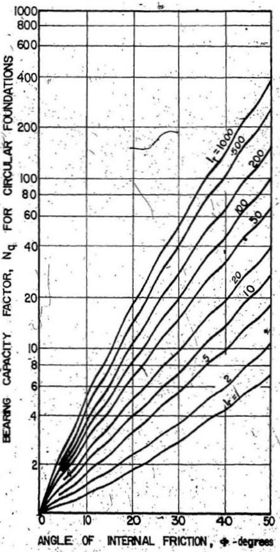

FIG. 20 BEARING CAPACITY FACTOR N_q FOR COMPRESSIBLE SOIL

(Vesic 1972)

the equation for the ultimate bearing capacity of foundations is the same in all the theories [Eqn. 6]. However, the values of the bearing capacity factors N_c, N_q and N_γ vary in each theory depending on the soil failure mechanism assumed and the different factors that are considered as affecting the bearing capacity. Fig. 21 shows summary for failure mechanisms assumed by different investigators.

However, for deep foundation, the value of N_γ becomes negligible compared to the other two terms. The values of N_c and N_q are those corresponding to a slip surface of a weightless soil and the value of N_γ is that corresponding to a slip surface for the condition $q/\gamma_s B = 0$, i.e., footing at the surface. Consequently, at great depths the bearing capacity of the base should be practically independent of its size and may be expressed as:

$$q_f = C\,N_c + p_o\,N_q \qquad [7a]$$

Some investigators such as Hu (1965) and Durgunoglu and Mitchell (1973) combined the factors N_q and N_γ in one term ($N_{\gamma q}$) and expressed the bearing capacity as:

$$q_f = C\,N_c + \gamma_s B\,N_{\gamma q} \qquad [14]$$

where $N_{\gamma q}$ is the bearing capacity factor for the friction-surcharge term.

The factors which influence the ultimate bearing capacity have been reviewed earlier. Important among these are the base roughness and base configuration.

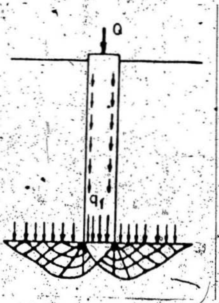

Terzaghi (1943)
Nowatzki and Karafiath (1972, 1978)

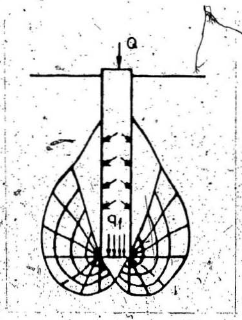

De Beer (1945)
Meyerhof (1951, 1961)

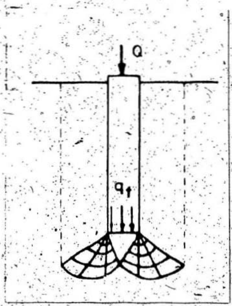

Berezantzev et al (1961)
Vesic (1963)

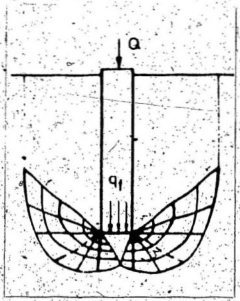

Biarez et al (1961)
Hu (1965)
Durgunoglu and Mitchell (1973, 1975)

FIG. 21 SUMMARY OF DIFFERENT FAILURE MECHANISMS

2.12.1 Base Roughness

The primary bearing capacity factors presented by Meyerhof (1951) and shown in Figs. 3, 4 and 5 apply only to perfectly rough bases ($\delta/\phi = 1$). Investigation by Meyerhof (1955) and others indicated that for cohesive soils, the roughness has very little influence on the bearing capacity. However, in cohesionless soils, the bearing capacity of a surface footing with a smooth base is significantly less than that for a footing with rough base. To account for this influence, Meyerhof has suggested that the N_γ factor be multiplied by a roughness factor r_γ expressed as:

$$r_\gamma = n_r + 1/2(1 - n_r^2) \qquad [28]$$

where n_r is the degree of roughness, defined by the ratio of the tangents of the base friction δ and the angle of internal friction ϕ:

$$n_r = (\tan\delta)/(\tan\phi) \qquad [29]$$

Equation [29] applies only to plane, horizontal bases at the soil surface.

This work was extended further by Meyerhof (1961a) for limiting conditions of perfectly rough ($\delta/\phi = 1$) and perfectly smooth ($\delta/\phi = 0$) bases for shallow and deep foundations. Bearing capacity factors as shown in Figs. 7, 8 and 9 were suggested.

The effect of roughness has also been considered in the numerical technique given by Nowatzki and Karafiath (1972, 1978). Friction angle between the cone and the soil (δ) was introduced as a parameter in their analysis. Durgunoglu and Mitchell (1973) concluded that, the bearing capacity factors for a given roughness should not be estimated by linear interpolation between perfectly smooth and perfectly rough values. They provided values for N_c and $N_{\gamma q}$ at different relative roughness. These values showed that bearing capacity factors increase nonlinearly with increasing roughness for cohesionless soils. In cohesive soils, base roughness has little or no influence on the bearing capacity factors.

2.12.2 Base Configuration

The influence of various non-planar base configuration (e.g. wedges and cones) on bearing capacity factors have been obtained, for different conditions, by Meyerhof (1961a), as shown in Figs. 6, 7 and 8. From these figures one can conclude that for a perfectly rough wedge there is little dependence of bearing capacity factors on the total apex angle (2α), for values of (2α) greater than 90°. That is, for rough wedges and cones with obtuse apex angles, the bearing capacity factors are nearly equal to those for plane and horizontal contact areas. However, for perfectly smooth wedges, the values of N_c and N_q increase with increasing total apex angle.

Recently the effect of cone angles on penetration resistance have been presented by Nowatzki and Karafiath (1972, 1978). Both theory and experiment showed that for soils at high relative densities, penetration resistance varies significantly with the size of the penetrometer apex angle.

Based on experiments on model tests, Durgunoglu and Mitchell (1973, 1975) presented solution for bearing capacity factors N_c and $N_{\gamma q}$ for wedge and cone shaped foundations. They concluded that, the bearing capacity factors for rough bases increase with decreasing values of base semi-apex angle (α) below approximately 15°, but for perfectly smooth wedges and cones, the bearing capacity factors increase with increasing base apex angle.

Although there are various theories for computing the ultimate bearing capacity of soils, the choice of a suitable theory for penetrometer tests is rather limited. The cone of the penetrometer is not really smooth. Similarly the cone angle has to be accounted for since it is unlike a flat foundation. Few theories are available at present which fully account for the base configuration, base roughness, penetrometer size, relative depth of penetration and soil compressibility. The theories which account for most of those factors are: Meyerhof's theory (1961a), theory of Nowatzki and Karafiath (1972, 1978) and theory of Durgunoglu and Mitchell (1973, 1975). It was, therefore, decided to choose these three theories for comparison with the results of the experiments reported here.

CHAPTER III

EXPERIMENTAL PROGRAM

3.1 General

As explained in the preceeding chapter, the penetration resistance is influenced by number of variables. The experimental program was designed to study the effect of these variables and the applicability of the different theoretical formulations to both 10 cm^2 Fugro type penetrometer and 45 cm^2 Memorial University penetrometer. The objectives of the experimental investigation are:

1. to study the influence of the following parameters on the penetration resistance:

    a) cone apex angle

    b) penetrometer base roughness

    c) penetrometer size

    d) soil friction angle

    e) saturation of soil

    f) rate of penetration

    g) depth of penetration

2. to develop a better understanding of the failure mechanism associated with static penetration resistance and the applicability of the theoretical formulae given by Meyerhof (1961a), Nowatzki and Karafiath (1972, 1978) and Durgunoglu and Mitchell (1973, 1975).

3. to illustrate methods of deducing the in-situ strength of soils from the results of cone penetration tests.

4. to evaluate the performance of static penetrometer in layered soils.

A detailed physical description of the two types of penetrometers used is given in Table 2. Tips for both penetrometers were detechable from the shaft and had various semi-apex angle and roughness as shown in Fig. 22. A complete listing of the penetrometer tips used in this investigation is given in Table 3.

Two types of soil target material were selected for this investigation, modelling clay and silica-70 sand. These were chosen as representative of clay (cohesive) and sand (cohesionless) targets. The ease and uniformity of preparing the samples and the commercial procurability of the soil were the other considerations in choosing the two types of soil. In all, about 200 tests were conducted, results of which will be discussed in the subsequent chapter.

3.2 Equipment, Facilities and Instrumentation

The general layout of the experimental facility is shown in Fig. 23. The standard rate of penetration for static cone penetration tests suggested by ASTM (D3441-75T) is 20 mm/sec. The penetrometer is connected to a hydraulic actuator which has a stroke of 55 cm. The hydraulic actuator is connected to a heavy duty pump (40 H.P. and 20 G.P.M.) of the M.T.S. (Measurements and testing system) model 410.31 digital function generator. This system is designed to provide simple yet flexible dynamic programming capabilities in M.T.S. closed loop electrohydraulic testing system. Selectable outputs include normal and inverted variable frequency sine, haversine, and haversquare and variable time single and dual slope ramps. The haversine and haversquare frequencies are step variable from 0.00001 to 990 HZ while ramp tests are step variable from 0.001 to 990,000 seconds. Using this

TABLE 2

PHYSICAL DESCRIPTION OF THE TWO SIZES OF PENETROMETER

Comparison	Fugro Type Penetrometer	Memorial University Penetrometer
Diameter of Cone	35.6 mm	76.2 mm
Base Area of Cone	10 cm^2	45 cm^2
Cone Angle	Adaptable to any end shape, in present investigation 30^o, 60^o and 90^o were used.	
Sleeve Diameter	35.6 mm	76.2 mm
Area of Sleeve	150 cm^2	625 cm^2
Length of Sleeve	13.4 cm	26.1 cm

FIG. 22 DIFFERENT TYPES OF CONES USED

TABLE 3

TYPES OF PENETROMETER TIPS

Penetrometer Diameter (mm)	Base semi-apex angle. α-degree*	Tip Material	Roughness (δ/ϕ)
35.6	15°	Stainless Steel	0.5
	30°	Polished Aluminum	0.6
	90°	Sanded Aluminum	0.75
	30°	Stainless Steel	0.5
	90°	Polished Aluminum	0.6
	15°	Sanded Aluminum	0.75
	90°	Stainless Steel	0.5
	15°	Polished Aluminum	0.6
	30°	Sanded Aluminum	0.75
76.2	15	Stainless Steel	0.5
	30	Polished Aluminum	0.6
	90	Sanded Aluminum	0.75
	30°	Stainless Steel	0.5
	90°	Polished Aluminum	0.6
	15°	Sanded Aluminum	0.75
	90°	Stainless Steel	0.5
	15°	Polished Aluminum	0.6
	30°	Sanded Aluminum	0.75

* A total of 18 different TIPS

FIG. 23 PHOTOGRAPH SHOWING EXPERIMENTAL FACILITY

system the velocity of penetration can be varied. The stroke of the actuator and consequently the depth of penetration can also be regulated and controlled.

The penetrometer is instrumented to measure the cone resistance and the sleeve side friction. The instrumentation for measuring these two quantities consists of two strain gauge load cells, cone load cell and sleeve load cell, (Fig. 24). A detailed specification of the strain gauges and the circuit diagram are shown in Appendix A.

The velocity of penetration was measured by a fixed pointer sliding on a resistance wire. The wire is stretched along the length of the moving shaft so that any movement in the shaft causes the change in the resistance wire with respect to a fixed pointer. This results in a change in voltage and when connected to the chart recorder, with a proper calibration, a direct plot of time vs. displacement is obtained.

The output signals from the cone load cell and friction sleeve load cell were recorded on a chart recorder of Gould 2000 series analog type. It is a self contained unit housed in a 250 mm mainframe chassis to accommodate up to three isolated recording channels. Each recording channel incorporates frictionless feedback sensors for closed-loop control of the pen at high speed. The Gould Model 13-4614-30 D.C. bridge preamplifier is a high gain preamplifier designed to work with resistance transducers, including strain gages and strain gage based transducers. It is designed for use with Gould 2000 series records, and receives its operating power from a companion pendrive amplifier located in the same analog channel of the recorder.

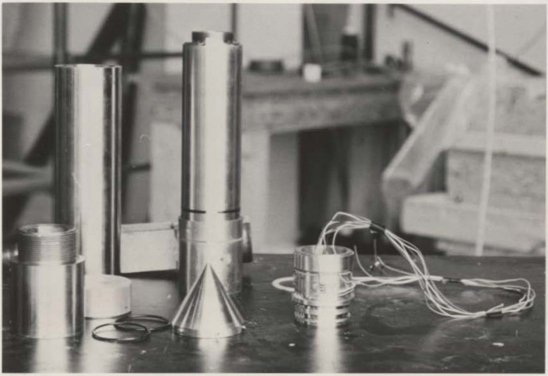

FIG. 24 CONE TIP ASSEMBLY SHOWING THE VARIOUS COMPONENTS

Three channels with three preamplifiers were used in this investigation. Two of them for recording cone and sleeve resistance and the third to check the linearity of the velocity of penetration.

The following time dependent parameters were obtained:

(1) displacement,

(2) cone thrust, and

(3) sleeve friction.

The actuator provides a constant velocity through the penetration, this could be verified from voltage variation vs. time relationship which is straight line. The penetration velocity is calculated by knowing the total time of voltage variation (calculated from the chart recorder) and the stroke of the actuator. With suitable calibration, the displacement of the penetrometer is calculated for each time division on chart, and for different penetration velocity. Thus, the recorded time vs. cone thrust and sleeve friction relationships is directly convertable to depth vs. cone thrust and sleeve friction profiles.

3.3 Surface Roughness

Penetrometer roughness is an important factor which influences penetration resistance. The determination of the roughness of the penetrometer material, therefore, must be made carefully. Roughness is always expressed as a ratio of the angle of friction between the penetrometer material and the soil (δ) to the soil friction angle (ϕ); i.e., relative roughness = δ/ϕ. Conventionally, the value of δ is determined by conducting direct shear tests using plates of the same material as that of the penetrometer. This value of δ is assumed to be the friction between the penetrometer and the soil.

In this investigation, the material roughness was quantitatively measured to ensure that any difference in the roughness between the plate used in the direct shear tests and that of the penetrometer cone is properly accounted for.

A quantitative evaluation of the surface roughness for the three types of penetrometer tips materials was made by using Taylor-Hobson No. 4 Talysurf and Rectilinear recorder. The equipment is shown in Fig. 25. The roughness is expressed (CSA B95, 1962) in terms of center line average (CLA) in microns over a cut-off length of 0.254 mm. The measured roughness values are presented in Table 4 for plates 6 X 6 cm which were used to determine the angle. Similarly the CLA values for the cones of different apex angles were determined. The results show a difference between the CLA values of the plates and the CLA values of the cones. A correction factor for the penetrometer relative roughness was made in the calculations and shown in Table 4. The roughness profiles obtained from the Talysurf recorder for stainless steel, polished aluminum and sanded aluminum are shown in Fig. 26.

3.4 Target Construction

3.4.1 Silca-70 Sand

Penetration tests on Silica-70 Sand were conducted in a wooden box 68.5 cm (2.25 ft.) wide, 91.5 cm (3 ft.) long and 91.5 cm (3 ft.) deep. The front side of the box is made up of three 30.5 cm (1 ft.) high removable sections. Water was not allowed to drain through the box (for saturated samples) by using plastic sheets to cover the sides

TABLE 4

CORRECTION FACTOR FOR δ FROM THE RESULTS OF TALYSURF RECORDER

Material / Tested Shape	Stainless Steel		Polished Aluminum		Sanded Aluminum	
	CLA Value	Correction for δ	CLA Value	Correction for δ	CLA Value	Correction for δ
Plate 6 cm X 6 cm	20		30		50	
Cone $\alpha = 15^o$	22.5	1.125	37.5	1.25	52.5	1.050
Cone $\alpha = 30^o$	22.5	1.125	32.5	1.0833	55	1.10
Cone $\alpha = 90^o$	22.5	1.125	40	1.33	60	1.20

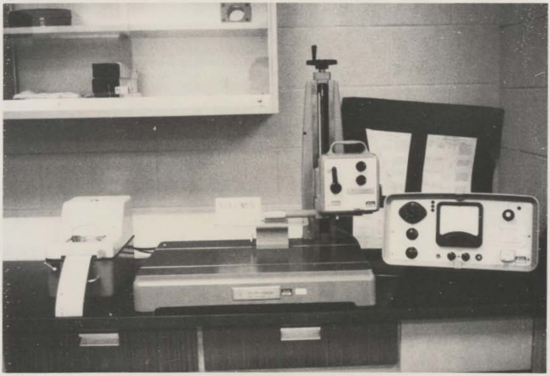

FIG. 25 PHOTOGRAPH SHOWING TALYSURF ROUGHNESS RECORDER

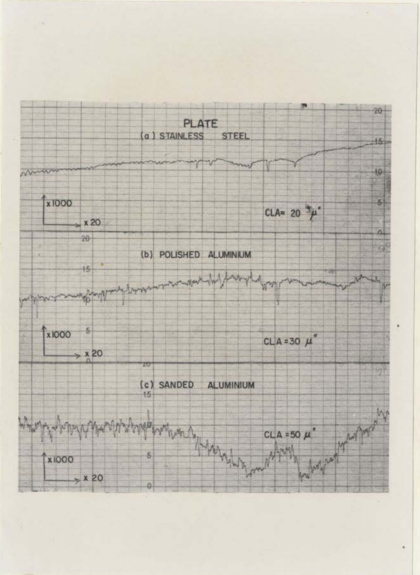

FIG. 26a RESULTS OF CLA ROUGHNESS MEASUREMENTS FOR PLATES 6 X 6 CM

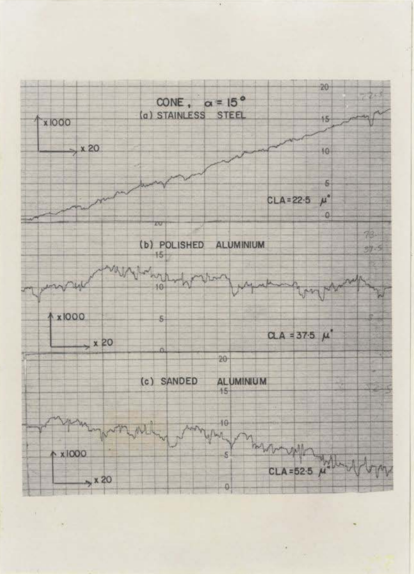

FIG. 26b RESULTS OF CLA ROUGHNESS MEASUREMENTS FOR CONES OF $\alpha = 15^{\circ}$

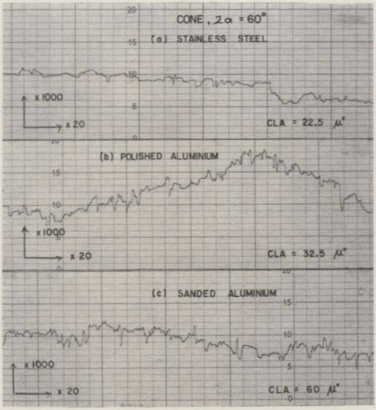

FIG. 26c RESULTS OF CLA ROUGHNESS MEASUREMENTS FOR CONES OF $\alpha = 30^\circ$

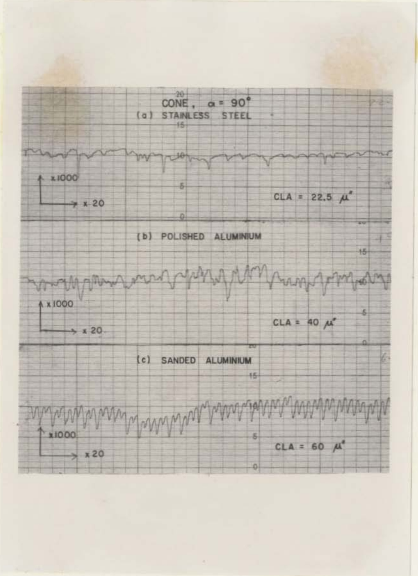

FIG. 26d RESULTS OF CLA ROUGHNESS MEASUREMENTS FOR CONES OF $\alpha = 90^{\circ}$

and the bottom of the box.

Silica-70 Sand compacted to different but uniform densities which were reproducible from test to test were used. At present there are many techniques available for preparing the sample. In this investigation, the raining technique was used for loose samples and the vibration technique was used for dense samples. The dense targets were constructed by placing sand in 15 cm (6 in.) layers and then compacting to the required density using a vibrator. Required densities were predetermined. Each layer consisting of a calculated weight of sand was placed and then vibrated to the determined volume to obtain the predetermined density. For construction of loose targets, the screen or raining technique was used. The dry material was poured through sieve held at a fixed height above the already formed target surface. As the soil deposit builds up, the screen is elevated to maintain a constant height of drop. This height was determined so that the measured amount of sand fills the volume to obtain the predetermined density.

Three different densities were chosen as follows:

(1) Dense sand = 1688 Kg/m^3

(2) Medium dense sand = 1530 Kg/m^3

(3) Loose sand = 1470 Kg/m^3

For the saturated target, the same procedure was adopted as previously explained. After the target was constructed, water was added at a slow rate through a hose and sprinkler placed at the top of the sample. There was some difficulty in preparing saturated targets in loose sand. As soon as water was added to the loose dry sand, some settlement occured to the surface of the target which increased its density above that estimated for dry conditions. The three different densities obtained for saturated sand were:

(1) dense sand = 1688 kg/m^3

(2) medium dense sand = 1543 kg/m^3

(3) loose sand = 1516 kg/m^3

3.4.2 Modelling Clay

Penetration tests on modelling clay were conducted in a steel test box of 1.0 m wide, 1.0 m long and 1.0 m deep. The front side of this box is also made up of three removable sections of 0.33 m height to simplify preparation of the samples in layers.

The material selected for testing was thoroughly dried and pulverized. It was then placed in a large concrete mixer (Fig. 27) and mixed with a metered amount of water to obtain a specific moisture content. The material was recycled until the mixture was hemogeneous and was then removed from the mixer. The moisture content was predetermined from Standard Proctor test, results of which are presented in a subsequent section. The soil mixture was placed in the steel testing box in a 15 cm layers and compacted with modified (AASHTO) hand hammer to the required density (predetermined from Standard Proctor test). The density was controlled by the number of blows per layer of soil. During target construction samples were collected at random locations for moisture content determinations. After construction of the target up to approximately mid-height, in-situ vane shear tests were performed. The vane shear tests for the upper half were performed

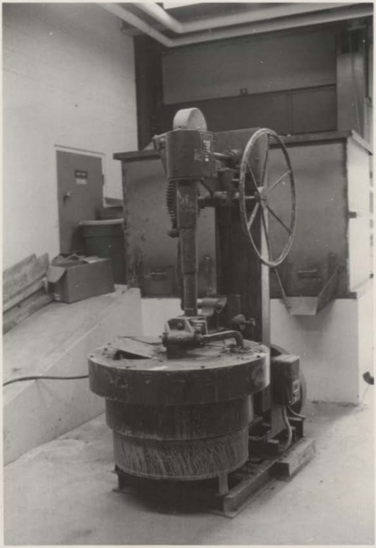

FIG. 27 PHOTOGRAPH SHOWING EQUIPMENT FOR MIXING CLAY SAMPLE

after penetration tests. Three different densities were used as shown in Table 5.

3.5 Target Properties

3.5.1 Index Properties

Tests were conducted on the sand and the clay targets to determine the physical properties of the soil. These included specific gravity, grain size analysis, Atterberg limits (Clay) and maximum and minimum void ratios (sand). The tests were performed immediately after preparation of the target.

The gradation curve for sand is given in Fig. 28 and some of the salient properties are given in Table 6. The soil is classified as medium to fine sand.

The grain size distribution of the modelling clay is shown in Fig. 29. According to M.I.T. system of soil classification it is classified as clayey silt with the properties as given in Table 7. Results of the Standard Proctor compaction test for this clay is shown in Fig. 30.

3.5.2 Shear Tests

The strength properties of silca-70 sand were determined using the triaxial compression tests and the direct shear tests. For modelling clay, the strength properties were determined using the triaxial compression tests and the vane shear tests.

Specimens of silca-70 sand were prepared in a triaxial cell to the desired uniform density, for the specimen size and shape (Lambe

TABLE 5

DIFFERENT DENSITIES OF THE MODELLING CLAY

Type of Clay	Water Content w%	Dry Density kg/m^3
Stiff Clay	25	1600
Medium Stiff Clay	30.4	1449
Soft Clay	40	1240

TABLE 6

CLASSIFICATION DATA FOR SILICA-70 SAND

Classification	Experimental Result
Mean Diameter (D_{50})	= 0.115 mm
Coefficient of Uniformity	= 1.95
Relative Density of Grains	= 2.608
Maximum Void Ratio	= 0.95
Minimum Void Ratio	= 0.45

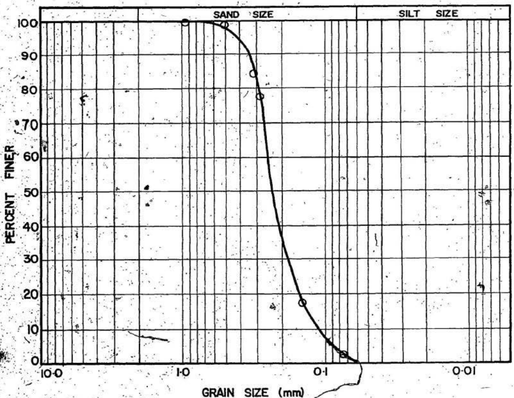

FIG. 28 GRAIN SIZE DISTRIBUTION FOR SILICA-70 SAND

TABLE 7

PROPERTIES OF THE MODELLING CLAY

Property	Experimental Result
Liquid Limit (L.L.)	37%
Plastic Limit (P.L.)	21%
Plasticity Index (P.I.)	16
Relative Density	2.83

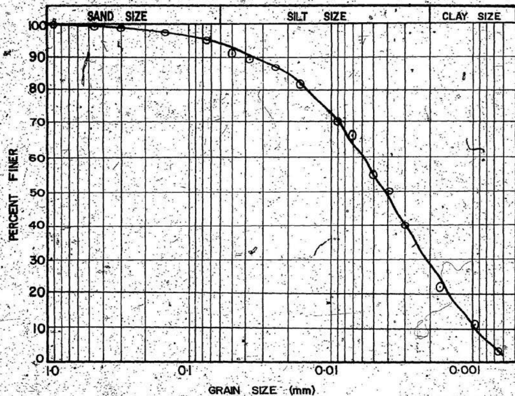

FIG. 29 GRAIN SIZE DISTRIBUTION FOR MODELLING CLAY

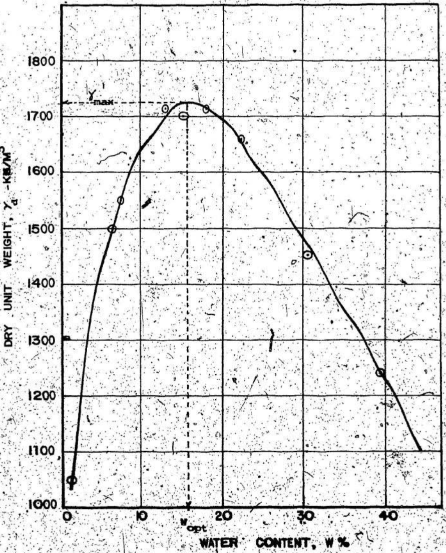

FIG. 38 STANDARD PROCTOR COMPACTION TEST FOR MODELLING CLAY

1951). Confining pressures of 34.45, 68.9, 103.35 and 295.6 kN/m^2 were used. Measurements were taken of the axial load with a calibrated proving ring and of axial deformation with a strain guage dial.

A total of 16 drained triaxial tests were conducted for sand at densities corresponding to those used in the penetration test. The results of these tests are plotted in Figures 31 and 32 which show the values of principle stress ratio (σ_1/σ_3) versus axial strain for the condition investigated. The peak values of soil friction angles were calculated from the results of these tests using the equation:

$$= \sin^{-1}\left[\frac{(\sigma_1/\sigma_3)_f - 1}{(\sigma_1/\sigma_3)_f + 1}\right] \qquad [31]$$

Table 8 shows a summary of triaxial peak friction angle. In Fig. 33 the peak friction angle is plotted against void ratio (e) for various confining pressures. From Fig. 31 and Fig. 32 it may be seen that peak principle stress ratio (σ_1/σ_3) decreases with increasing confining pressure for a given void ratio. This explains why the failure envelope shown in Fig. 34 for the Mohr's circle is slightly curved.

For the modelling clay, 12 tests were performed using 12 undisturbed samples which were collected after preparing the targets for the penetration tests. The confining pressures used are 78.9, 157.8, 236.7 and 276.2 kN/m^2. The results of the triaxial test are shown in Figs. 35, 36 and 37 for the three types of soil tested. Cohesion of the soil and the friction angle were obtained from the shear envelope. Table 9 summarizes the results of the triaxial tests. It is seen that the shear strength of the clay decreases with increasing consistency.

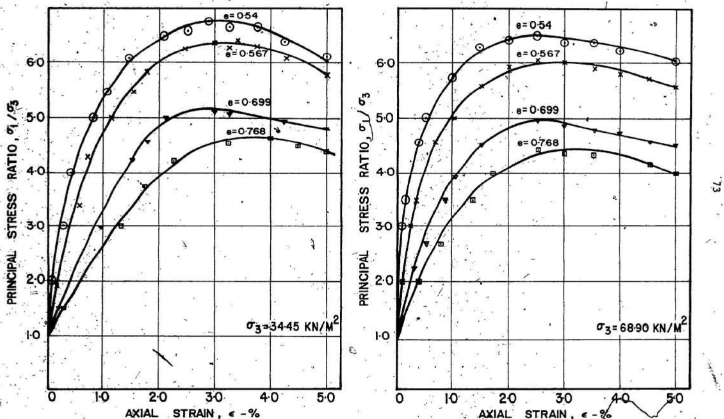

FIG. 31 STRESS-STRAIN RELATIONSHIP FOR SILICA-70 SAND DETERMINED FROM TRIAXIAL TEST

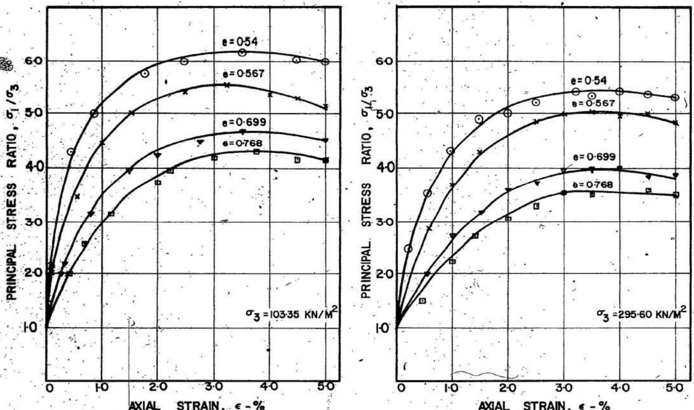

FIG. 32 STRESS-STRAIN RELATIONSHIP FOR SILICA-70 SAND DETERMINED FROM TRIAXIAL TEST

TABLE 8

SUMMARY OF TRIAXIAL PEAK FRICTION ANGLE OF SILICA-70 SAND

Confining Pressure σ_3 (kN/m^2)	Initial Density γ (Kg/m^3)	Density Index I_D	Peak Friction angle (ϕ^0)
34.45	1688	0.8	47.8
	1659	0.766	46.8
	1530	0.50	42.5
[5 psi]	1470	0.365	40.1
68.9	1688	0.8	47.0
	1659	0.766	46.1
	1530	0.5	41.6
[10 psi]	1470	0.365	39.2
103.35	1688	0.8	46.0
	1659	0.766	44.9
	1530	0.50	40.5
[15 psi]	1470	0.365	38.2
295.6	1688	0.8	43.5
	1659	0.766	42.0
	1530	0.50	37.5
[40 psi]	1470	0.365	35.5

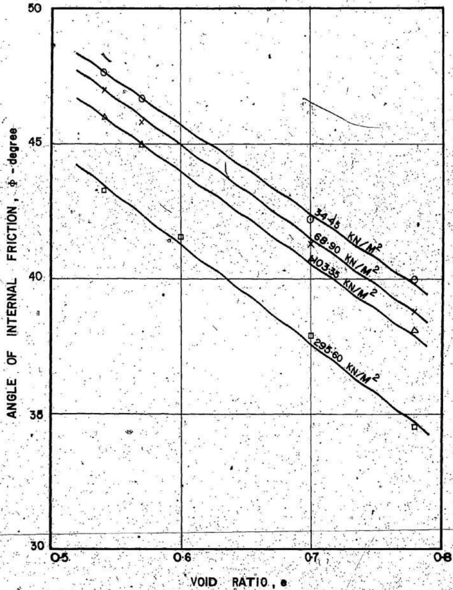

FIG. 33 PEAK FRICTION ANGLE VERSUS VOID RATIO (e) FOR SILICA-70 SAND

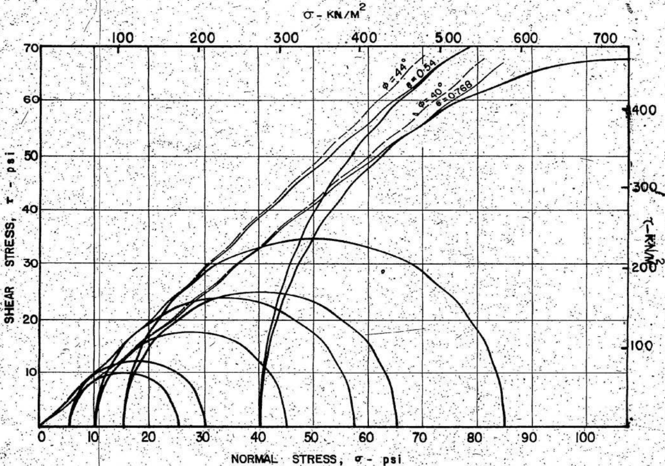

FIG. 34 FAILURE ENVELOPES FOR SILICA-70 SAND

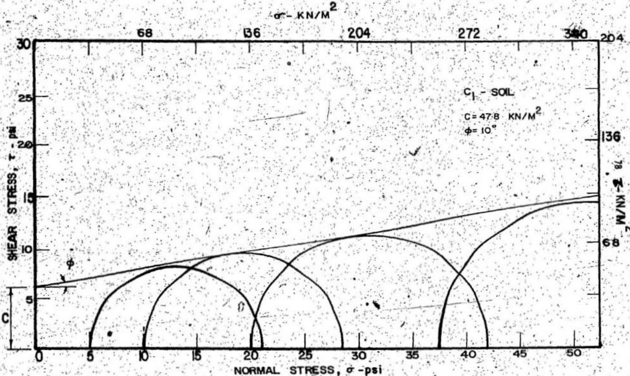

FIG. 35 RESULTS OF TRIAXIAL COMPRESSION TEST FOR THE MODELLING CLAY (STIFF CLAY)

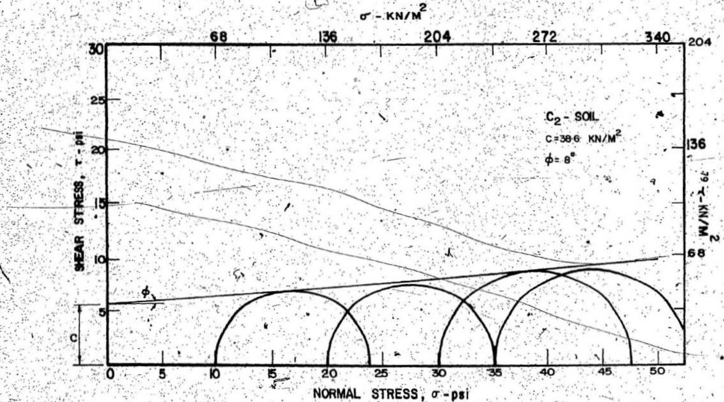

FIG. 36 RESULTS OF TRIAXIAL COMPRESSION TEST FOR THE MODELLING CLAY (MEDIUM STIFF CLAY)

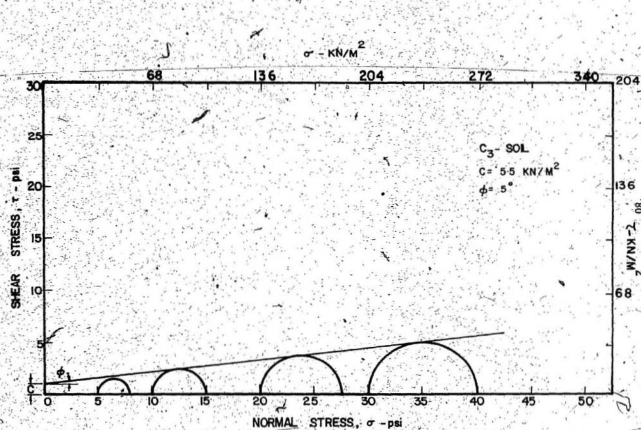

FIG. 37 RESULTS OF TRIAXIAL COMPRESSION TEST FOR THE MODELLING CLAY (SOFT CLAY)

A series of direct shear tests was done on Silica-70 sand to determine the values of the soil friction angle to facilitate a determination of δ/ϕ. The tests were conducted in a constant rate of strain shear box WF25000 of Wykeham-Farrance direct shear apparatus. A horizontal constant rate of strain is placed upon the lower half of the box while the upper half is kept stationary. The resulting shear force is measured from the upper half of the box, using a proving ring. A photograph of the apparatus is shown in Fig. 38. Results of soil to soil direct shear tests are shown in Table 10 and presented in Fig. 39. The values of the angle of friction obtained from direct shear tests is compared with the values obtained from triaxial tests, and shown in Fig. 40.

The strength properties of the modelling clay can be determined from vane shear test as well as from triaxial compression test. Samples at different locations were collected during and after preparing the clay target and vane shear tests were conducted on these samples. The results of these tests are presented in Table 11.

Values of shearing strength determined from vane shear tests are in good agreement with the values obtained from triaxial compression tests.

3.5.3 Penetrometer to Soil Friction Angle

To determine the friction angle between the penetrometer material and soil, and to establish a basis for the variation of δ/ϕ with void ratio, tests were conducted in the WF 25000 shear box in which the upper half of the box was filled with Silca-70 sand at a desired

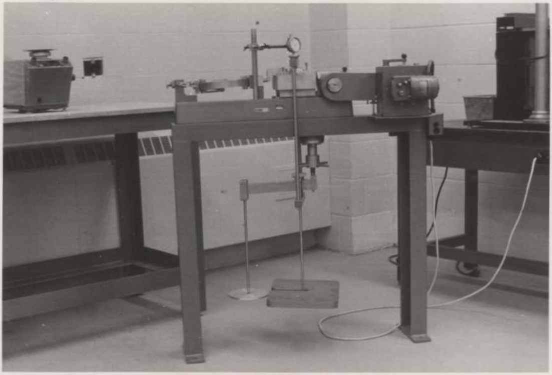

FIG. 38 SHEAR BOX APPARATUS

TABLE 9

RESULTS OF TRIAXIAL TEST FOR MODELLING CLAY (DRAINED)

Dry Density (Kg/m^3)	Water Content (w%)	Cohesion $C - kN/m^2$	Friction Angle ϕ-degree
1600	25	47.8	10
1449	30.4	38.6	8
1240	40	5.5	5

TABLE 10

RESULTS OF DIRECT SHEAR TEST

Normal Stress on Failure Plane (kN/m^2)	Initial Density γ (Kg/m^3)	Density Index I_D	Angle of Internal Friction ϕ-degree
163.4	1688	0.8	45.8
	1539	0.5	42.8
	1467	0.365	41.3
326.8	1688	0.8	43.8
	1539	0.5	41.0
	1467	0.365	39.0
653.6	1688	0.8	41.2
	1539	0.5	38.2
	1467	0.365	36.6

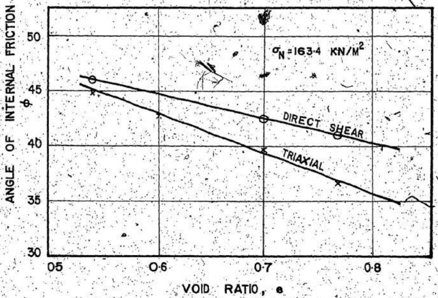

FIG. 40 COMPARISON OF TRIAXIAL AND DIRECT SHEAR TESTS

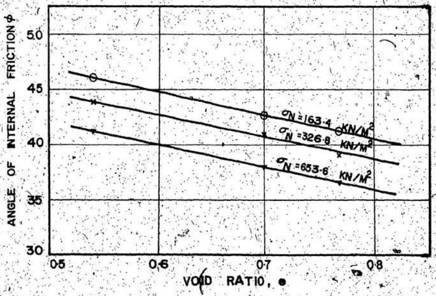

FIG. 39 SOIL TO SOIL FRICTION ANGLES OF SILICA-70 SAND FROM DIRECT SHEAR TEST

TABLE 11

RESULTS OF VANE SHEAR TEST FOR MODELLING CLAY

Dry Density (Kg/m^3)	Water Content (w%)	Bulk Density (Kg/m^3)	Cohesion $C - kN/m^2$
1600	25	2010	47.1
1449	30.4	1889	38.00
1240	40	1735	5.35

initial density, and the lower half of the shear box was replaced by a solid plate of penetrometer material. The three different materials tested were:

(1) Stainless Steel

(2) Polished Aluminum, and

(3) Sanded Aluminum

Three densities of soil were used:

(1) dense dry sand, $= 1688\ kN/m^3$

(2) medium dense sand, $= 1530\ kN/m^3$

(3) loose dry sand, $= 1470\ kN/m^3$

A total of 9 tests were conducted using normal stresses of 163.4, 326.8 and 653.6 kN/m^2. The results of the roughness values (δ/ϕ) are summarized in Table 12.

The values of direct shear test must be corrected for the cone shapes. The correction factor can be obtained from the results of the Talysurf on both plates and cone shapes as shown in Table 4. To simplify the calculation average correction factors of 1.125, 1.2 and 1.166 are suggested for stainless steel, polished aluminum and sanded aluminum respectively based on the values given in Table 4.

The corrected values of relative roughness (δ/ϕ) can be summarized as:

(1) Stainless Steel $\delta/\phi = 0.5$

(2) Polished Aluminum $\delta/\phi = 0.6$

(3) Sanded Aluminum $\delta/\phi = 0.75$

TABLE 12

RESULTS OF TESTS FOR PENETROMETER ROUGHNESS

Relative Density I_D	Soil To Soil Friction Angle (ϕ)	Stainless Steel To Soil Friction		Polished Aluminum To Soil Friction		Sanded Aluminum To Soil Friction	
		δ	δ/ϕ	δ	δ/ϕ	δ	δ/ϕ
0.8	43.5°	19°	0.437	22.2	0.51	27.8°	0.639
0.5	41.0°	18.6°	0.45	20.8	0.50	26	0.634
0.365	39.0°	17.0°	0.435	19.2	0.49	25.2	0.64
	δ/ϕ average	0.44		0.50		0.64	

3.6 Layered Soil

Samples were prepared in cylindrical steel moulds of 45.0 cm diameter and 90.0 cm height. layers of silica-70 sand and modelling clay of different strength were used to obtain four types of layered soil. Each type is described below:

A) Type I

A 16.8 cm layer of stiff clay underlain by a layer of dense sand (height = 16 cm) and finally a bottom layer of stiff clay of 43.5 cm height.

B) Type II

A top layer of loose sand followed by an intermediate layer of sand-clay mixture (50% sand and 50% clay) and finally a bottom layer of stiff clay. The heights of the layers were 13, 13 and 41.5 cm respectively.

C) Type III

A top layer of soft clay overlying a layer of stiff clay and at the bottom a layer of soft clay (d_1 = 13 cm, d_2 = 18 cm, d_3 = 41.5 cm).

D) Type IV

A layer of soft clay on top with a layer of medium dense sand below and finally a layer of soft clay (d_1 = 13 cm, d_2 = 13 cm, d_3 = 41.5 cm).

A summary of the type of soil targets is given in Table 13.

TABLE 13

TYPES OF SOIL TARGETS

Target Symbol	Type of Target	Dry Density (Kg/m^3)	Target Properties
S_1	Dense Dry Sand	1688	$\phi = 44.0^o$, $C = 0$
S_2	Medium Dense Dry Sand	1530	$\phi = 40.0^0$, $C = 0$
S_3	Loose Dry Sand	1470	$\phi = 38.0^o$, $C = 0$
S_4	Wet Sand (Dense)	1688	$\phi = 43.0^o$, $C = 0$
S_5	Wet Sand (Medium)	1543	$\phi = 38.5^o$, $C = 0$
S_6	Wet Sand (Loose)	1516	$\phi = 36.5^o$, $C = 0$
C_1	Stiff Clay	1600	$\phi = 10^o$, $C = 47.8\ kN/m^2$, $w = 25\%$
C_2	Medium Stiff Clay	1449	$\phi = 8^o$, $C = 38.6\ kN/m^2$, $w = 30.4\%$
C_3	Soft Clay	1240	$\phi = 5^o$, $C = 5.5\ kN/m^2$, $w = 40\%$
C_4	Powder Or Dry Clay	1200	$\phi = 20^o$, $C = 9.7\ kN/m^2$, $w = 0.9\%$

CHAPTER IV

TEST RESULTS, ANALYSIS AND DISCUSSION

4.1 General

A series of static penetration tests were performed on both silica-70 sand (cohesionless soil) and modelling clay (cohesive soil). The properties of these soils were presented in the preceeding chapter. Comparison was made between the experimental results of penetration tests with the different theoretical methods available in the literature. Three of the theoretical methods which account explicitly for the factors affecting penetration resistance were chosen as follows:

1. Meyerhof (1961a) provided solutions for both cohesive and cohesionless soils for limiting conditions of base roughness and for both deep and shallow foundations.

2. Nowatzki and Karafiath (1972, 1978) employed numerical technique for analysis of the influence of apex angle on the penetration resistance of cohesionless-soil. They also studied the influence of base roughness, penetrometer size, soil friction angle and relative depth of penetration.

3. Durgunoglu and Mitchell (1973, 1975) suggested a failure mechanism based on the results of laboratory model tests. They also provided a theoretical relationship for the ultimate base resistance which account explicitly for base semi-apex angle (α), base roughness (δ/ϕ) and relative depth of penetration (D/B) for both cohesionless and cohesive soils.

Results are presented in this chapter in the following format:

a) Tests on sand: comparison of the three theoretical methods with the experimental values, for dry sand to select the most appropriate theoretical approach.

b) Parameters Influencing Penetration Resistance: evaluation of the effect of various parameters on the penetration resistance using the theory chosen and the experimental results, for sand.

c) Tests on Saturated Sand: experiments with saturated sand to study the effect of various parameters on penetration resistance.

d) Tests on Clay: comparison of the experimental results and the theoretical values for modelling clay to choose the most appropriate theory.

e) Parameters Influencing Penetration Resistance in Clay: evaluation of the effects of the different physical parameters in modelling clay.

f) Effect of Velocity of Penetration on Cohesive Soils: studies on strain-rate effects on penetration resistance of cohesive soils.

g) Layered Soils: tests on different types of layered soils.

Typical raw data for some of the penetration tests conducted in this investigation are shown in Figs. 41, 42 and 43 for cohesive, cohesionless and layered soils respectively. Similar penetration records were obtained from the chart recorder for each test. Fig. 41a is the record of the velocity of penetration and was obtained in each test to check the linearity of the velocity with time. Fig. 41b and 41c are the records of sleeve and cone resistance respectively. Cone resistance at any required depth can be obtained by using the calibration chart for the cone load cell in combination with the velocity record and cone resistance output. Unit cone resistance at any depth was then

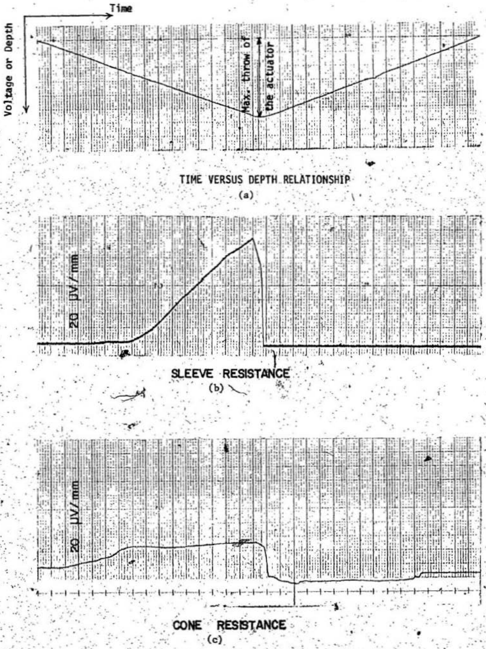

FIG. 41 TYPICAL OUTPUT FROM THE PENETRATION TEST FOR COHESIVE SOIL

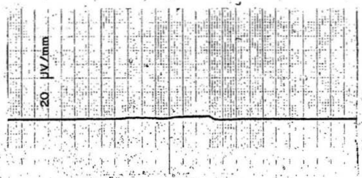

SLEEVE RESISTANCE
(a)

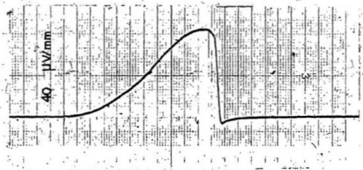

CONE RESISTANCE
(b)

FIG. 42 TYPICAL OUTPUT FROM THE PENETRATION TEST FOR COHESIONLESS SOILS

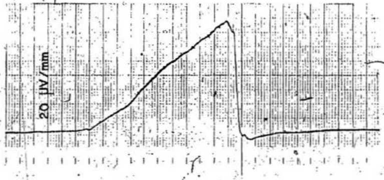

(a)

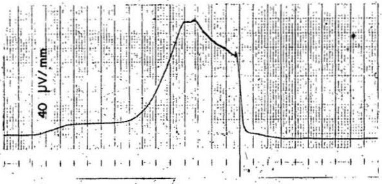

(b)

FIG. 43 TYPICAL OUTPUT FROM THE PENETRATION TEST FOR LAYERED SOIL calculated as the resistance per unit cross sectional area of the penetrometer. Sleeve resistance was obtained in a way similar to the cone resistance. Unit sleeve friction was determined by dividing the sleeve force by the effective surface area of the sleeve. The term unit penetration resistance used in this investigation is the sum of both unit cone resistance and unit sleeve resistance.

4.2 Tests on Dry Sand

The objective of this part of the analysis is to compare the laboratory results on dry sand with the three theoretical methods mentioned previously. The results are presented in Fig. 39 through Fig. 46 in the form of unit penetration resistance q_f (kN/m^2) versus penetration depth D (cm). Theoretical values using the peak friction angle from triaxial tests are also presented on the same figures. Different tests were conducted with different types of cones as well as different soil types. Fig. 44 is for the penetrometer with a cone semi-apex angle $\alpha = 30^\circ$, relative roughness $\delta/\phi = 0.75$, diameter B = 35.6 mm and soil density index $I_D = 0.8$, while Figure 45 is for the Memorial University penetrometer of 76.2 mm diameter. Figs. 46, 47 and 48 are for a penetrometer with a value for $\alpha = 30^\circ$, $\delta/\phi = 0.5$ and B = 35.6 mm, for three density indicies of 0.8, 0.5 and 0.365 respectively. Finally Figs. 49, 50 and 51 are for a penetrometer with a semi-apex angle of $\alpha = 15^\circ$, $\delta/\phi = 0.75$ and B = 35.6 mm for the same three density indicies.

Analyses of the results of the tests in sand lead to the following conclusions:

(1) Meyerhof's values are greater than the experimental values

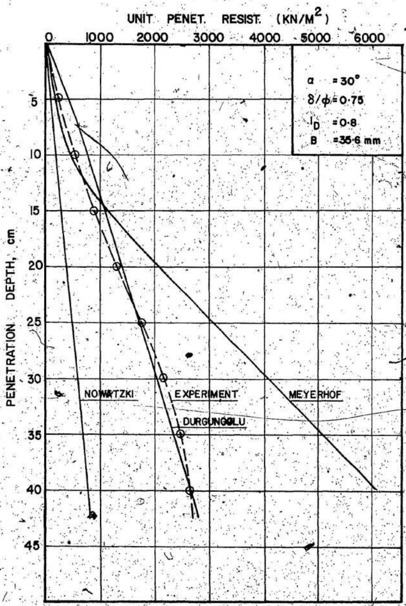

FIG. 46 COMPARISON OF MEASURED AND PREDICTED STATIC PENETRATION CURVES FOR SILICA-70 SAND (B =35.6 mm)

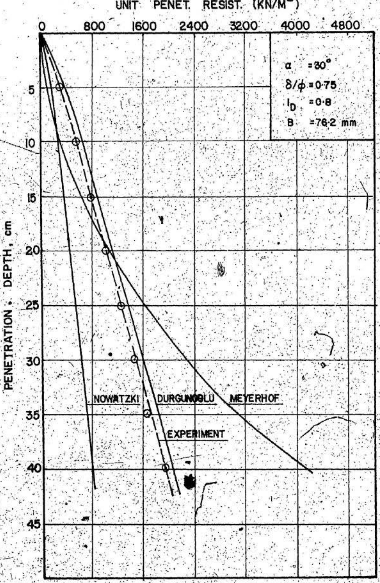

FIG. 45 COMPARISON OF MEASURED AND PREDICTED STATIC PENETRATION CURVES FOR SILICA-70 SAND (B = 76.2 mm)

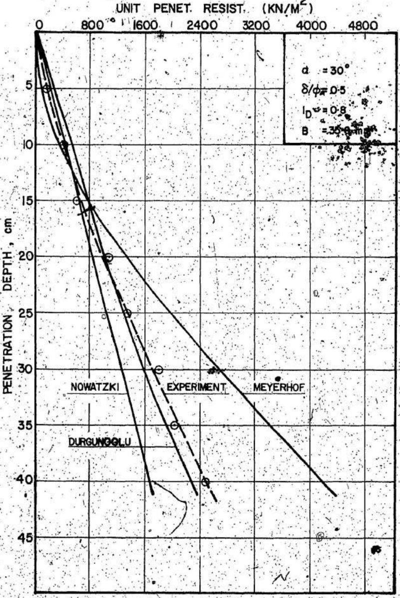

FIG. 46 COMPARISON OF MEASURED AND PREDICTED STATIC PENETRATION CURVES FOR SILICA-70 SAND ((DENSE SAND)

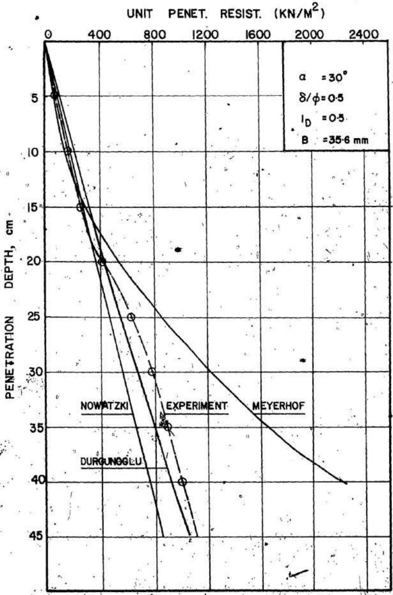

FIG. 47 COMPARISON OF MEASURED AND PREDICTED STATIC PENETRATION CURVES FOR SILICA-70 SAND (MEDIUM DENSE)

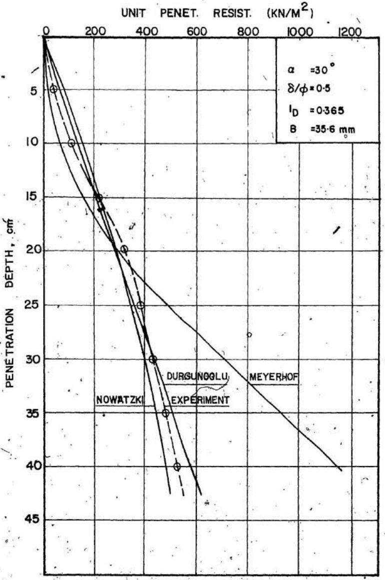

FIG. 48 COMPARISON OF MEASURED AND PREDICTED STATIC PENETRATION CURVES FOR SILICA-70 SAND (LOOSE SAND)

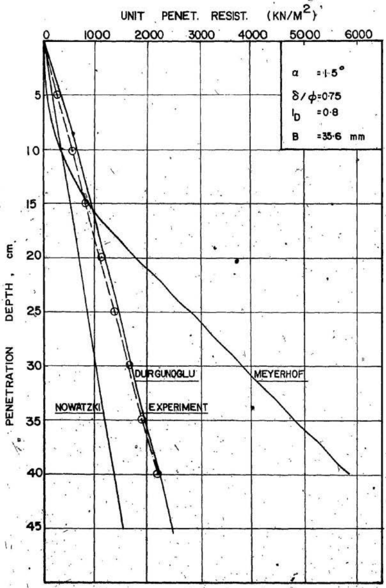

FIG. 49 COMPARISON OF MEASURED AND PREDICTED STATIC PENETRATION CURVES FOR SILICA-70 SAND (DENSE SAND)

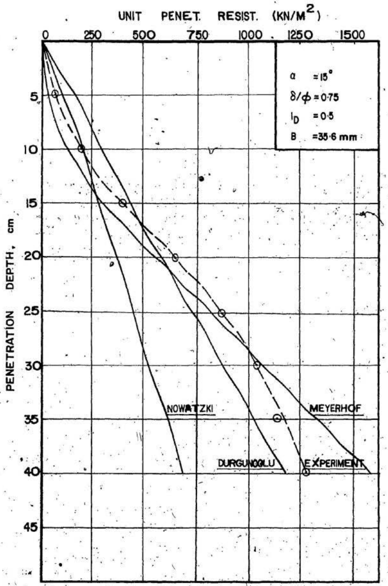

FIG. 50 COMPARISON OF MEASURED AND PREDICTED STATIC PENETRATION CURVES FOR SILICA-70 SAND (MEDIUM DENSE)

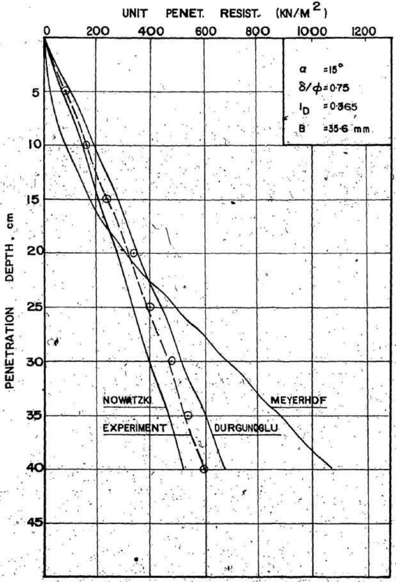

FIG. 51 COMPARISON OF MEASURED AND PREDICTED STATIC PENETRATION CURVES FOR SILICA-70 SAND (LOOSE SAND)

for D/B > 4 and less than the experimental values for relative depth values less than 4. Meyerhof has proposed two different theories for shallow and deep foundations and hence two different sets of bearing capacity factors. It is seen that for shallow foundations, using Meyerhof theory will give conservative values of penetration resistance and for deep foundations, the theory overestimates the resistance values. These high values are a result of the failure mechanism assumed by Meyerhof for deep foundation which involves a greater shear surface. The slip lines revert back to the shaft with a larger size of the affected soil mass. A comparison of the three theoretical methods chosen here also shows that in the shallow foundation zone, all the theories predict almost same values, while in the deep foundation zone, there is significant difference.

(2) Values of Nowatzki and Karafiath are always lower than the experimental values. The difference increases with increasing depth of penetration. It is seen that this theory under estimates the penetration resistance compared to the experimental values, and the error is pronounced in the deep foundation situation. Comparing the three theoretical methods, this theory is the most conservative of all. This is because Nowatzki and Karafiath assumed the failure mechanism shown in Fig. 17 where the slip lines stop at the base of the penetrometer. They disregarded the effect of shear failure above the level of the base of the cone and expressed the weight of the soil above the base level as an effective surcharge.

(3) Values obtained from the theory of Durgunoglu and Mitchell are in close agreement with the experimental values. This is true for all the figures presented irrespective of the soil type and penetro-

meter variables. These theoretical values are intermediate values between the other two theoretical methods. This can be explained by examining the failure mechanism shown in Fig. 18 which is an intermediate case between Meyerhof's shape and that of Nowatzki and Karafiath. The theory of Durgunoglu and Mitchell was therefore chosen for further comparisons because of its good correlation with the present series of experiments.

4.3 Parameters Influencing Penetration Resistance

In this section the influence of soil friction angle, penetrometer base apex angle, penetrometer size and roughness, relative depth of penetration and velocity of penetration are examined. At the same time a comparison will be made between the experimental values and the theoretical values based on the theory of Durgunoglu and Mitchell for the above variables.

4.3.1 Angle of Soil Shear Resistance

Density index is an indirect indicator of the angle of internal friction of cohesionless soils. The higher the density index the higher the angle of internal friction. To study the influence of the angle of internal friction on static penetration resistance, targets of silica-70 sand with different density indicies were prepared. Three different density indicies and consequently three soil friction angles were used to represent dense sand, medium dense sand and loose sand, these are S_1, S_2 and S_3 soils.

The influence of the angle of internal friction on penetration resistance is presented in Figs. 52 and 53 in the form of unit penetration resistance q_f (kN/m^2) versus penetration depth (cm) for

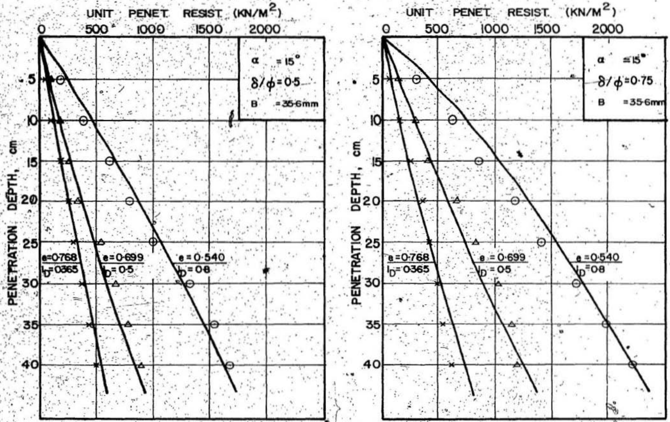

(Firm lines are theoretical graphs- Points are experimental data)

FIG. 52 INFLUENCE OF SOIL DENSITY ON STATIC PENETRATION RESISTANCE OF SILICA-70 SAND

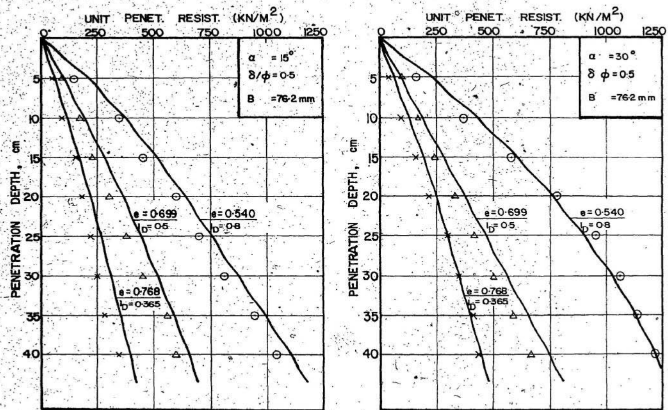

(Firm lines are theoretical graphs- Points are experimental data)

FIG. 53 INFLUENCE OF SOIL DENSITY ON STATIC PENETRATION RESISTANCE OF SILICA-70 SAND different soil density indicies. Theoretical values based on the theory of Durgunoglu and Mitchell are also presented on the same figures.

It is seen from both theoretical and experimental results in these figures that the penetration resistance increases significantly with increasing soil friction angle. The variation of the static penetration resistance with the value of density index for silica-70 sand is shown in Figs. 54, 55 and 56 for the two sizes of the penetrometer. Three different ratios of relative depths (D/B) 1, 5 and 10 are presented for the 35.6 mm penetrometer and two ratios 1 and 5 are presented for the 76.2 mm penetrometer.

Analysis of the data in these figures shows that penetration resistance is very sensitive to soil density, i.e., to soil friction angle. It increases rapidly with increasing soil density and the rate of increasing is higher for higher densities. It was also noticed that the variation of penetration resistance with relative depth is a linear variation, the slope of these lines decrease with decreasing relative depth. The type of variation is the same for the two sizes of the penetrometer.

4.3.2 Cone Apex Angle

Another factor which affects the penetration resistance significantly is the cone semi-apex angle α. For the 76.2 mm penetrometer, with a roughness of 0.5 and soil density index 0.8, Fig. 57a shows the relation between unit penetration resistance and penetration depth. Curves were drawn for cone semi-apex angles of 15^{o}, 30^{o} and 90^{o}. For the 35.6 mm penetrometer with the same variables, similar relationship is shown in Fig. 57b. The figures show that unit penetration resistance

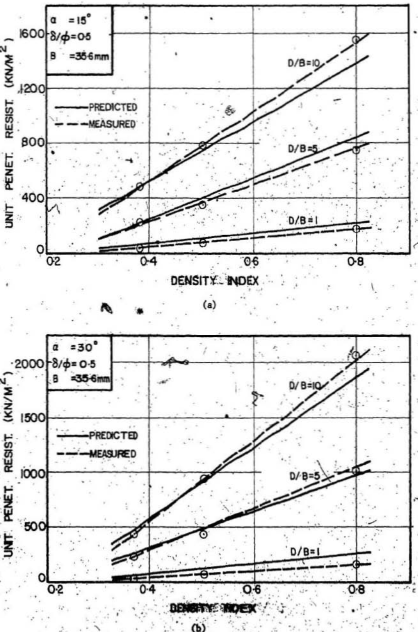

FIG. 54 VARIATION OF UNIT PENETRATION RESISTANCE WITH DENSITY INDEX OF SILICA-70 SAND

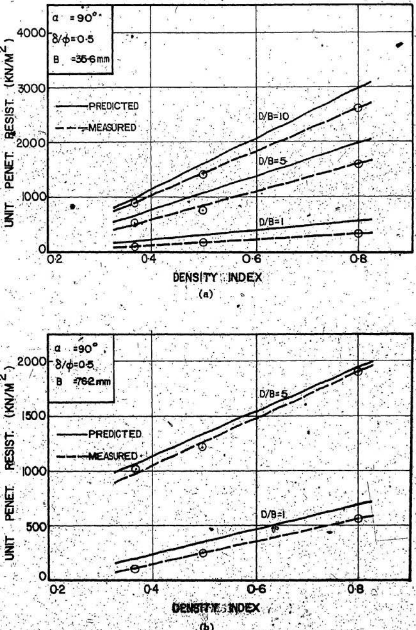

FIG. 55 VARIATION OF UNIT PENETRATION RESISTANCE WITH DENSITY INDEX OF SILICA-70 SAND

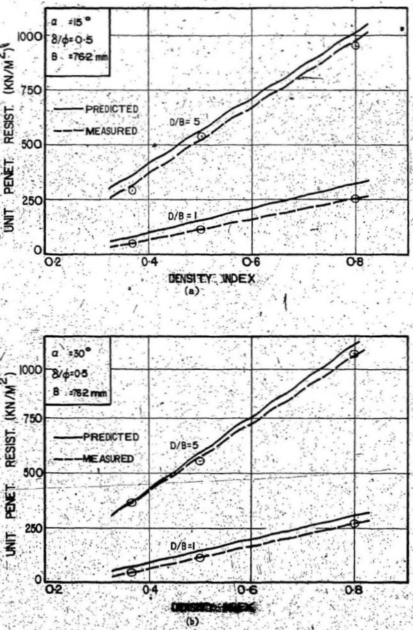

FIG. 56 VARIATION OF UNIT PENETRATION RESISTANCE WITH DENSITY INDEX OF SILICA-70 SAND

increases with increasing cone semi-apex angle in all the tests.

The penetration resistance is shown as a function of the cone semi-apex angle for the 35.6 mm diameter penetrometer in Fig. 58. The penetration resistance was taken at three relative depths, D/B = 1, 5 and 10 for this discussion. Similar curves for the 76.2 mm diameter penetrometer are shown in Fig. 59 at two relative depths D/B = 1 and 5. Theoretical curves were drawn in all cases. It is seen that the correlation between the experimental values and the theory is good.

From Fig. 58 it can be seen that an increase of semi-apex angle from 15° to 30° causes an increase of 34% in penetration resistance at relative depth of 5 and 15% increase at relative depth of 1, while an increase of semi-apex angle from 30° to 90° causes a corresponding increase in penetration resistance of 36% at relative depth 5 and 77% increase at relative depth 1. The effect of a change in the semi-apex angle is more pronounced at greater depths. Further, the rate of increase in penetration resistance is far rapid than in the region of smaller angles. A similar phenomenon is also seen for the 76.2 mm diameter penetrometer (Fig. 59).

4.3.3 Base Roughness

The effect of base roughness on unit penetration resistance was studied using tips of different materials, stainless steel, polished aluminum and sanded aluminum. The materials have different relative roughness of 0.5, 0.6 and 0.75 respectively. Fig. 60a shows the relationship between unitppenetration resistance and penetration depth for the 76.2 mm penetrometer for the three different materials. For

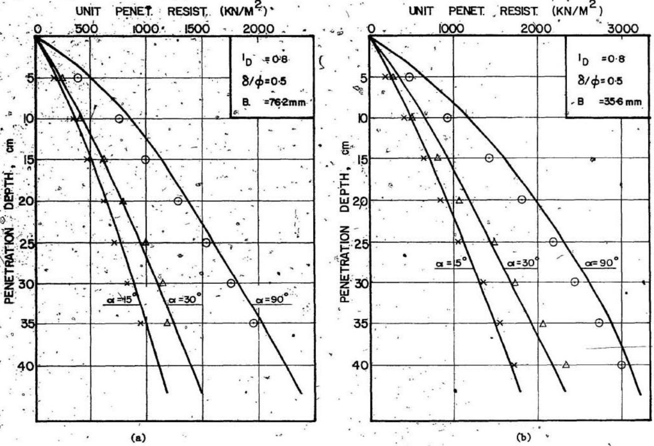

FIG. 57 INFLUENCE OF CONE SEMI-APEX ANGLE ON STATIC PENETRATION RESISTANCE OF SILICA-70 SAND

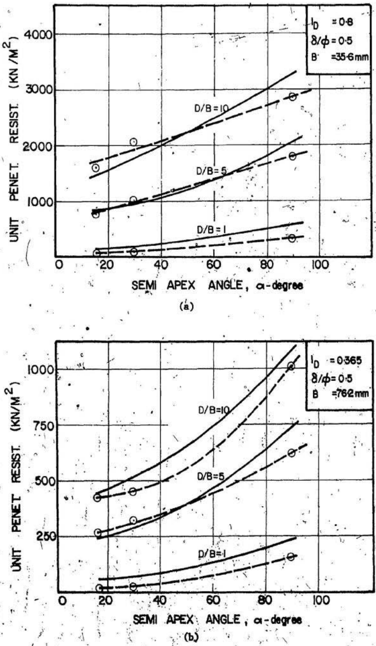

FIG. 58 VARIATION OF UNIT PENETRATION RESISTANCE WITH CONE SEMI-APEX ANGLE (α) FOR SILICA-70 SAND

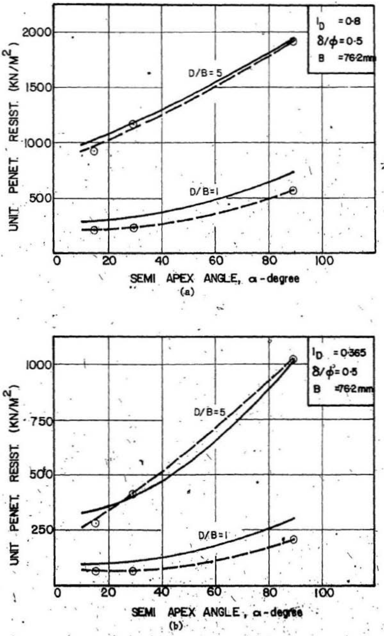

FIG. 59 VARIATION OF UNIT PENETRATION RESISTANCE WITH CONE SEMI-APEX ANGLE (α) FOR SILICA-70 SAND

the 35.6 mm penetrometer the same relation is shown in Fig. 60b. From Fig. 60a, b, it can be seen that there is a significant effect of the base roughness on unit penetration resistance. Penetration resistance increases with increasing roughness at any depth and for any density index value.

The variation of unit penetration resistance as a function of roughness is presented in Figs. 61 and 62 for the two penetrometers. At any relative depth and for both the penetrometers, unit penetration resistance increases with increasing base roughness. Theoretical curves shown in Figs. 61 and 62 are in good agreement with the experimental results.

4.3.4 Penetrometer Size

The influence of penetrometer size on static penetration resistance was studied by conducting penetration tests with two sizes of penetrometer keeping the other parameters constant. Figs. 63 and 64 show the relation between unit penetration resistance and penetration depth for the two types of penetrometer. The theoretical curves are also shown in these figures. It can be seen that the unit penetration resistance decreases with increasing size at any depth and for a given cone semi-apex angle and base roughness. This brings out clearly the effect of the foundation width in the soil bearing capacity and is in conformity with theory.

4.3.5 Rate of Penetration

To check the influence of the rate of penetration on the penetration resistance, tests were conducted using different velocities of penetration of 0.4, 2.0 and 4.0 cm/sec. The results are presented in Fig. 65

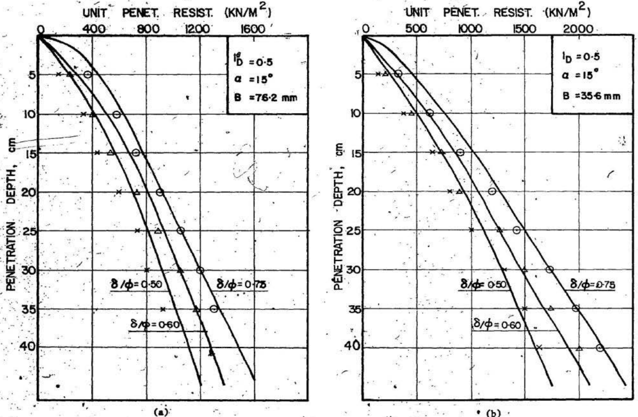

FIG. 60 INFLUENCE OF BASE ROUGHNESS ON STATIC PENETRATION RESISTANCE OF SILICA-70 SAND

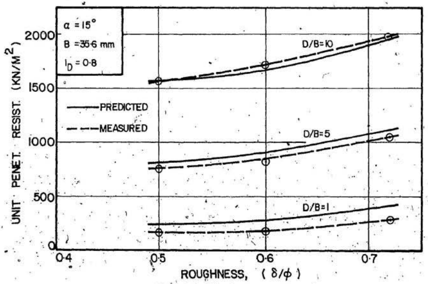

(a)

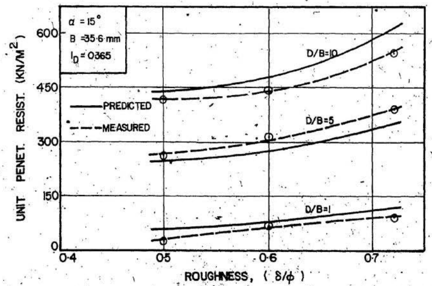

(b)

FIG. 61 VARIATION OF UNIT PENETRATION RESISTANCE WITH BASE ROUGHNESS FOR SILICA-70 SAND

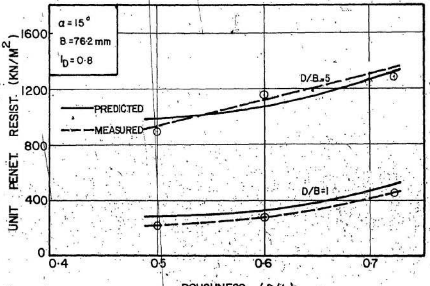

(a)

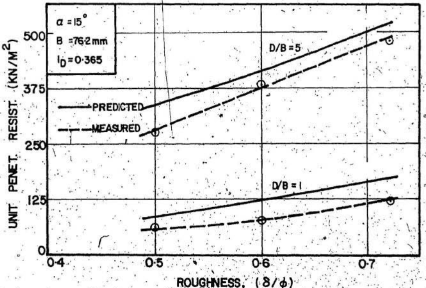

(b)

FIG. 62 VARIATION OF UNIT PENETRATION RESISTANCE WITH BASE ROUGHNESS FOR SILICA-70 SAND

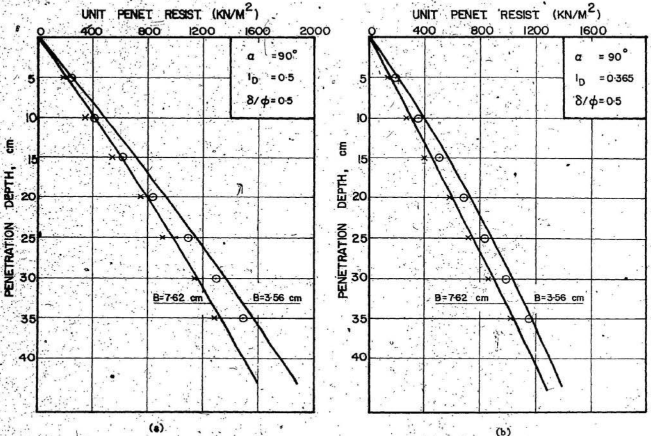

FIG. 63 INFLUENCE OF PENETROMETER SIZE ON STATIC PENETRATION RESISTANCE OF SILICA-70 SAND

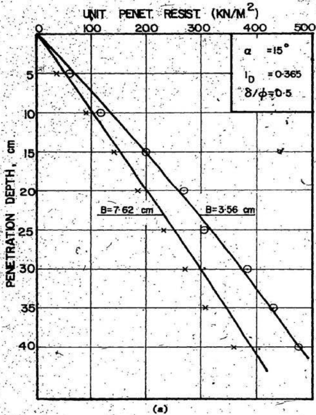

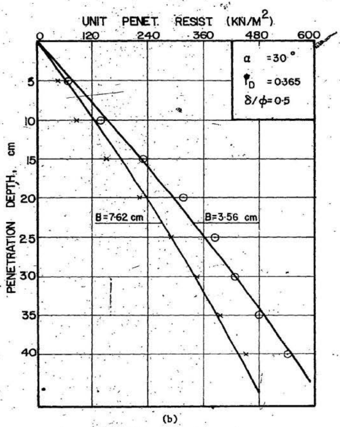

FIG. 64 . INFLUENCE OF PENETROMETER SIZE ON STATIC PENETRATION RESISTANCE OF SILICA-70 SAND

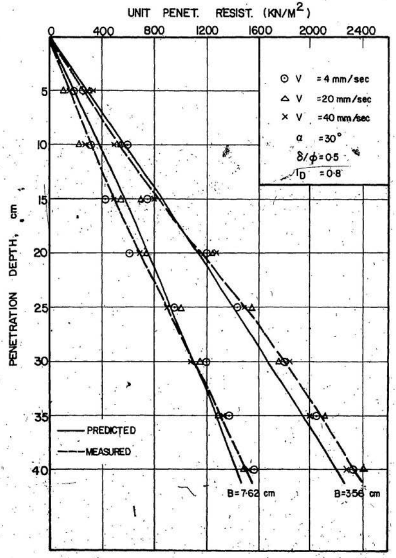

FIG. 65 INFLUENCE OF THE RATE OF PENETRATION ON STATIC PENETRATION RESISTANCE OF SILICA-70 SAND

for the two penetrometers. Figure 65 also shows the curves of static penetration obtained from theory. It is seen that experimental values at different penetration rates are very nearly the same and in close agreement with theory.

4.4 Tests on Saturated Sand

The objective of these tests is to study the influence of the variables already discussed on the unit penetration resistance in saturated sand.

4.4.1 Angle of Soil Shear Resistance

Since the density index of the sand is an indication of its friction angle, three density indicies were chosen as was done for dry sand. These are given in Table 13 (Soils S_4, S_5 and S_6). Fig. 66 shows the relation between penetration resistance and depth at different density indicies for the two penetrometers. The variation of the penetration resistance with density index is shown in Fig. 67a for the 76.2 mm penetrometer and in Fig. 67b for the 35.6 mm penetrometer at different relative depths. It may be seen that at any depth, penetration resistance is very sensitive to any change in soil density index and consequently to soil friction angle. It increases rapidly with increasing soil density index and the rate of increase is much higher than in the dry case. It is also noticed that the variation between D_r and q_f is linear with a smaller slope for lower relative depths.

4.4.2 Cone Apex Angle

The influence of cone apex angle on penetration resistance in saturated sand is illustrated in Fig. 68 where the relation between

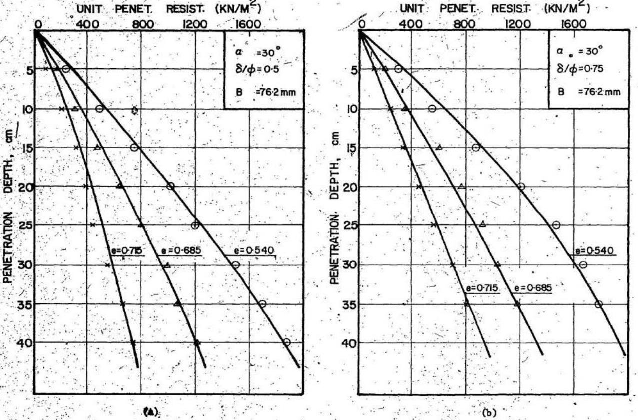

FIG. 66 INFLUENCE OF SOIL DENSITY ON STATIC PENETRATION RESISTANCE OF SATURATED SILICA-70 SAND

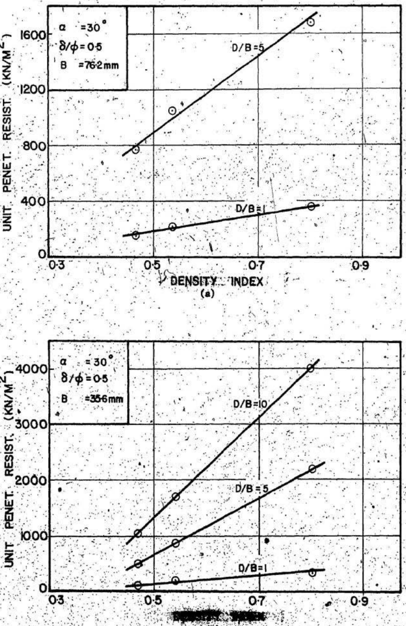

FIG. 67 VARIATION OF UNIT PENETRATION RESISTANCE WITH DENSITY INDEX OF SATURATED SILICA-70 SAND

unit penetration resistance and depth is drawn for different cone semi-apex angles. The influence of the semi-apex angle on the penetration resistance is shown in Fig. 69 for different relative depths. The phenomenon observed in dry sand is confirmed in saturated sand also.

4.4.3 Base Roughness

Fig. 70 shows the unit penetration resistance versus depth drawn for different values of base roughness. The effect of base roughness on the penetration resistance at different relative depths is shown in Fig. 71. The results are similar to the dry case, unit penetration resistance increases with increasing base roughness.

4.4.4 Penetrometer Size

The two penetrometers were used in the saturated soil and experiments were conducted as was done in dry soil. Comparable results are shown in Fig. 72. This again clearly demonstrates that the penetrometer size effects static penetration resistance whether the sand is dry or saturated. At any depth, penetration resistance is greater for the smaller penetrometer. For different cone angle and different soil densities, static penetration resistance with the 35.6 mm penetrometer is always higher than that from the 76.2 mm penetrometer.

4.4.5 Rate of Penetration

Similar to the dry sand, the effect of the rate of penetration on the resistance of saturated sand was also studied. The results are similar to those in dry sand. No significant effect for the rate of penetration on static resistance of saturated sand was noticed as shown in Fig. 73.

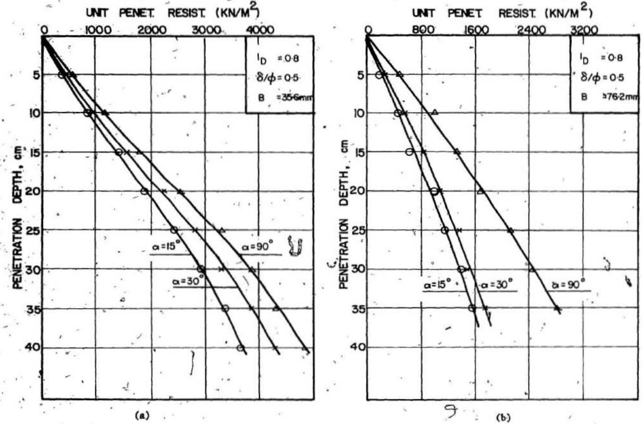

FIG. 68 INFLUENCE OF CONE SEMI-APEX ANGLE ON STATIC PENETRATION RESISTANCE OF SATURATED SILICA-70 SAND

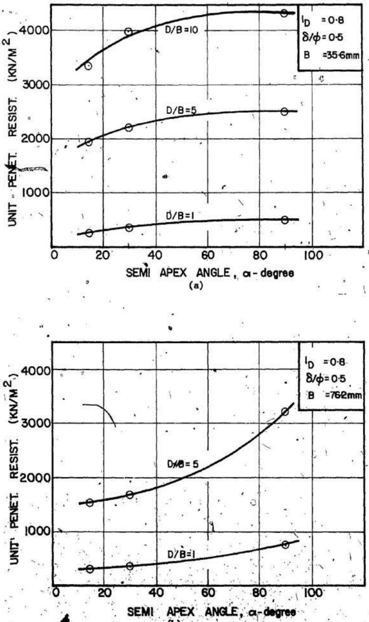

FIG. 69 VARIATION OF UNIT PENETRATION RESISTANCE WITH CONE SEMI-APEX ANGLE FOR SATURATED SILICA-70 SAND

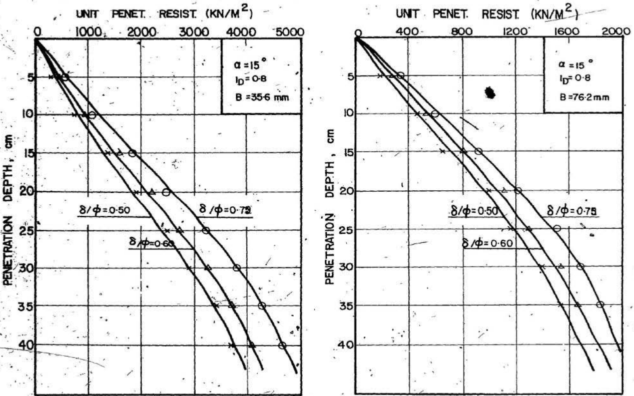

(a) (b)

FIG. 70 INFLUENCE OF BASE ROUGHNESS ON STATIC PENETRATION RESISTANCE OF SATURATED SILICA-70 SAND

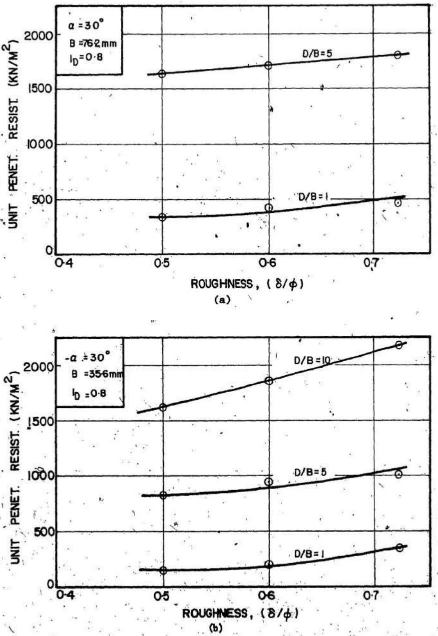

FIG. 71 VARIATION OF UNIT PENETRATION RESISTANCE WITH BASE ROUGHNESS FOR SATURATED SILICA-70 SAND

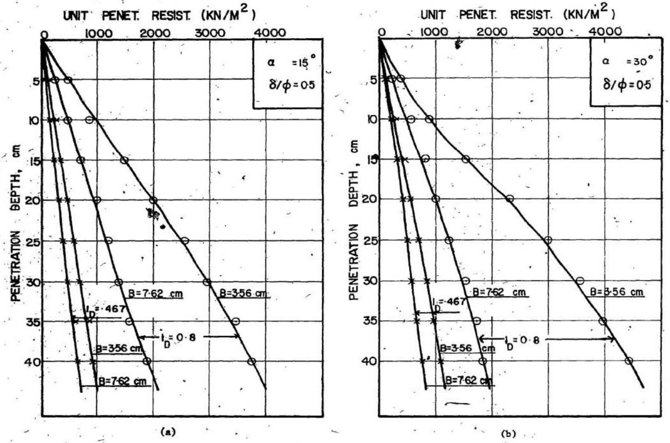

FIG. 72 INFLUENCE OF PENETROMETER SIZE ON STATIC PENETRATION RESISTANCE OF SATURATED SILICA-70 SAND

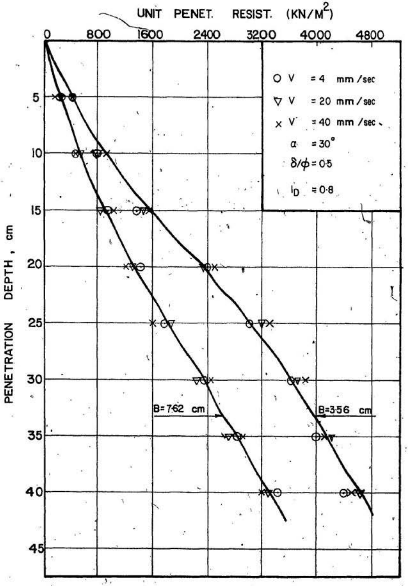

FIG. 73 INFLUENCE OF PENETRATION VELOCITY ON STATIC PENETRATION RESISTANCE OF SATURATED SILICA-70 SAND

4.4.6 Influence of Saturation

It was noticed earlier in paragraph 4.4.1 that the penetration resistance in saturated sand is higher compared to that in dry sand. Fig. 74 shows this comparison for both penetrometers for different soil properties. Contarary to an intuitive feeling that saturation would decrease the strength due to pore pressure effects in the case of sand, saturation actually increases the soil resistance. At present there are no theoretical approaches to compute the penetration resistance in saturated sands. Schmertmann (1975) has also noticed a similar phenomenon for sands. An earlier work by Drozd (1965) indicates the same type of behaviour for saturated sand in dynamic and free fall penetration testing. This effect of pore pressure in sands and clays is discussed further at the end of this chapter.

4.5 Summary For Cohesionless-Soil

From test results on cohesionless-soil, some conclusions may be drawn and summarized as follows:

(1) Penetration resistance is very sensitive to the soil density and consequently to soil friction angle. It increases rapidly with increasing density.

(2) Penetration resistance increases with increasing cone apex angle.

(3) Penetration resistance increases with increasing base roughness.

(4) Penetration resistance increases with decreasing penetrometer diameter at any depth.

(5) Penetration resistance of cohesionless soil is independent

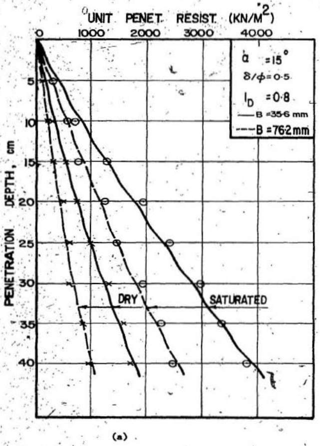

FIG. 74 COMPARISON OF STATIC PENETRATION RESISTANCE FOR DRY AND SATURATED SILICA-70 SAND

of the rate of penetration for the rates up to 4 cm/sec tested here.

(6) For saturated sand, the penetration resistance values are higher than those of the dry case. Penetration resistance increases due to generation of negative pore pressure in cohesionless soils.

(7) There is a good agreement between the theory of Durgunoglu and Mitchell and the experimental values. This theory may be used with confidence for cohesionless soils.

(8) Both the 45 cm^2 Memorial University penetrometer and the 10 cm^2 Fugro Type penetrometer give similar results except that the values obtained from the 10 cm^2 penetrometer are higher than the values obtained from the 45 cm^2 penetrometer. This is in conformity with bearing capacity theory.

4.6 Tests On Clay

To choose an appropriate theoretical analysis for cohesive soils, results of the penetration tests performed on the clay target were compared with the theoretical values of Meyerhof (1961a) and Durgunoglu and Mitchell (1973, 1975). The numerical technique suggested by Nowatzki and Karafiath (1972, 1978) and used earlier for cohesionless soils is not applicable for cohesive soils. In their analysis, Nowatzki and Karafiath assumed that the stress boundary conditions at the free surface and along the wall of the hole caused by the penetrometer are stable and that the soil behind this hole tends to fail and failure surfaces developed towards the hole. The latter situation occurs almost exclusively in cohesionless soils. Even a very small amount of cohesion is sufficient to insure stability of the hole and thus the above theory is not relevant in cohesive soils.

The results of penetration tests in this section are presented in Fig. 75 through Fig. 78 in the form of unit penetration resistance $q_f(kN/m^2)$ versus penetration depth D (cm). Theoretical values using both Meyerhof's theory and that of Durgunoglu and Mitchell are also shown on these figures. The combination of the different variables are shown on each of these figures.

It may be seen from the data presented that Meyerhof's theoretical values are greater than the experimental values for $D/B > 4$ and less than the experimental values for D/B less than 4. A similar phenomenon observed previously in the case of cohesionless-soils was explained in section 4.2. The values of Durgunoglu and Mitchell are in better agreement with the experimental values for stiff clay (Fig. 75 a, b) and medium stiff clay (Fig. 76b) and for soft clay the agreement is not good. The theoretical values are always higher than the experimental values in soft clay indicating the effect of soil compressibility on the static penetration resistance.

The ratios of predicted to measured penetration resistance are presented in Tables 14 and 15. It may be seen that these ratios are always greater than unity for Meyerhof's values (Table 14). Comparison with the values of Durgunoglu and Mitchell (Table 15), gives ratios which are close to unity for dense deposit, indicating the validity of this method for general shear condition. However, for low densities, these ratios are larger than one, indicating the significant influence of soil compressibility on penetration resistance. The use of bearing capacity factors formulated for general shear conditions will cause overestimation of the penetration resistance of compressible deposits.

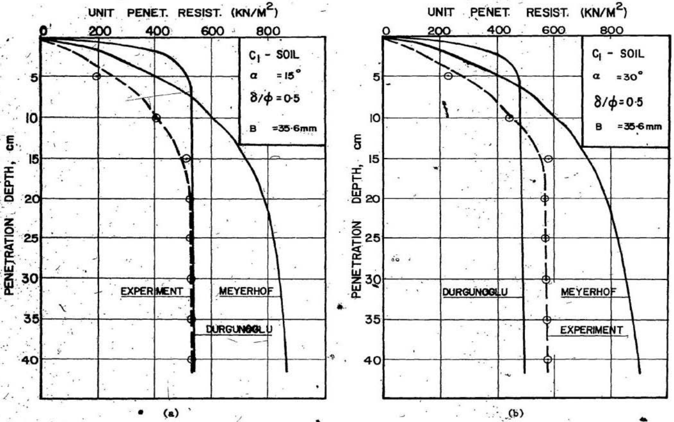

FIG. 75 COMPARISON OF MEASURED AND PREDICTED STATIC PENETRATION CURVES FOR MODELLING CLAY

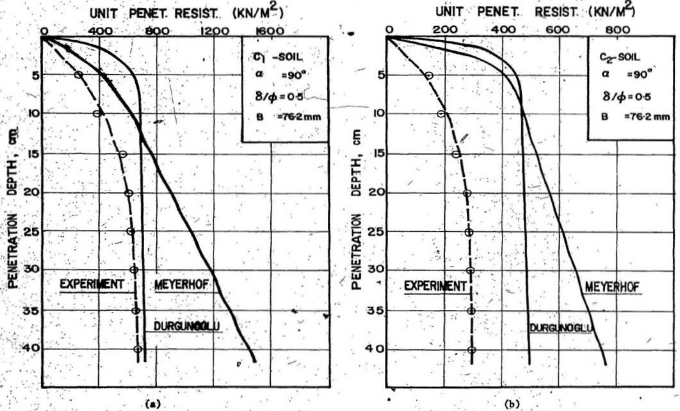

FIG. 76 COMPARISON OF MEASURED AND PREDICTED STATIC PENETRATION CURVES FOR MODELLING CLAY

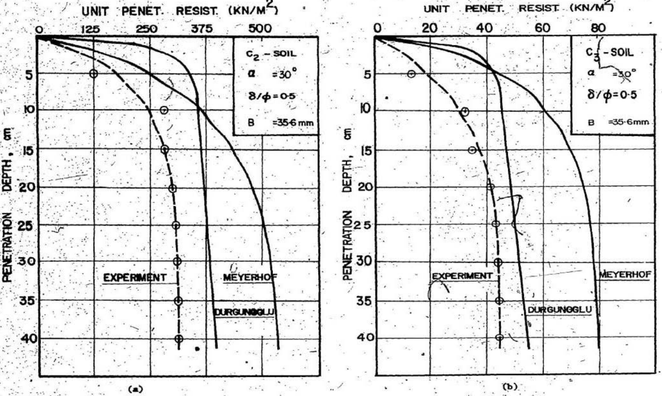

FIG. 77. COMPARISON OF MEASURED AND PREDICTED STATIC PENETRATION CURVES FOR MODELLING CLAY

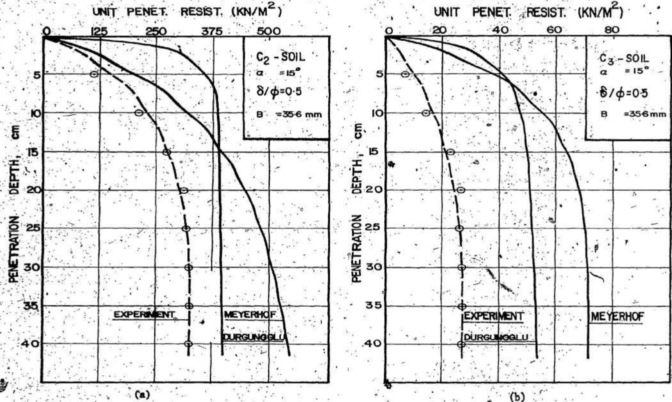

FIG. 78 COMPARISON OF MEASURED AND PREDICTED STATIC PENETRATION CURVES FOR MODELLING CLAY

TABLE 14

RATIOS OF PREDICTED TO MEASURED PENETRATION RESISTANCE FOR MODELLING CLAY USING MEYERHOF FAILURE MECHANISM

Soil Type	Dry Density (Kg/m^3)	Cohesion (kN/m^2)	Water Content (w%)	$\frac{q_f \text{ predicted}}{q_f \text{ measured}}$		
				D/B = 2.8	D/B = 5.6	D/B = 9.8
V. Soft Clay	1240	5.5	40	1.62	1.76	1.76
Relatively Medium Stiff Clay	1449	38.6	30.4	1.13	1.67	1.7
Relatively Stiff Clay	1600	47.8	25	1.22	1.43	1.53

TABLE 15

RATIOS OF PREDICTED TO MEASURED PENETRATION RESISTANCE FOR MODELLING CLAY USING DURGUNOGLU AND MITCHELL'S FAILURE MECHANISM

Soil Type	Dry Density (Kg/m^3)	Cohesion (kN/m^2)	Water Content (w%)	predicted q_f / measured q_f		
				D/B = 2.8	D/B = 5.6	D/B = 9.8
V. Soft Clay	1240	5.5	40	1.3	1.7	1.76
Relatively Medium Stiff Clay	1449	38.6	30.4	1.24	1.19	1.18
Relatively Stiff Clay	1600	47.8	25.0	1.12	0.85	0.86

In compressible soils, the shear surface is restricted to a smaller zone around the penetrometer tip as suggested by Vesic (1963) for punching or local shear failure types.

4.7 Parameters Affecting Penetration Resistance in Clay

The objective of this part is to study experimentally the influence of the different penetrometer and soil variables on the penetration resistance of cohesive soils. Since base roughness has little or no influence on the penetration resistance of the cohesive soils (Durgunoglu and Mitchell 1973), the variables to be examined are soil shearing strength, penetrometer size, cone apex angle and relatvie depth of penetration.

Fig. 79 shows the relation between unit penetration resistance q_f (kN/m^2) and penetration depth D (cm) for the modelling clay which has different shearing strength depending on its water content and its density. The dry clay sample had residual water content of 0.9%. Tests on this dry sample (C_4) shows that the soil behaves like a cohesionless material, this is shown in Fig. 79. When the water content is increased to 25% and the sample made into a stiff clay target, the penetration response is similar to that normally obtained in clay soils. When the water content is increased from 25% to 30.4% the penetration resistance decreases by approximately 30%. The reduction in the actual shear strength of the soil in this process is 20%. When the soil is a soft clay with 40% water content, the reduction in shear strength and the corresponding change in shear strength are drastically different. It can thus be seen that the degree of saturation has an important effect on the penetration resistance.

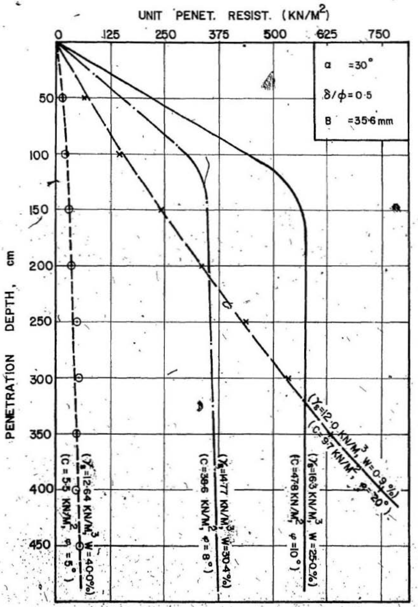

FIG. 79 COMPARISON OF PENETRATION RESISTANCE IN MODELLING CLAY

The variation of penetration resistance with cone semi-apex angle is illustrated in Fig. 80 for stiff clay for the two types of penetrometers. The variation is shown for different relative depths. From this figure one can infer that there is a significant increase in the penetration resistance with increasing cone semi-apex angle at any relative depth. In Fig. 80a at a relative depth of 10, there is an increase of 12% in penetration resistance for an increase from 15° to 30° in cone semi-apex angle. When the cone semi-apex increases from 30° to 90° at the same relative depth, an increase of 32% in penetration resistance was observed. At lower relative depth ($D/B = 5$), an increase of 12% was noticed corresponding to a change of cone semi-apex angle from 15° to 30°, while an increase of 50% was noticed for a change of semi-apex angle from 30° to 90°. The influence of cone apex angle on penetration resistance is more significant at lower relative depths than at higher values.

The influence of penetrometer size on unit penetration resistance, is shown in Fig. 81. Both the penetrometers have a cone semi-apex angle = 30° and relative roughness = 0.5. A similar comparison is shown in Fig. 82 for the two penetrometers but with a cone semi-apex angle of 15°. It may be seen from these figures that, irrespective of soil shear strength and cone semi-apex angle, penetration resistance for the 35.6 mm penetrometer is always higher than the values obtained using the 76.2 mm penetrometer at any depth. The difference between the two values are greater for stiff clay and it decreases with decreasing shear strength for clay.

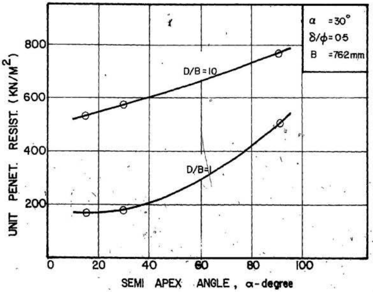

(a)

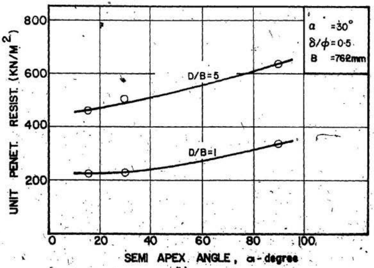

(b)

FIG. 80 VARIATION OF UNIT PENETRATION RESISTANCE WITH SEMI-APEX ANGLE FOR MODELLING CLAY

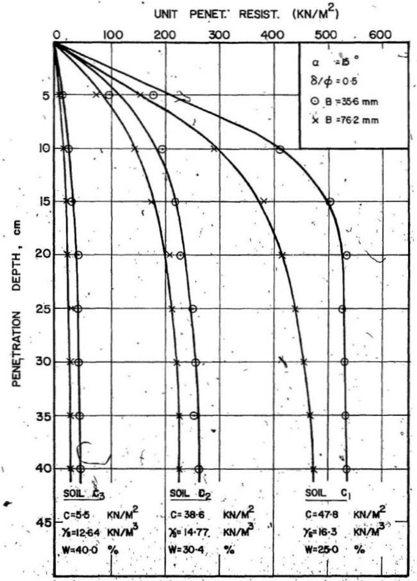

FIG. 81 INFLUENCE OF PENETROMETER SIZE ON STATIC PENETRATION RESISTANCE OF MODELLING CLAY

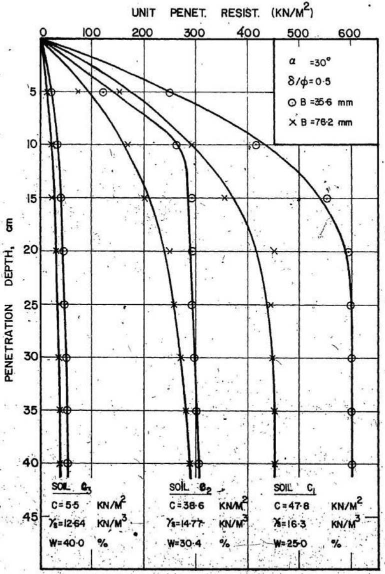

FIG. 82 INFLUENCE OF PENETROMETER SIZE ON STATIC PENETRATION RESISTANCE OF MODELLING CLAY

4.8 Effect of the Rate of Penetration on Static Resistance of Cohesive Soils

The aim of these tests is to study the influence of the rate of penetration on the shear strength of cohesive soils, since the rate of penetration represents an important factor which significantly affects the shear strength and consequently the penetration resistance of cohesive soils. As reported by Amar et al (1975), the penetration resistance for cohesive soils varies ~~with~~ the speed of penetration, when the speed varies from 1 to 10. Amar et al (1975) observed an increase in resistance of about 40% for soft clays and nearly 100% for Plateau silt.

Penetration tests were conducted on clay targets of varying strength, 5.5 kN/m^2, 38.6 kN/m^2 and 47.8 kN/m^2. These tests were performed at five different penetration rates, 0.88 cm/sec, 1.76 cm/sec, 4.4 cm/sec, 8.8 cm/sec and 22 cm/sec. Other variables such as cone semi-apex angle (α = 30^o), base roughness (δ/ϕ = 0.5) and penetrometer diameter (B = 3.56 cm) were kept constant. Figures 83, 84 and 85 show the results of these tests for stiff, medium stiff and soft clay respectively. In these figures, the unit cone resistance and unit sleeve friction profiles are plotted to penetration depths of 40 cm for the five different penetration velocities. The results clearly demonstrate that an increase in the penetration velocity causes a corresponding increase in both cone and sleeve resistance for all types of the clay. For stiff clay, an increase of 30% in cone resistance was noticed when the velocity increased 10 times, and an increase of 45% was noticed when the velocity increased 25 times. For medium stiff clay, when the velocity increased 25 times an increase of 66% occurred in the cone

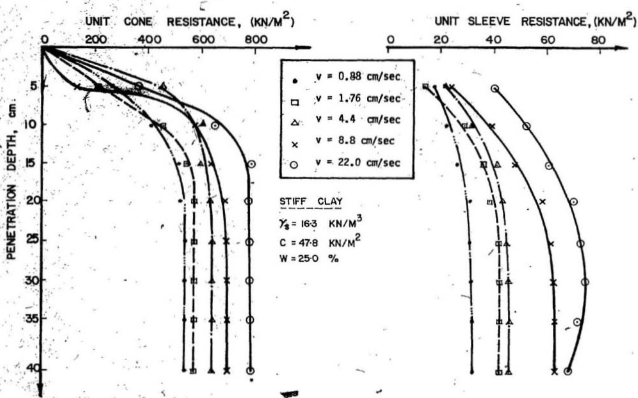

FIG. 83 INFLUENCE OF PENETRATION VELOCITY ON CONE AND SLEEVE RESISTANCE FOR MODELLING CLAY (STIFF CLAY)

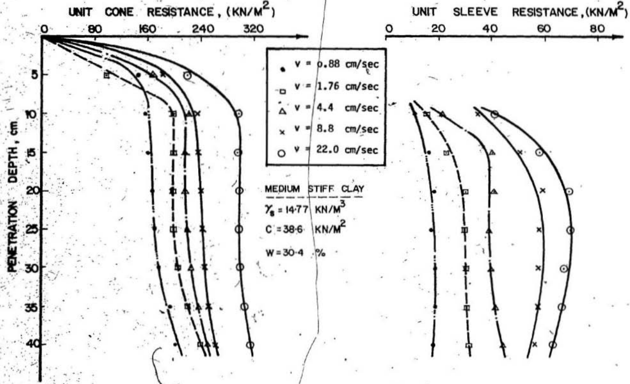

FIG. 84 INFLUENCE OF PENETRATION VELOCITY ON CONE AND SLEEVE RESISTANCE FOR MODELLING CLAY (MEDIUM STIFF)

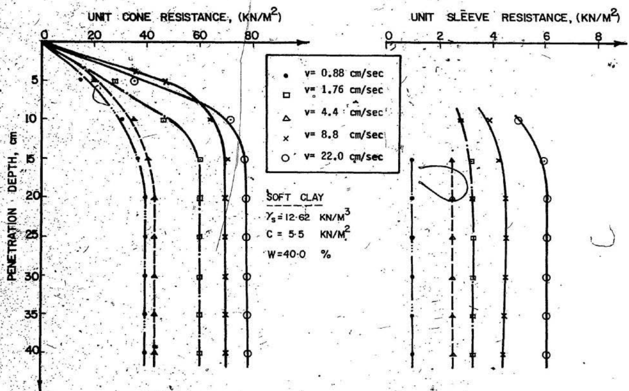

FIG. 85 INFLUENCE OF PENETRATION VELOCITY ON CONE AND SLEEVE RESISTANCE FOR MODELLING CLAY (SOFT CLAY)

resistance while for soft clay the corresponding increase was 75%.

4.9 Strain Rate Effect

It has been long recognized that the shear strength of many soil types is dependent upon shearing rate, (Casagrande and Shannon 1949). For many of these types the shear rate effect is too complex to permit mathematical definition or prediction. However, successful treatment of the shear rate effect for saturated clays for both small strain and large strain loading has been accomplished recently by Turange and Freitage (1970). They observed that for saturated clays, cone index varied with penetration rate according to the relation:

$$\frac{CI_x}{CI_s} = \left(\frac{\left(\frac{V}{d}\right)_x}{\left(\frac{V}{d}\right)_s}\right)^M \qquad [32]$$

wherein:

CI_x = cone index of penetration V_x with cone of diameter d_x,

CI_s = cone index of standard cone,

V = penetration rate,

d = diameter of 30° right circular cone, and

M = exponent of shear rate factor.

The above expression was found to hold good for speeds ranging from 0.051 to 431.8 cm/sec, for diameters from 0.27 to 7.7 cm and saturated soils ranging from silt to heavy clay. The exponent ranged from 0.091 to 0.109 for these conditions.

Wismer and Luth (1972 a, b) checked the applicability of the above expression using a horizontal high speed penetrometer, suggested a correlation term

$$\frac{CI_s}{\gamma L} = \left(\frac{V/L}{V_s/d_s}\right)^{0.1} \qquad [33]$$

where the V/L term is the velocity/length term. Expression [33] was used in this investigation to determine theoretical values for unit cone resistance at different penetration velocities. The interpretation of the results in this paragraph is based on the cone resistance values at penetration depth greater than 4D ($\approx$ 20 cm), this depth being the depth at which a constant value of cone and sleeve resistance is obtained. A comparison of the measured and the predicted values of cone penetration resistance using expression [33] is presented in Tables 16, 17 and 18 and shown graphically in Figures 86, 87 and 88 for stiff, medium stiff and soft clays respectively. The ratios of the predicted and measured cone resistance are also presented in the tables. It may be seen that these ratios are close to unity for the stiff and medium stiff clay indicating the validity of expression [33] for dense deposits. However, from Fig. 88 and Table 18 the difference between theoretical and experimental values is found to be large. The ratios of predicted to measured values are smaller than one, indicating that the use of expression [33] to predict cone penetration resistance in relatively compressible soils at any velocity underestimates the resistance.

4.10 Effect of the Pore Pressure on the Unit Penetration Resistance

The pore pressure field around a penetrating cone penetrometer can exert a major influence on the magnitude of the measured penetration

TABLE 16

COMPARISON OF MEASURED AND PREDICTED CONE RESISTANCE USING EXPRESSION [33] FOR STIFF MODELLING CLAY

Penetration Velocity cm/sec	Predicted Cone Resistance kN/m^2	Measured Cone Resistance kN/m^2	$\frac{\text{Predicted } q_c}{\text{Measured } q_c}$
0.88	53.6	53.4	1.004
4.4	63.0	62.7	1.004
8.8	67.56	67.1	1.006
22.0	74.0	72.8	1.045

TABLE 17

COMPARISON OF MEASURED AND PREDICTED CONE RESISTANCE USING EXPRESSION [33] FOR MEDIUM STIFF MODELLING CLAY

Penetration Velocity cm/sec	Predicted Cone Resistance kN/m^2	Measured Cone Resistance kN/m^2	$\frac{\text{Predicted } q_c}{\text{Measured } q_c}$
0.88	2.14	1.95	1.097
4.4	2.5	2.4	1.042
8.8	2.7	2.55	1.095
22.0	2.96	3.10	0.954

TABLE 18

COMPARISON OF MEASURED AND PREDICTED CONE RESISTANCE USING EXPRESSION [33] FOR SOFT MODELLING CLAY

Penetration Velocity cm/sec	Measured Cone Resistance kN/m^2	Predicted Cone Resistance kN/m^2	$\frac{q_c \text{ predicted}}{q_c \text{ measured}}$
0.88	0.396	0.4	0.99
4.4	0.46	0.6	0.766
8.8	0.5	0.7	0.714
22	0.55	0.725	0.728

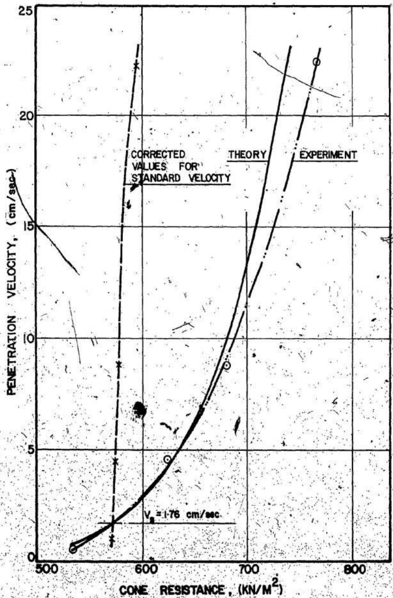

FIG. 56 COMPARISON OF MEASURED AND PREDICTED CONE PENETRATION RESISTANCE FOR STIFF MODELLING CLAY

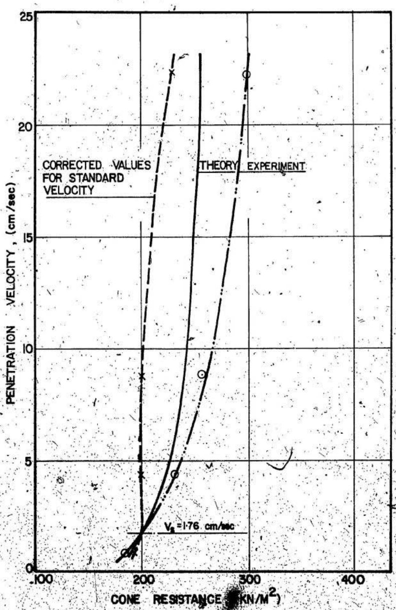

FIG. 87 COMPARISON OF MEASURED AND PREDICTED CONE PENETRATION RESISTANCE FOR MEDIUM STIFF MODELLING CLAY

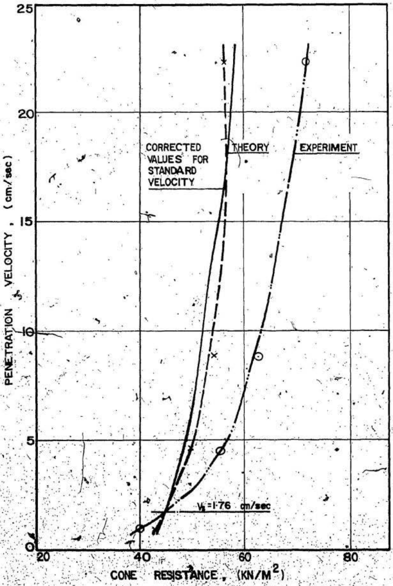

FIG. 88. COMPARISON OF MEASURED AND PREDICTED CONE PENETRATION RESISTANCE FOR SOFT MODELLING CLAY

resistance q_c. The measured penetration resistance might be different from that which would be obtained under a fully drained condition. It is reasonable to expect, therefore, that the penetration resistance of such soils would be dependent on water content and that interpretation of data obtained from tests in saturated soils should be done with care.

Schmertmann (1974 a, b) studied the effect of pore pressure on static cone resistance. He used a cone-piezometer to measure the excess hydrostatic pore pressure in the field for both cohesive and cohesionless soils. The piezometer recorded a positive pore pressure in case of cohesive soils and a negative pore pressure in case of cohesionless soils. Cone penetration tests were performed in the same sites for drained and undrained conditions. For undrained conditions, an increase of about 50% was recorded for cohesionless soils while a decrease of about 16% was recorded for cohesive soils compared to the drained tests. Schmertmann concluded that, the positive pore pressure reduces q_c in cohesive soils while the negative pore pressure increases q_c in cohesionless-soils.

One can conceptually visualize this phenomenon in cohesive and cohesionless soils. In case of cohesive soils, the permeability of the material is small and always results in an excess pore pressure. This causes a reduction in penetration resistance since the pore pressure is not dissipated. In the case of cohesionless soils, the rate of penetration appears to virtually cause a pore pressure dissipation at a high rate resulting in a negative pore pressure as the penetrometer advances.

Fig. 74 shows a comparison of unit penetration resistance for dry and saturated silica-70 sand (cohesionless soil). It is clearly demonstrated that, penetration resistance in saturated cohesionless soils is always higher than the penetration resistance in dry cohesionless soils irrespective of the soil density or penetrometer properties. An increase of about 60% was noticed for $I_D = 0.8$ and at a depth = 40 cm. This is due to the creation of negative pore pressure which tends to increase the unit penetration resistance.

For the modelling clay (cohesive soil), Fig. 79 shows the relation between unit penetration resistance and penetration depth at different water contents. It may be seen that penetration resistance decreases with increasing water content, which is in part a result of the creation of a positive pore pressure.

The phenomenon of pore water pressure and its effect on penetration resistance was also studied by Freitag et al (1970) who provided values of apparent cohesion as a function of relative density for Yuma sand at various water contents. Fig. 89 shows these values. From the figure it is clear that cohesion decreases with increasing water content at the same relative density.

Another explanation for this phenomenon was given by Melzer (1974), based on experimental studies using WES cone penetrometer and Lean clay exhibiting different degree of saturation. He stated that with decreasing degree of saturation, the frictional component of the soil bearing capacity becomes more dominant. As a consequence, the cone penetration resistance increases with decreasing degree of saturation at a given relative depth, as indicated in Figure 90.

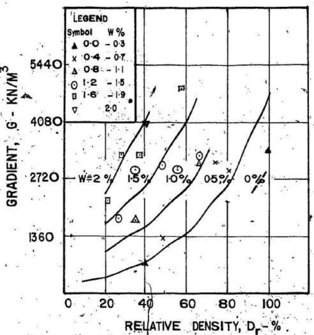

FIG. 89 PENETRATION RESISTANCE GRADIENTS FOR MOIST YUMA SAND

(Freitag et al 1970)

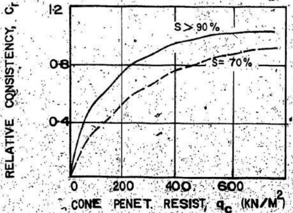

FIG. 90 INFLUENCE OF DEGREE OF SATURATION (s) ON RELATION BETWEEN C_r AND q_c FOR LEAN CLAY

(Melzer 1974)

4.11 Experiment on Layered Soils

The problem of foundations on layered soil was treated by Button (1951) who assumed that a circular failure surface will occur in case of a footing on a two layered cohesive soil. This work has been further extended by Reddy and Srinivasan(1967), who considered nonhomogeneity and anisotropy of soil with respect to shear strength. They presented numerical results in the form of graphs that can be readily used to calculate the bearing capacity of strip footing on a two layered cohesive soil. These graphs take into account the anisotropy of the soils and are similar in shape to that for isotropic case. An increase of about 15% in bearing capacity will result if $K < 1$ and a decrease of 30% if $K > 1$. "K" being defined as the coefficient of anisotropy, the ratio of the cohesive strength of the two layers ($K = C_2/C_1$).

Another extension of Button's analysis of the bearing capacity for footing on layered clays was carried out by Meyerhof and Brown (1967). They proved experimentally that the assumption of a cylindrical failure surface was incorrect. For a homogenous and isotropic solution, the assumption of a cylindrical surface leads to a value of N_c, which is about 7% higher than that obtained by the rigorous Prandtl solution. Where the subsoil is neither homogenous nor isotropic, it is known that the failure surface will no longer be cylindrical, and that the error associated with the assumption of a cylindrical failure surface will increase with increasing nonhomogeneity.

Button's analysis gave results which were in all cases higher than those obtained experimentally. The mode of failure which occurs in almost all cases was a combination of punching through the top layer and mobilization of the full bearing capacity of the lower layer.

None of the presently available solutions in the literature describe efficiently the failure mechanism associated with static penetration resistance of layered soils. In this investigation, preliminary tests on layered soil using the 10 cm^2 Fugro type penetrometer and the 45 cm^2 Memorial University penetrometer were conducted. Four types of layered system using silica-70 sand and the modelling clay were tested. A profile of the different layering combinations used, is shown in Fig. 91. Results are presented below:

(1) Type I. Figure 92 represents the relation between unit penetration resistance and penetration depth for this layered system. The sudden change of the value of penetration resistance in moving from layer to layer is clearly demonstrated in this figure. Analysis of the data of this test gives the following results:

1. The change in penetration resistance for the top layer is very small with an average value of 300 kN/m^2 for the small penetrometer and of 175 kN/m^2 for the 45 cm^2 penetrometer.

2. In the second layer, which is a dense sand deposit, the unit penetration resistance reaches its maximum value.

3. For bottom layer, unit resistance decreases up to a value of 1500 kN/m^2 for small penetrometer and up to 1100 kN/m^2 for the big penetrometer and it becomes almost constant at these values.

4. The general shape of the unit penetration resistance versus penetration depth is almost the same for the two sizes of the penetrometers, but the values of the small one are always higher than the values for the larger diameter at the same depth.

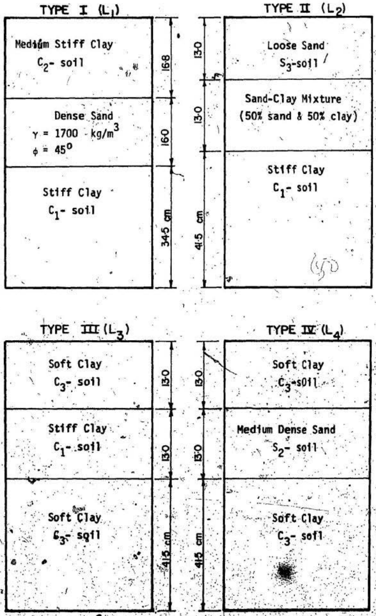

FIG. 91 PROFILE OF DIFFERENT LAYERING COMBINATIONS

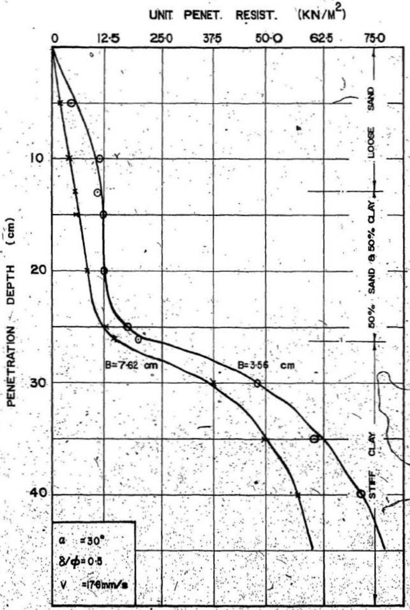

FIG. 92 STATIC PENETRATION RESISTANCE OF LAYERED SOILS (TYPE I)

(2) Type II. Figure 92 shows the results of tests in this soil. The following observations are made:

1. The penetration resistance in the loose sand is small. An average of 50 kN/m^2 (small penetrometer) and an average of 35 kN/m^2 (big penetrometer) is observed.

2. In the mixed layer, no significant increase in the unit penetration is observed, it is almost constant along the entire depth of the layer with an average of 125 and 75 kN/m^2 for small and big size penetrometer respectively.

3. At the bottom, the stiff clay layer, there is a sudden increase in the value of the penetration resistance which reaches its maximum. At the maximum depth of penetration in this layer, a resistance of 775 kN/m^2 (small size one), and 550 kN/m^2 (big size one) are recorded.

(3) Type III. Fig. 93 shows the results of tests in type III layered soil. Examining this figure, one can notice the sudden increase in penetration resistance between the top and the mid layers and also the sudden decrease between the mid and the bottom layer.

1. For the top soft clay layer, the increase in penetration resistance is very samll from 0.0 to 100 kN/m^2 (35.6 mm penetrometer) and from 0.0 to 55 kN/m^2 (76.2 mm penetrometer).

2. For the stiff clay layer, penetration resistance increases rapidly with depth, till it reaches its maximum, 625 kN/m^2 (35.6 mm penetrometer) and 239 kN/m^2 (76.2 mm penetrometer).

3. For the bottom layer, penetration resistance decreases till it reaches its constant value of 200 kN/m^2 (35.6 mm penetrometer) and 150 kN/m^2 (76.2 mm penetrometer).

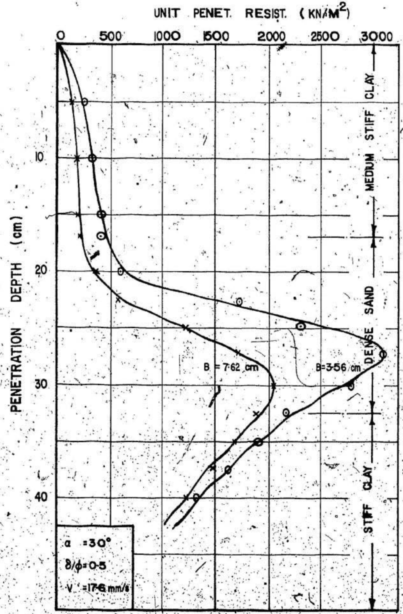

FIG. 93 STATIC PENETRATION RESISTANCE OF LAYERED SOILS (TYPE II)

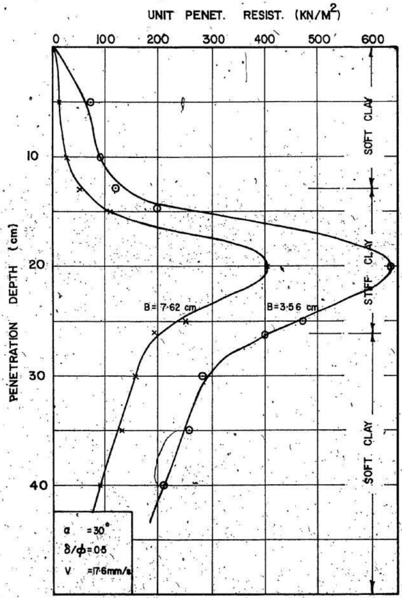

FIG. 94 STATIC PENETRATION RESISTANCE OF LAYERED SOILS (TYPE III)

(4) Type IV. The test results in this type of soil is presented in Fig. 94 which is similar to Figure 93 with a slight difference in the value of penetration resistance.

1. For the top layer, the change in penetration resistance is from 0.0 to 225 kN/m^2 for small size penetrometer and from 0.0 to 65 kN/m^2 for the larger penetrometer.

2. The maximum value of penetration resistance occurs in the middle layer, at a value of 950 kN/m^2 (35.6 mm penetrometer) and 280 kN/m^2 (76.2 mm penetrometer).

3. The average value of penetration resistance in the bottom layer is 275 kN/m^2 for the 35.6 mm penetrometer and 150 kN/m^2 for the 76.2 mm penetrometer.

At this time there are no well defined theoretical methods for a satisfactory calculation of the penetration resistance in layered systems similar to those used in this investigation for cohesive and cohesionless soils. An attempt was made to use the approahhes of Meyerhof (1961a) and Durgunoglu and Mitchell (1973) to correlate the experimental results obtained here. It is felt that a substantial modification of these theories would be required for evolving a meaningful analysis. It will be also necessary to experimentally observe the shape of the failure surface particularly when penetration occurs in the transition zone. The complexity of the problem could be explained further with reference to Figs. 92 to 94. When the penetrometer enters from one layer to the immediately succeeding layer below, there is always an interaction between the two layers as far as the slip lines are concerned. The strength of the underlying layer

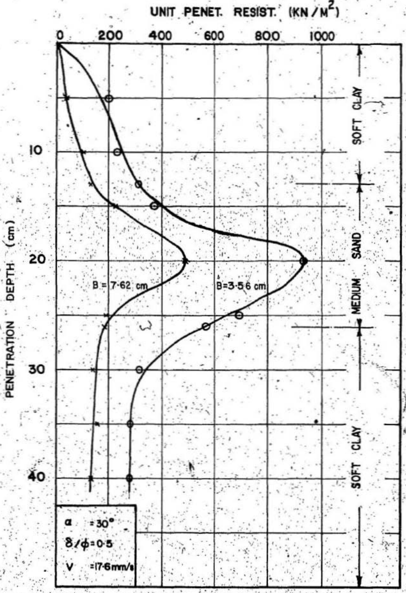

FIG. 95 STATIC PENETRATION RESISTANCE OF LAYERED SOILS (TYPE IV)

will be fully mobilized only when the entire failure zone is restricted to that layer without any interaction with the overlying soil type. This can be very clearly observed in all the experimental data presented. When there is a transition from a weak layer to a stronger layer, the full advantage of the better soil is obtained only after substantial penetration into that layer. Any theory that will be proposed has to take this phenomenon into account and be able to predict the optimum depth of penetration to make the best use of the properties of the individual layer. This is an interesting phenomenon that was noticed and is to be pursued as a separate research problem.

4.12 Interpretation of Field Test Results

Although a good correlation has been shown in the preceeding paragraphs, an interpretation of field tests is an art based on experience. This is due to the fact that more than one variable is to be evaluated from the available measurements, generally by trial and error. In the evaluation of the cone penetrometer, methods have been developed for use in specific soil types. For example, De Beer (1945) has developed a method that is applicable particularly to soils in Belgium. An angle of 30^0 is initially assumed for the soil and values of the apparent angle of internal friction and cohesion are computed from field cone resistance values. Similarly modification of this method is used for cohesive and cohesive frictional soils. There are other methods in practice suggested by Meyerhof (1961a), Janbu and Senneset (1974), Schmertmann (1975) and Durgunoglu and Mitchell (1973, 1975). The detailed review of these methods is given by Lunne and Mitchell (1977). The method of Durgunoglu and Mitchell is a reverse application to their theory, its use in cohesive friction soils involves measurements with two penetrometers of different sizes from which the values of C and ϕ can be found out.

A detailed discussion of the methods is not made in this section as they are well documented and are not particularly relevant here. However, computations were made using the various methods in the experiments reported here and also to the tests on Monterey sand No. 0 reported by Durgunoglu and Mitchell (1973). The results are tabulated in Table 19 through 30. Fig. 96 shows a comparison of ϕ values computed by different theories.

From these calculations it is seen that the methods of De Beer (1945) and Meyerhof (1961a) are simple but they constantly yield low values of ϕ. Theory of Durgunoglu and Mitchell (1973) requires a knowledge of cone roughness and the coefficient of earth pressure at rest. Values obtained by this method are close to the measured values. Janbu's method is applicalbe only to cases where q_c varies linearly with depth or at least close to a linear variation. Schmertmann's method is empirical and reliable results can be obtained only if the coefficient of earth pressure at rest is known.

TABLE 19

DE BEER METHOD FOR SILICA-70 SAND

	Dense Sand $\gamma_s = 17.2$ kN/m^3				Medium Dense $\gamma_s = 15.60$ kN/m^3				Loose Sand $\gamma_s = 14.98$ kN/m^3			
Depth in cm	q_c kN/m^2	$\gamma_s D$ kN/m^2	$q_c/\gamma_s D$	ϕ degree	q_c kN/m^2	$\gamma_s D$ kN/m^2	$q_c/\gamma_s D$	ϕ degree	q_c kN/m^2	$\gamma_s D$ kN/m^2	$q_c/\gamma_s D$	ϕ degree
5.0	183	0.86	213	32	60	0.78	77	26	51	0.75	67	24.5
10.0	373	1.72	217	32	160	1.56	102	27	120	1.5	80	25.8
15.0	660	2.58	256	33	262	2.34	112	28.1	232	2.247	103	27.8
20.0	1030	3.44	300	33.8	500	3.12	160	30.5	322	3	107	28
25.0	1400	4.3	326	34.3	650	3.9	167	31	382	3.75	102	27.5
30.0	1750	5.16	339	34.8	800	4.68	171	31	400	4.5	89	27
35.0	2120	6.06	352	34.9	920	5.46	168	31	450	5.2	86	27
40.0	2413	6.88	351	34.9	1040	6.24	167	31	550	5.9	91	27.2
Average ϕ	33.5°				30.0°				26.5°			

TABLE 20

DE BEER METHOD FOR MONTEREY SAND NO. 0

	Dense Sand $\gamma_s = 16.81$ kN/m^3				Medium Dense $\gamma_s = 15.96$ kN/m^3				Loose Sand $\gamma_s = 15.53$ kN/m^3			
Depth cm	q_c kN/m^2	$\gamma_s D$ kN/m^2	$q_c/\gamma_s D$	ϕ degree	q_c kN/m^2	$\gamma_s D$ kN/m^2	$q_c/\gamma_s D$	ϕ degree	q_c kN/m^2	$\gamma_s D$ kN/m^2	$q_c/\gamma_s D$	ϕ degree
5	255	0.84	303	33.8	115	0.8	144	30.0	103	0.78	132	29
10	517	1.6	323	34.2	250	1.6	157	30.2	150	1.55	97	27.9
15	819	2.52	325	34.2	377	2.4	157	30.2	222	2.33	95	27.8
20	1103	3.36	328	34.3	510	3.2	159	30.3	300	3.1	96.6	28
25	1495	4.2	356	34.9	657	4.0	165	30.4	360	3.9	92.7	27.5
30	1840	5.04	365	35.2	800	4.8	167	30.4	423	4.7	90.7	27
ϕ average	34.5°				30.2°				28.0°			

TABLE 21

MEYERHOF METHOD FOR SILICA-70 SAND

	Dense Sand $\gamma_s = 17.20\ kN/m^3$		Medium Dense $\gamma_s = 15.60\ kN/m^3$		Loose Sand $\gamma_s = 14.98\ kN/m^3$	
Depth cm	$N_q = q_c/\gamma D$	ϕ-degree	$N_q = q_c/\gamma D$	ϕ-degree	$N_q = q_c/\gamma D$	ϕ-degree
5.0	216.8	40.5	78.4	36.1	69	35.9
10.0	221.0	40.8	104.5	37.0	81.6	36.4
15.0	260	41.2	114.2	37.5	105.2	37.0
20.0	305	42.0	163	39.0	109.4	37.2
25.0	332.0	42.2	170	39.10	103.9	37.0
30.0	345.0	42.5	179	39.20	90.7	36.8
35.0	358.8	42.6	171.8	39.0	87	36.5
40.0	357.0	42.6	170.0	39.0	93.5	37.0
ϕ average	41.5°		38.5°		36.5°	

TABLE 22

MEYERHOF METHOD FOR MONTEREY SAND NO. 0

	Dense Sand $\gamma_s = 17.1$ kN/m^3		Medium Dense $\gamma_s = 16.27$ kN/m^3		Loose Sand $\gamma_s = 15.83$ kN/m^3	
Depth cm	$N_q = q_c/\gamma_s D$	ϕ degree	$N_q = q_c/\gamma_s D$	ϕ degree	$N_q = q_c/\gamma_s D$	ϕ degree
5	303.5	41.8	144	38.2	132	37.5
10	322.9	41.9	136.6	38.5	97	36.5
15	325.0	41.9	157.0	38.5	95.0	36.5
20	328	42.0	159.0	38.5	95.6	36.5
25	335.95	42.1	164.7	38.6	92.7	36.2
30	365	42.2	167.0	38.6	90.7	36.0
ϕ average	42.0°		38.5°		36.5°	

TABLE 23

DURGUNOGLU AND MITCHELL METHOD FOR SILICA-70 SAND

	Dense Sand $\gamma_s = 17.2\ kN/m^3$			Medium Dense $\gamma_s = 15.60\ kN/m^3$			Loose Sand $\gamma_s = 14.98\ kN/m^3$		
Relative Depth (D/B)	q_f kN/m^2	$N_{\gamma q}\ \xi_{\gamma q}$	ϕ degree	q_f kN/m^2	$N_{\gamma q}\ \xi_{\gamma q}$	ϕ degree	q_f kN/m^2	$N_{\gamma q}\ \xi_{\gamma q}$	ϕ degree
1.4	183	305	45.1	60	110	40	51	97.5	37.5
2.8	373	620	45.1	160	294	41	120	229	39
4.2	660	1098	45.1	262	481	41.2	232	443	40
5.6	1030	1669	45.5	500	918	42	322	615	40
7.0	1400	2329	45.5	650	1193	42.5	382	730	40
8.4	1750	2912	45.5	800	1469	42.4	400	764	39.5
9.8	2120	3528	45.5	920	1689	42.5	450	860	39
11.2	2413	4015	45.4	1040	1909	42.4	550	1051	39
ϕ average		45.0^o			41.0^o			39.0^o	

TABLE 24

MEASURED AND PREDICTED VALUES OF ϕ FOR MONTEREY SAND NO. 0 AS GIVEN BY DURGUNOGLU AND MITCHELL

Type of Sand	γ_s kN/m^3	ϕ-Predicted degree	ϕ-Measured degree	$\frac{\phi\text{-Predicted}}{\phi\text{-Measured}}$
Dense Sand	17.1	45.6	46.8	0.97
Medium Sand	16.27	42.9	42.9	1
Loose Sand	15.83	39.7	39.7	1

TABLE 25

JANBU METHOD FOR SILICA-70 SAND

γ_s kN/m^3	Slope N_p	$N_q = N_p + 1$	tan ϕ	ϕ degree
17.2	305	306	1.04	46.0°
15.60	147	148	0.9	41.7°
14.98	91	92	0.8	38.7°

TABLE 26

JANBU METHOD FOR MONTEREY SAND NO. 0

γ_s kN/m^3	Slope N_p	$N_q = N_p + 1$	tan ϕ	ϕ degree
17.10	303	304	1.00	45°
16.27	159	160	0.95	43.6°
15.83	96	97	0.88	41.4°

TABLE 27

SCHMERTMANN METHOD FOR SILICA-70 SAND

γ Kg/cm^3	Depth (max) cm	q_f Kg/cm^2	γD Kg/cm^2	Relative Density I_D%	ϕ degree
0.001688	40.0	24.13	0.068	80	43.5°
0.00153	40.0	11.00	0.060	45.0	39°
0.00147	40.0	6.00	0.0588	30.0	37°

TABLE 28

SCHMERTMANN METHOD FOR MONTEREY SAND NO. 0

γ Kg/cm^3	Depth (max) cm	q_f Kg/cm^2	γD Kg/cm^2	Relative Density I_D%	ϕ degree
0.001681	30.0	18.40	0.05	70	42.2
0.001596	30.0	8.00	0.048	35	37.8
0.001553	30.0	4.23	0.047	18	35.5

TABLE 29

SUMMARY OF ALL RESULTS (VALUES OF ϕ)

Types of Sand	Unit Weight kN/m^3	Triaxial Test	De Beer (1945)	Meyerhof (1961a)	Durgunoglu and Mitchell (1973)	Janbu (1974)	Schmertmann (1975)
Silica-70 Dense	17.20	44^o	33.5	41.5	45.0	46	43.5
Silica-70 Medium Dense	15.60	40.0	30	38.5	41.0	41.7	39
Silica-70 Loose	14.98	38^o	26.5	36.5	39.0	38.7	37
Monterey Sand No. 0 Dense	17.10	46.6	34.5	42	45.6	46	42.2
Monterey Sand No. 0 Medium Dense	16.27	42.9	30.2	38.5	42.9	43.6	37.8
Monterey Sand No. 0 Loose	15.83	39.7	28	36.5	39.7	41.4	35.5

TABLE 30

DURGUNOGLU AND MITCHELL METHOD FOR THE MODELLING CLAY

Type of Clay	Water Content w%	γ_s (dry) kN/m^3	C-Predicted kN/m^2	C-Measured kN/m^2	$\frac{\text{C Predicted}}{\text{C Measured}}$
Stiff Clay	25	16.30	52.9	47.8	1.106
Medium Stiff Clay	30.4	14.77	33.1	38.6	0.858
Soft Clay	40	12.64	4.6	5.5	0.836

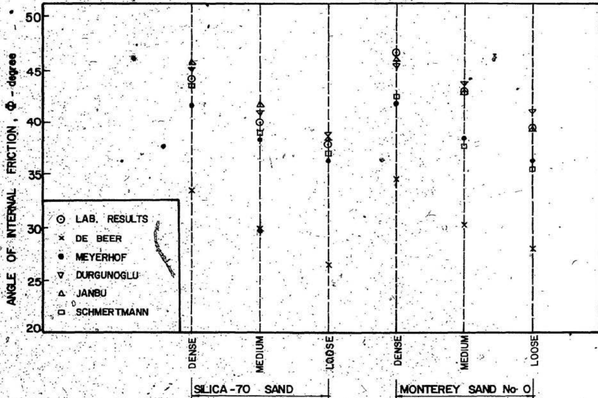

FIG. 96 COMPARISON OF ϕ VALUES COMPUTED BY DIFFERENT THEORIES

CHAPTER V

SUMMARY AND CONCLUSIONS

The research reported here is part of a comprehensive program to develop a 45 cm^2 (nominal) free fall impact penetrometer for use in the oceans. Evaluation of quasi static penetration tests was made in conjunction with a standard 10 cm^2 Fugro type penetrometer.

Three theoretical methods, Meyerhof (1961a), Nowatzki and Karafiath (1973, 1978) and Durgunoglu and Mitchell (1973, 1975) were considered and compared with the results of controlled laboratory penetration tests conducted on a fine sand (silica-70) and on silty clay (modelling clay). Variables such as the penetrometer roughness, base apex angle, relative depth and the angle of shear resistance of soil were considered. Experiments were also conducted in layered soils.

The following conclusions are drawn from the present investigation pertinent to the range of variables investigated in this study.

1. Among the various solutions available for the penetrometer problem, only those of Meyerhof (1961a), Nowatzki and Karafiath (1972, 1978) and Durgunoglu and Mitchell (1973, 1975) take into account the penetrometer roughness, base apex angle and relative depth which influence the penetration resistance.

2. Meyerhof's method overestimates the penetration resistance in the deep foundation zone and is conservative in the shallow foundation region, while the method of Nowatzki and Karafiath is always conservative.

3. The agreement between measured and predicted values using

the theory of Durgunoglu and Mitchell for cohesionless and cohesive soils was quite good. This analytical method can be reliably used for predicting the static penetration resistance of relatively incompressible soils.

4. Tests in dry sand showed that penetration resistance is influenced by the angle of shear resistance for the soil, the apex angle of the cone, the base roughness and the size of the penetrometer. The penetration resistance is highly sensitive to changes in the soil strength as shown in tests on soils of three different density indicies. Increasing apex angle of the cone results in increased penetration resistance. Similarly, increasing relative roughness of the cone increases the penetration resistance. An increase in the diameter of the penetrometer decreases correspondingly the resistance to penetration. This phenomenon can be logically explained with reference to bearing capacity equations. Although the larger diameter penetrometer consistently gave lesser penetration resistance, the effects of the various other parameters were similar to both penetrometers.

5. Tests in silty clay show that the resistance to penetration is influenced by the soil cohesion, cone apex angle penetrometer diameter and soil compressibility. In medium stiff and stiff clays, the penetration resistance is sensitive to the shear strength of the soil. The influence of cone apex angle is similar to that observed in sand. An increase in the diameter of the penetrometer reduces the penetration resistance, similar to the effect observed in sand. Cone roughness has no perceptable effect in clays. Interpretation of tests in clay requires some caution. Results on compressible soft clay show that they are not amenable to reliable analysis, due to local and punching shear failure.

The effects of various parameters on the larger penetrometer is similar to that observed in the standard one.

6. Rate of penetration is an important variable, since the results are to be finally used for the free fall penetrometer. Penetration rates of 0.4 cm/sec to 22 cm/sec were tested. In this range, tests on sand showed no rate effects. However, the clay was found sensitive to the strain rate effect. It may also be qualified here that the velocity of the free fall penetration tests is in the order of 7.5 m/sec and the results obtained in this investigation need not necessary hold good for a direct application. At those speeds, some effect even in sands is likely.

7. Tests on saturated sand and clay show that pore water causes some abnormalities in cone penetration test results. In sands, a negative pore pressure is developed, resulting in a higher penetration resistance while in clays the pore water pressure increases causing a decrease in the resistance.

8. Tests on layered soils show that the relative strength of the stronger layer can be used to advantage in foundation designs, if the depth at which maximum penetration resistance occurs can be determined.

9. Tests with the two types of penetrometer show that the behaviour and response of the 45 cm^2 penetrometer is similar to the standard Fugro type penetrometer, except that the absolute values of penetration resistance are smaller when the diameter increases. The Memorial University penetrometer can thus be used in practice with as much confidence as the standard penetrometer.

Recommendations for further research:

a) Pore pressure is a factor to be reckoned with when the penetrometer is used at sea. Limited references are available in the literature where this effect is quantitatively evaluated. It is suggested that further research efforts be made in this area.

b) Compressibility of the soil will be a problem in testing surficial underconsolidated ocean sidements. Reliable reduction factors are necessary to interpret the results on such soils. This is an area to be studied further.

c) Higher penetration rates in the range measured for the free fall cone penetrometer tests is reported (Chaudhuri, 1979) to have an influence even on sand targets. Efforts should be made to investigate this influence.

d) Research on layered soils is an area that should be pursued further, in the light of the interesting observations made in this investigation.

REFERENCES

1. Amar, S., Baguelin, F., Jezequel, J.F. and LE Mehaute, A. (1975), "In Situ Shear Resistance of Clays", Proceedings of the Conference on In Situ Measurements of Soil Properties, ASCE, Vol. 1, pp. 22-45.

2. Baligh, M.M. (1976), "Cavity Expansions in Sands With Curved Envelopes", Journal of the Geotechnical Engineering Division, Proceedings, ASCE, Vol. 102, No. GT11.

3. Baligh, M.M. and Vivatrat, V. (1979), "In Situ Measurements in a Marine Clay", Preprint, Behaviour of Offshore Structures (BOSS) Conference, London, England.

4. Bell, A.L. (1915), "Lateral Pressure and Resistance of Clay and the Supporting Power of Clay Foundations", Proceedings, Institution of Civil Engineers (London), V. 199, pp. 233-272.

5. Berezantzev, V.G., Khristoforov, V.S. and Golubkov, V.N. (1961), "Load Bearing Capacity and Deformation of Piled Foundations," Proceedings of the 5th International Conference on Soil Mechanics and Foundation Engineering, Paris, pp. 11-15.

6. Biarez, J., Burel, M. and Wack, B. (1961), "Contribution a l'etude de la force portante des foundations", Proceedings of the 5th International Conference on Soil Mechanics and Foundation Engineering, Paris, pp. 603-609.

7. Bishop, R.F., Hill, R. and Mott, N.F. (1945), "The Theory of Indentation and Hardness Test", Proceedings of the Physical Society, Vol. 57, pp. 147-159.

8. Brinch Hansen, J. (1961), "A General Formula for Bearing Capacity", Bulletion No. 11, Danish Geotechnical Institute, Copenhagen, pp. 38-46.

9. Brinch Hansen, J. (1970), "A Revised and External Formula for Bearing Capacity", Bulletin No. 28, Danish Geotechnical Institute, Copenhagen, pp. 5-11.

10. Button, S.J. (1953), "The Bearing Capacity of Footing on a Two-Layer Cohesive Soils", Proceedings, 3rd International Conference on Soil Mechanics and Foundation Engineering, Vol. 1, pp. 332-335.

11. Casagrande, A. and Shannon, W.L. (1949), "Strength of Soils Under Dynamic Loads", Transaction, ASCE, Vol. 114.

12. Chari, T.R., Smith, W.G. and Zielinski, A. (1978), "Use of Free Fall Penetrometer in Sea Floor Engineering", Conference Record, Ocean 78, IEEE-MTS Conference, pp. 686-691.

13. Chari, T.R., Muthukrishnaiah, K. and Zielinski, A. (1979), "Performance Evaluation of a Free Fall Penetrometer", First Canadian conference on Marine Geotechnical Engineering, Calgary, Alberta, April 1979.

14. Chaudhuri, S.N., (1979), "Free Fall Impact Penetration Tests in Soils", Master Thesis, Memorial University of Newfoundland, St. John's, July 1979.

15. CSA Standard B95-1962. Surface Texture (Roughness, Waviness and Lay). Canadian Standard Association, Ottawa, Canada.

16. Cox, A.D. (1962), "Axially Symmetric Plastic Deformation Soils -II, Indention of Ponderable Soils", International Journal of Mech. Sci., Vol. 4, pp. 371.

17. Dayal, U. (1974), "Instrumented Impact Penetrometer", Ph.D. Thesis, Memorial University of Newfoundland, Canada.

18. De Beer, E.E. (1945), "Etudes des Fonditions sur Pilotis et des Fonditions Directes", Annales Des Travaux Publics de Belgique 46, pp. 1-78.

19. De Beer, E.E. (1967), "Bearing Capacity and Settlement of Shallow Foundations on Sand", Proceedings, Symposium on Bearing Capacity and Settlement of Foundations, Duke University, pp. 15-34.

20. De Ruiter, J. (1975), "The Use of In-Situ Testing for North Sea Soil Studies", Preprints, Offshore Europe 75, Aberdeen, pp. 219.1-219.10.

21. Drozd, K. (1965), "The Influence of Variable Moisture Content in Sand on the Results of Dynamic Penetration Test", Proceedings, 6th International Conference on Soil Mechanics and Foundation Engineering, Vol. 3, pp. 335-336.

22. Durgunoglu, H.T. and Mitchell, J.K. (1973), "Static Penetration Resistance of Soils", Research Report Prepared for NASA Headquarters, Washington, D.C., April 1973, University of California, Berkeley.

23. Durgunoglu, H.T. and Mitchell, J.K. (1974), "Influence of Penetrometer Characteristics on Static Penetration Resistance", Proceedings, European Symposium on Penetration Testing, Vol. II, pp. 133-139.

24. Durgunoglu, H.T. and Mitchell, J.K. (1975), "Static Penetration Resistance of Soils, I-Analysis, II-Evaluation", Proceedings of the Conference on In-Situ Measurement of Soil Properties, ASCE, Vol. 1, pp. 172-189.

25. ESOPT, 1974. European Symposium on Penetration Testing, Stockholm,

June 1974, Vol. 1, State-Of-The-Art Report.

26. Ferguson, G.H., McClelland, B. and Bell, W.D. (1977), "Seafloor Cone Penetrometer for Deep Penetration Measurements of Ocean Sediment Strength", The 9th Offshore Technology Conference, OTC 2787, Vol. I, pp. 471-478.

27. Freitag, D.R., Green, A.J. and Melzer, K.J. (1970), "Performance Evaluation of Wheels for Lunar Vechicles", U.S. Army Engineer Waterways Experiment Station, Vicksburg, Mississippi, Technical Report M-70-2.

28. Graham, J. (1968), "Plastic Failure in Cohesionless Soils", Geotechnique, Vol. 18, No. 3, pp. 301-316.

29. Harr, M.E. (1966), "Foundations of Theoretical Soil Mechanics", McGraw Hill Book Company Publications.

30. Hu, G.C. (1965), "Bearing Capacity of Foundation with Overburden Shear", Sols-Soils, Vol. I, No. 13, June 1965, pp. 11-18.

31. Janbu, N. and Senneset, K. (1974), "Effective Stress Interpretation of In-Situ Static Penetration Tests", Proceedings, ESOPT, Stockholm, Vol. 2.2, pp. 181-194.

32. Johnes, J.M. (1976), "The Use of an Impact Penetrometer in Remote Sensing Study of the Sea Bed Properties", 2nd CSCE Hydrotechnical Conference, Atlantic Region, Amherst, N.S..

33. Lambe, T.W. (1915), "Soil Testing for Engineers", Series in Soil Engineering, 1st edition, John Wiley and Sons, Inc..

34. Lundgren, H. and Mortensen, K. (1953), "Determination by the Theory of Plasticity of the Bearing Capacity of Continuous Footings on Sand", Proceedings, 3rd International Conference on Soil Mechanics and Foundation Engineering, Vol. 1, pp. 409.

35. Lunne, T.A. and Mitchell, J.K. (1977), "Sand Strength from Cone Penetration Resistance", Report of Civil Engineering Dept., University of California, Berkeley, September 1977.

36. Melzer, K.J. (1974), "Use of WES Cone Penetrometer in Cohesive Soils", Proceedings, ESOPT 1974, Stockholm, Vol. 2.2, pp. 263-268.

37. Meyerhof, G.G. (1951), "The Ultimate Bearing Capacity of Foundations", Geotechnique, Vol. 2.2, pp. 301.

38. Meyerhof, G.G. (1955), "Influence of Roughness of Base and Ground Water Conditions on the Ultimate Bearing Capacity of Foundation", Geotechnique, Vol. 5, pp. 227.

39. Meyerhof, G.G. (1961a), "The Ultimate Bearing Capacity of Wedge-

Shaped Foundations", Proceedings, 5th International Conference on Soil Mechanics and Foundation Engineering, Vol. 2, pp. 105-109.

40. Meyerhof, G.G. (1961b), "Discussion of Shallow Foundations. Influence of the Dimensions and the Shape of the Foundations", Proceedings, 5th International Conference on Soil Mechanics and Foundation Engineering, Vol. 3, pp. 193-195.

41. Meyerhof, G.G. (1963), "Some Recent Research on the Bearing Capacity of Foundations", Canadian Geotechnical Journal, Vol. 1, No. 1, pp. 16-26.

42. Meyerhof, G.G and Brown, J.D. (1967), "Discussion, Bearing Capacity of Footing on Layered Soil", Proceedings, ASCE, SMS, Sept. 1967, pp. 361-363.

43. Nowatzki, E.A. and Karafiath, L.L. (1972), "The Effect of Cone Angle on Penetration Resistance", Highway Research Board No. 405, pp. 51-59.

44. Nowatzki, E.A. and Karafiath, L.L. (1978), "Soil Mechanics for Offroad Vehicle Engineering", Series on Rock and Soil Mechanics, Vol. 2 (1974/77), No. 5, Trans. Tech. Publications.

45. Prandtl, L. (1920), "Uber Die Harte Plasticher Korperu", Nachrichten Von Der Gesellschaft Der Wissen Chaften Zu Geottingen, Mathemtish, Physikalische Klasse, pp. 74-85.

46. Ohde, J. (1936), "The Theory of Earth Pressure With Special Reference to Earth Pressure Distribution", Bautechnik, 16:150-761.

47. Reddy, A.S. and Srinivasan, R.J. (1967), "Bearing Capacity of Footings on Layered Clays", Proceedings, ASCE, SM2, March 1967, pp. 83-99.

48. Reissner, H. (1924), "Zum Erddruckproblem", Proceedings, 1st International Congress of Applied Mechanics, Delft, pp. 295-311.

49. Sanglart, G. (1972), "The Penetrometer and Soil Exploration", Developments in Geotechnical Engineering, Elsevier Publishing Company.

50. Schmertmann, J. (1974), "Penetration Pore Pressure Effects on Quasi-Static Cone Bearing, q_c", ESOPT, Stockholm, Vol. 2.3, pp. 345-352.

51. Schmertmann, J. (1975), "Measurement of In-Situ Shear Strength", Proceedings of the Conference on In-Situ Measurements of Soil Properties, ASCE, Vol. II, June 1975, pp. 57-138.

52. Skempton, A.W. (1951), "The Bearing Capacity of Clays", Proceedings, Building Research Congress, London, Vol.1, pp. 180-189.

53. Sokolovski, V.V. (1960), "Statics of Soil Media", 2nd ed. (translated from Russian by D.H. Jones and A.N. Schofield), Butterworths, London.

54. Terzaghi, K. (1943), "Theoretical Soil Mechanics", Wiley, New York.

55. Turnage, G.W. and Freitag, D.R. (1970), "Effects of Cone Velocity and Size on Soil Penetration Resistance", ASAE, Paper 69-970.

56. Vesic, A.S. (1963), "Bearing Capacity of Deep Foundations in Sand", Highway Research Board Record, No. 39, pp. 112-135.

57. Vesic, A.S. (1972), "Expansion of Cavities in Infinite Soil Mass", Journal of Soil Mechanics and Foundation Division, ASCE, Vol. 98, No. SM3, pp. 265-290.

58. Vesic, A.S. (1975), "Bearing Capacity of Shallow Foundations", Foundation Engineering Handbook by Winter Korn, H.F. and Fang, H., pp. 121-147.

59. Wismer, R.D. and Luth, H.J. (1972a), "Rate Effects in Soil Cutting," Journal of Terramechanics, Vol. 8, No. 3, pp. 11-21.

60. Wismer, R.D. and Luth, H.J. (1972b), "Performance of Plane Soil Cutting Blades in Clay", Transactions of ASAE, Feb. 1972, Vol. 15, No. 1, pp. 211-216.

61. Zuidberg, H.M. (1975), "The Sea Calf, a Submersible Cone Penetrometer Rig", Marine Geotechnology, Vol. 1, No. 1, pp. 15-32.

APPENDIX A

SPECIFICATIONS OF THE STRAIN GAGES USED IN THE PENETROMETERS

The strain gages used in the penetrometers are of EA-06-125BT-120 series constant strain gages widely used in experimental stress analysis.

The gages are of open-faced construction with a 0.03 mm, tough, flexible polyimide film backing. They have the following specifications:

Temperature Range:	$-100^{\circ}F$ ($-75^{\circ}C$) to $+350^{\circ}F$ ($+175^{\circ}C$) for continuous use in static measurements, $-320^{\circ}F$ ($-195^{\circ}C$) to $+400^{\circ}F$ ($+205^{\circ}C$) for special or short term exposure.
Strain Limits:	Approximately 5% for gage lengths 1/8" (3.2 mm) and larger; and approximately 3% for gage lengths under 1/8" (3.2 mm).
Resistance:	The resistance in Ohms for the EA series gages is $120.0 \pm 0.15\%$.
Gage Factor:	The gage factor at $75^{\circ}F$ is $2.075 \pm 0.5\%$.
Fatigue Life:	10^8 cycles at $\pm 1200\mu''/''$ ($\mu m/m$); 10^6 cycles at ± 1500 $\mu''/''$ ($\mu m/m$); 10^5 cycles at $\pm 1800\mu''/''$ ($\mu m/m$). 10^6 cycles at $2800\mu''/''$ ($\mu m/m$) unidirectional, tension or compression only. Longer gage lengths and lower resistance result in greater endurance and less scatter in fatigue life.

The circuit diagrams for cone load cell and sleeve load cell are showin in Figures A.1 and A.2 respectively.

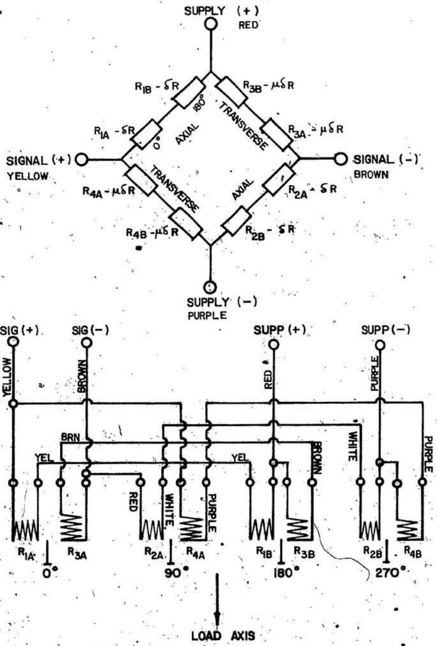

FIG. A.1 CIRCUIT DIAGRAM FOR CONE LOAD CELL

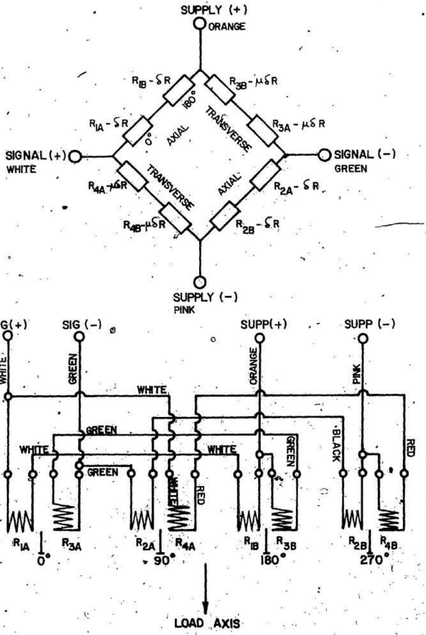

FIG. A.2 CIRCUIT DIAGRAM FOR SLEEVE LOAD CELL

APPENDIX B

APPLICATION OF PLASTICITY THEORY TO PROBLEMS INVOLVING PENETRATION RESISTANCE

A finite difference approximation based on the method of characteristics was used in the numerical analysis of the differential equations of the axially symmetric case which is applicable to penetration or bearing capacity problems. To derive the differential equation for the axially symmetric case, consider the equilibrium of the element shown in Fig. B.1. The main difference between the axially symmetric case and the plane strain condition is that the circumferential stress is the intermediate principal stress (σ_2) and is equal to the minor principal stress (σ_3). Because of the axial symmetry, the formulation of the equilibrium equations is done more efficiently in polar coordinate as shown in Fig. B.1, where the symbols σ_γ, σ_λ, σ_Z, $\tau_{\lambda Z}$, $\tau_{\gamma Z}$ and $\tau_{\gamma\lambda}$ are the stress components acting on the soil mass. The principal stress directions and orientation definition are analogus to those of the plane strain case given by Sokolovski (1960) and are shown in Fig. B.2. The angle θ is a function of the local stress state within the soil mass and therefore Sokolovski proposed the general relationship:

$$\theta = (1 - K)\ \pi/4 + (K\Delta - \delta) + n\pi \qquad [B.1]$$

where

δ = obliquity angle in the classical soil mechanics sense i.e.

$\delta = \arctan[\tau_{xz}/(\sigma_x + \psi)]$

$\Delta = \arcsin(\sin\delta/\sin\phi)$

K = +1 (passive); −1 (active)

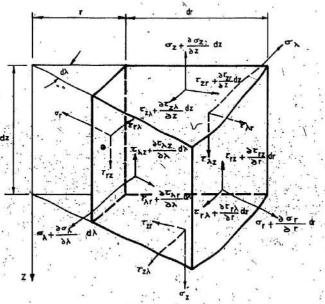

FIG. B.1 STRESSES ON ELEMENT - POLAR COORDINATES

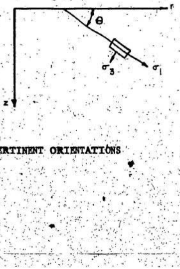

FIG. B.2 PERTINENT ORIENTATIONS

n = any integer; usually 0 or $\pm$ 1

Axial symmetry requires that the shear stresses $\tau_{\lambda z}$ and $\tau_{\lambda r}$ vanish so that at equilibrium the summation of the forces in the r and z directions yields:

$$\partial\sigma_r/\partial r + \partial\tau_{zr}/\partial z + (\sigma_r - \sigma_\lambda)n/r \qquad [B.2a]$$

$$\partial\tau_{rz}/\partial r + \partial\sigma_z/\partial z + \gamma + n\tau_{zr}/r = 0 \qquad [B.2b]$$

where n is a constant which is zero for plane strain conditions and 1 for the axially symmetric case.

The basic equations of the transformation of stress components between stresses in polar coordinates and principal stresses when $\sigma_1 > (\sigma_2 = \sigma_3)$ is:

$$\sigma_1 = (\sigma_r + \sigma_z)/2 + \{1/4(\sigma_r - \sigma_z)^2 + \tau_{rz}^2\}^{1/2} \qquad [B.3a]$$

$$\sigma_3 = (\sigma_r + \sigma_z)/2 - \{1/4(\sigma_r - \sigma_z)^2 + \tau_{rz}^2\}^{1/2} \qquad [B.3b]$$

$$\sigma_\lambda = \sigma_2 = \sigma_3 \qquad [B.3c]$$

From which

$$\sigma_r = (\sigma_1 + \sigma_3)/2 + (\sigma_1 - \sigma_3)/2 \text{ Cos } 2\theta \qquad [B.4a]$$

$$\sigma_z = \sigma_1 + \sigma_3/2 - \sigma_1 - \sigma_3/z \text{ Cos } 2\theta \qquad [B.4b]$$

$$\tau_{rz} = (\sigma_1 - \sigma_3)/2 \text{ Sin } 2\theta \qquad [B.4c]$$

Substituting Equations (B.4) into Equations (B.3) and following the same mathematical procedure described by Sokolovski (1960) and given in detail by Nowatzki and Karafiath (1978) the following general differential equations are obtained for the axially symmetric case $(n = 1)$:

$$dz = dr\ \tan(\theta \pm \mu) \qquad \text{[B.5a]}$$

$$d\sigma \pm 2\sigma \tan\phi\ d\theta - (dz \pm \tan\phi\ dr)\gamma + n\sigma/r[\sin\phi\ dr \pm \tan\phi\ (1 - \sin\phi)dz] = 0 \qquad \text{[B.5b]}$$

The corresponding recurrence relations are:

$$dz = dr\ \tan(\theta \pm \mu) \qquad \text{[B.6a]}$$

$$d\sigma \pm 2\sigma \tan\phi\ d\theta - (dz \pm \tan\phi\ dr)\gamma + n\sigma/r[\sin\phi\ dr \pm \tan\phi\ (1 - \sin\phi)dz] = 0 \qquad \text{[B.6b]}$$

The corresponding recurrence relationships are:

$$\sigma_{i,j} = \Big[2\sigma_{i-1,j}\ \sigma_{i,j-1}[1 - \tan\phi(\theta_{i-1,j} - \theta_{i,j-1})] + \bar{\bar{C}}\sigma_{i,j-1} + \bar{\bar{D}}\sigma_{i-1,j} - \sigma_{i-1,j}\ \sigma_{i,j-1}\Big(\bar{\bar{A}}/r_{i-1,j} + \bar{\bar{B}}/r_{i,j-1}\Big)\Big]\Big/\Big[\sigma_{i,j-1} + \sigma_{i-1,j}\Big] \qquad \text{[B.6c]}$$

and

$$\theta_{i,j} = \sigma_{i,j} \text{[illegible]} \sigma_{i-1,j} + 2\tan\phi\ (\sigma_{i-1,j}\ \theta_{i-1,j} + \sigma_{i,j-1}\ \theta_{i,j-1}) - \bar{\bar{C}} + \bar{\bar{D}} + (\sigma_{i-1,j}\ \bar{\bar{A}}/r_{i-1,j}) - (\sigma_{i,j-1}\ \bar{\bar{B}}/r_{i,j-1}\Big]\Big/\Big[2\tan\phi\ (\sigma_{i-1,j} + \sigma_{i,j-1})\Big] \qquad \text{[B.6d]}$$

$$\bar{A} = \sin\phi(r_{i,j} - r_{i-1,j}) - \tan\phi(1 - \sin\phi)\ (z_{i,j} - z_{i-1,j})$$

$$\bar{B} = \sin\phi(r_{i,j} - r_{i,j-1}) + \tan\phi(1 - \sin\phi)\ (z_{i,j} - z_{i,j-1})$$

$$\bar{C} = \gamma[z_{i,j} - z_{i-1,j} - \tan\phi(r_{i,j} - r_{i-1,j})]$$

$$\bar{D} = \gamma[z_{i,j} - z_{i,j-1} + \tan\phi(r_{i,j} - r_{i,j-1})]$$

The expressions for r and z in this case are:

$$z_{i,j} = z_{i-1,j} + \alpha_2(r_{i,j} - r_{i-1,j}) \quad \text{[B.6e]}$$

or

$$z_{i,j} = z_{i,j-1} - \alpha_1(r_{i,j} - r_{i,j-1}) \quad \text{[B.6f]}$$

$$r_{i,j} = (z_{i-1,j} - z_{i,j-1} + \alpha_1 r_{i,j-1} - \alpha_2 r_{i-1,j})/(\alpha_1 - \alpha_2) \quad \text{[B.6g]}$$

where

$$\alpha_1 = \tan(\theta_{i,j-1} + \mu)$$

$$\alpha_2 = \tan(\theta_{i-1,j} - \mu)$$

To apply these recurrence relations to the problem of cone penetration resistance, the geometric boundary conditions as well as the stress boundary conditions must be formulated appropriately and included in a computer program.

A Computer Program to Determine Cone Penetration Resistance Using the Finite Difference Approximation:

The geometric boundary conditions are simply mathematical descriptions of the cone geometry and its position or depth in terms of r, z and R_0 as shown in Fig. B.3. As reported by Nowatzki and Karafiath (1978), the stress boundary conditions at the free surface and along the wall of the hole are stable, or the soil behind the hole tends to fail and failure surfaces develops towards the hole. The latter situation occurs almost exclusively in cohesionless soils, since a very small

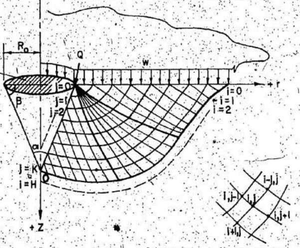

FIG. B.3 GEOMETRY FOR AXIALLY SYMMETRIC (CONE PENETROMETER) PROBLEM amount of cohesion is sufficient to insure stability of the hole for small depth of penetration, and therefore, the program is valid only for cohesionless soils.

The boundary conditions at the soil-cone interface are of the GOURSAT type (Harr 1966) that require the specification of a relationship for the geometry and another one for the direction of the major principal stress. The first relationship is defined by the angle (β) which the interface makes with the horizontal, while the latter condition is satisfied by assuming that the direction of σ_1 is constant and corresponds to a specified angle of interface friction (δ). For these conditions the numerical computation of the slip line field geometry and the associated stresses is straight forward. The stress boundary condition on the horizontal plane through the base of the cone is given by the surcharge and overburden pressure γD (Fig. B.3):

$$\sigma = \gamma D/(1 - \mathrm{Sin}(\phi)) \qquad \text{[B.7a]}$$

$$\theta = 0.0 \qquad \text{[B.7b]}$$

The slip-line field and associated stresses in the passive zone are computed by Equations [B.6] starting with these boundary values andsan assumed value for the horizontal extent of the passive zone ($L \approx 3d$). In the radial shear zone, the same equations are used, but special consideration is given to the central point (0) where the j-lines converge. This point is a degenerated slip line, where θ changes from its value at the passive boundary to that specified at the active zone boundary. Point (0) is called singular point. In numerical solution precedure, the singular point is obtained by dividing the total change in θ by the number of i-lines converging at that point. This result in an equal $\Delta\theta$ increment between adjacent i-lines at the singular point.

$$\theta_{passive} = 0.0 \tag{B.8a}$$

$$\theta_{active} = (1 - K)\pi/4 + (K\Delta - \delta) + n\pi \tag{B.8b}$$

The σ values for each increment are computed from the equation:

$$\sigma = \sigma \exp(2(\sigma - \sigma_o)\tan\phi) \tag{B.8c}$$

With these values of σ and θ for each slip line at point 0, the coordinates as well as the σ and θ values for all other points in the radial shear zone can be computed by Equations [B.6]. In the active zone the same equations are used, except for the points at the loaded surface of the cone itself. Here $\theta_{i,j}$ is assigned and the following conditions pertain (Nowatzki and Karafiath 1978):

$$z_{i,j} = z_o + (R_o - r_{i,j})\tan\beta' \tag{B.9a}$$

$$r_{i,j} = \left[r_{i-1,j}\tan[(\theta_{i,j} + \theta_{i-1,j})/2 - \mu] - z_{i-1,j} + R_o\tan\beta' + Z_o\right] \Big/ \left[\tan[(\theta_{i,j} + \theta_{i-1,j})/2 - \mu] + \tan\beta'\right] \tag{B.9b}$$

$$\sigma_{i,j} = \sigma_{i-1,j} + \sigma_{i-1,j}(\theta_{i,j} - \theta_{i-1,j})\tan\phi + \bar{\bar{C}} - (\sigma_{i-1,j}\,\bar{\bar{A}}/r_{i-1,j}) \tag{B.9c}$$

where

β' = complement to half the cone apex angle.

$\mu = \pi/4 - \phi/2$

z_0 = depth to which base of cone has penetrated

R_0 = radius of cone base

The numerical computation is performed and adjustments made, using iteration techniques, to the value assumed for the horizontal extent of the passive zone until the slip line field closes according to the required accuracy, on the axis of symmetry at the apex of the cone.

At this stage, the calculation for penetration resistance starts. If the face of the cone encloses an angle $\alpha/2$ with the vertical then the following relationship for penetration resistance, P, holds:

$$P = \int_A [\sigma_n \text{Sin}(\alpha/2) + \tau \text{Cos}(\alpha/2)] dA \qquad \text{[B.10a]}$$

where

$$\tau = (\sigma_n + \psi)\tan\delta \qquad \text{[B.10b]}$$

therefore

$$P = \int_A [\sigma_n \text{Sin}(\alpha/2) + \sigma_n \text{Cos}(\alpha/2) \tan\delta + \psi \text{Cos}(\alpha/2) \tan\delta] dA \qquad \text{[B.10c]}$$

The method of computation outlined above is well suited for the analysis of the effect of various input parameters on cone penetration resistance. The output of the given computer program is the slip line field and the unit penetration resistance at the required depth.

Input Data

a) control card (2I 10)

Columns 1 - 5 Number of data set to be calculated

11 - 20 Number of depths at which the above data sets are to be used.

b) Slip-lines characteristic card (F5.0, 6I5)

Columns 1 - 5 assumed length of passive zone

6 - 15 number of j-slip lines

16 - 25 number of i-slip lines

26 - 35 i-line ends the passive zone

36 - 45 j-line starts the radial shear zone

46 - 55 i-line ends the radial shear zone

56 - 65 i-line starts the active zone

c) penetrometer and soil properties card

Columns 1 - 10 penetrometer diameter (B - DIAM)

11 - 20 penetrometer cone angle (2α - ALFA)

21 - 30 penetrometer to soil friction angle (δ - DELTA)

31 - 40 unit weight of soil (γ - GAMA)

41 - 50 cohesion of soil (C — COHES)

d) depth versus friction angle card

Columns 1 - 10 depth of penetrometer base

11 - 20 angle of internal friction at this depth

Notes

1. Data cards must be in proper sequence.
2. Units must be considered.
3. For N sets of data, N cards for slip-lines characteristic are required. Also N cards of penetrometer and soil properties are needed.

4. For M sets of points, M cards of depth versus friction angle are required for each of the above sets.

Output of the Computer Code

For each data set, the slip lines characteristics and penetrometer and soil properties are printed out. For each set of depth and the corresponding friction angle, R-cord, Z-cord, sigma and theta at each (I,J) point in the slip line field are printed out in the following sequence:

1. Prescribed values at the boundary of the passive zone.
2. Values inside the passive zone.
3. Transitional values from passive to active zone.
4. Values of the radial shear zone.
5. Values of the active zone.

At the end of each slip lines configuration, the unit penetration resistance at this depth is printed out.

LISTING OF THE COMPUTER PROGRAM TO DETERMINE CONE PENETRATION RESISTANCE USING THE FINITE DIFFERENCE APPROXAMATION

```
//54200502 JOB (4200,502C,3,8),GAWAD,CLASS=C
// EXEC WATFIV,REGION.GO=129K
//GC.SYSIN DD *
$COMPILE         ,TIME=180,PAGES=800
C
C       **************************************************************
C       * PROGRAM TO DETERMINE PENETRATION RESISTANCE AND THE SHAPE OF   *
C       * FAILURE AS AN APPLICATION OF PLASTICITY THEORY                 *
C       **************************************************************
C
C
C       N     =NUMBER OF DATA SETS
C       M     =NUMBER OF GIVEN SETS OF DEPTH AND FRICTION ANGLE
C       ALFA  =APEX ANGLE OF THE CONE
C       DELTA =PENETROMETER TO SOIL FRICTION ANGLE
C       FI    =ANGLE OF INTERNAL FRICTION
C       GAMA  =UNIT WEIGHT OF SOIL
C       DIAM  =DIAMETER OF THE CONE BASE
C       C     =COHESION OF THE SOIL
C       --------------------------------------------------------------
C
C       THE PROGRAM IS CONVERTED INTO DUBLE PRECISON.
C
C
      IMPLICIT REAL*8(A-H,O-Z)
      DIMENSION THETA(40,20),SIGMA(40,20),R(40,20),Z(40,20),P(20)
     1,CHECK(100)
      READ 2,N,M
    2 FORMAT(2I10)
C                    READ AND PRINT CONE ANGLE, ROUGHNESS,DIAMETER
C                    *****************************************
C
C
      DO 99 KM=1,N
      READ 1,PASL,JL,IL,IFP,ISR,IFR,ISA
    1 FORMAT(F5.0,6I5)
      PRINT 111,JL,IL,ISR,ISA
  111 FORMAT(1H1,30X,'SLIP LINES CHARACTERSTICS',/,30X,24(1H*)///
     1,5X,'J-LINES---------------------------=',I10,//,5X,
     2'I-LINES---------------------------=',I10,//,5X,'I-START RADIAL SH'
     3,'EAR ZONE=',I10,//,5X,'I-START OF ACTIVE ZONE----=',I10,//)
      READ 5,DIAM,ALFA,DELTA,GAMA,COHES
    5 FORMAT(5F10.0)
      PRINT 15,KM,DIAM,ALFA,DELTA,GAMA,COHES
   15 FORMAT(/////,30X,'DATA SET NO',I5,/,30X,17(1H*),//,5X,
     1          'DIAMETER OF THE CONE------=',F8.4//5X,
     2          'CONE APEX ANGLE-----------=',F8.4,//,5X,
     3          'ROUGHNESS ANGLE-----------=',F8.4//5X,
     4          'UNIT WEIGHT OF SOIL-------=',F15.8//5X,
     5          'COHESION OF SOIL----------=',F15.8)
      PI=22./7.
      ALFA=ALFA*PI/180.
      DELTA=DELTA*PI/180.
      BETA=PI/2.-ALFA/2.0
      DELTAI=DELTA-BETA
      DO 98 KL=1,M
      READ 6,DEPTH,FI
    6 FORMAT(2F10.0)
      PRINT7,DEPTH,FI
    7 FORMAT(///,10X,'PENETRATION DEPTH---=',F10.5/10X
     1,'FRICTION ANGLE----=',F10.5X//,11X,'I',11X,'J',12X,'R-CORD',
```

```
     218X,'Z-CORD',12X,'THETA',15X,'SIGMA',/,11X,'-',11X,'-',
     312X,'------',18X,'-----',12X,'-----',15X,'-----')
      FI=FI*PI/180.
      DEL=DARSIN(DSIN(DELTA)/DSIN(FI))
      THETA(JL,1)=0.0
      SIGMA(JL,1)=(GAMA*DEPTH)/(1.-DSIN(FI))
      R(JL,1) =DIAM/2.0
      Z(JL,1)=0.0
      IST=1
      PASL1=PASL
C     ASSUMED VALUE OF EPS.
C
      EPS=0.02
  500 JM=JL-1
      DO 10 I=1,JM
      DJL=JL-1
      R(JL-I,I+1)=R(JL+1-I,I)+PASL1/DJL
      THETA(JL-I,I+1)=THETA(JL+1-I,I)
      SIGMA(JL-I,I+1)=SIGMA(JL+1-I,I)
      Z(JL-I,I+1)=Z(JL+1-I,I)
   10 CONTINUE
C     ******************************************************************
C     *                  CALCULATION OF THE PASSIVE ZONE.              *
C     ******************************************************************
C
C
      EMU=PI/4.-FI/2.
      N1=JL-1
      DO 30 K=1,N1
      K1=K+1
      DO 31 J=K1,JL
      I=JL-J+K1
      ALFA1=DTAN(THETA(I,J-1)+EMU)
      ALFA2=DTAN(THETA(I-1,J)-EMU)
      R(I,J)=(Z(I-1,J)-Z(I,J-1)+ALFA1*R(I,J-1)-ALFA2*R(I-1,J))/
     1(ALFA1-ALFA2)
      Z(I,J)=Z(I,J-1)+ALFA1*(R(I,J)-R(I,J-1))
      A1=DSIN(FI)*(R(I,J)-R(I-1,J))
      A2=(1.-DSIN(FI))*(Z(I,J)-Z(I-1,J))
      A=A1-DTAN(FI)*A2
      B1=DSIN(FI)*(R(I,J)-R(I,J-1))
      B22=1.-DSIN(FI)
      B3=Z(I,J)-Z(I,J-1)
      B2=B22*B3
      B=B1+DTAN(FI)*B2
      C=GAMA*(Z(I,J)-Z(I-1,J)-DTAN(FI)*(R(I,J)-R(I-1,J)))
      D=GAMA*(Z(I,J)-Z(I,J-1)+DTAN(FI)*(R(I,J)-R(I,J-1)))
      T1=SIGMA(I-1,J)*THETA(I-1,J)+SIGMA(I,J-1)*THETA(I,J-1)
      T2=SIGMA(I-1,J)/R(I-1,J)
      T3=SIGMA(I,J-1)/R(I,J-1)
      T4=2.*DTAN(FI)*(SIGMA(I-1,J)+SIGMA(I,J-1))
      THETA(I,J)=(SIGMA(I,J-1)-SIGMA(I-1,J)+2.*DTAN(FI)*T1-C+D+T2*A-T3*B
     1)/T4
      S1=2.*SIGMA(I-1,J)*SIGMA(I,J-1)
      S2=THETA(I-1,J)-THETA(I,J-1)
      S22=1.-DTAN(FI)*S2
      S3=SIGMA(I-1,J)*SIGMA(I,J-1)
      S4=A/R(I-1,J)+B/R(I,J-1)
      S5=SIGMA(I,J-1)+SIGMA(I-1,J)
      SIGMA(I,J)=(S1*S22+C*SIGMA(I,J-1)+D*SIGMA(I-1,J)-S3*S4)/S5
   31 CONTINUE
```

```
   30 CONTINUE
C     ****************************************************************
C     *              CALCULATION OF RADIAL SHEAR ZONE                 *
C     ****************************************************************
C
C
      THETAP=0.0
      LRAD=IFR-ISR+1
      THETAA=PI+(-1.*DEL-DELTA)
      DELTH=(THETAA-THETAP)/LRAD
      DO40 I=1,LRAD
      THETA(I+JL,1)=THETA(I-1+JL,1)+DELTH
      SIGMA(I+JL,1)=SIGMA(JL,1)*DEXP(2*(DELTH)*DTAN(FI))
      R(I+JL,1)=DIAM/2.
      Z(I+JL,1)=0.0
   40 CONTINUE
      DO 50 J=2,JL
      DO 51 I=ISR,IFR
      ALFA1=DTAN(THETA(I,J-1)+EMU)
      ALFA2=DTAN(THETA(I-1,J)-EMU)
      R(I,J)=(Z(I-1,J)-Z(I,J-1)+ALFA1*R(I,J-1)-ALFA2*R(I-1,J))/
     1(ALFA1-ALFA2)
      Z(I,J)=Z(I,J-1)+ALFA1*(R(I,J)-R(I,J-1))
      A1=DSIN(FI)*(R(I,J)-R(I-1,J))
      A2=(1.-DSIN(FI))*(Z(I,J)-Z(I-1,J))
      A=A1-DTAN(FI)*A2
      B1=DSIN(FI)*(R(I,J)-R(I,J-1))
      B22=1.-DSIN(FI)
      B3=Z(I,J)-Z(I,J-1)
      B2=B22*B3
      B=B1+DTAN(FI)*B2
      C=GAMA*(Z(I,J)-Z(I-1,J)-DTAN(FI)*(R(I,J)-R(I-1,J)))
      D=GAMA*(Z(I,J)-Z(I,J-1)+DTAN(FI)*(R(I,J)-R(I,J-1)))
      T1=SIGMA(I-1,J)*THETA(I-1,J)+SIGMA(I,J-1)*THETA(I,J-1)
      T2=SIGMA(I-1,J)/R(I-1,J)
      T3=SIGMA(I,J-1)/R(I,J-1)
      T4=2.*DTAN(FI)*(SIGMA(I-1,J)+SIGMA(I,J-1))
      THETA(I,J)=(SIGMA(I,J-1)-SIGMA(I-1,J)+2.*DTAN(FI)*T1-C+D+T2*A-T3*B
     1)/T4
      S1=2.*SIGMA(I-1,J)*SIGMA(I,J-1)
      S2=THETA(I-1,J)-THETA(I,J-1)
      S22=1.-DTAN(FI)*S2
      S3=SIGMA(I-1,J)*SIGMA(I,J-1)
      S4=A/R(I-1,J)+B/R(I,J-1)
      S5=SIGMA(I,J-1)+SIGMA(I-1,J)
      SIGMA(I,J)=(S1*S22+C*SIGMA(I,J-1)+D*SIGMA(I-1,J)-S3*S4)/S5
   51 CONTINUE
   50 CONTINUE
C     ****************************************************************
C     *                 CALCULATION OF ACTIVE ZONE                    *
C     ****************************************************************
C
C
C
C     ASSIGNING VALUE OF THETA AT THE INTERFACE
C     ----------------------
C
      DO 60 J=2,JL
      I=ISA+J-2
      THETA(I,J)=THETAA
   60 CONTINUE
```

```
C
C        CALCULATION OF THE POINTS AT THE INTERFACE
C        ------------------------------------------
C
      DO 61 J1=2,JL
      I=ISA+J1-2
      ALFA3=PI-ALFA
      R(I,J1)=(R(I-1,J1)*DTAN((THETA(I,J1)+THETA(I-1,J1))/2.-EMU)-
     1Z(I-1,J1)+
     1DIAM/2.*DTAN(BETA ))/(DTAN((THETA(I,J1)+THETA(I-1,J1))/2.-EMU)
     2+DTAN(BETA))
C
C       CHECK THE VALUE OF R-CORD. IF+VE,CONTINUE,IF -VE,DECREASE THE
C       LENGTH OF THE PASSIVE ZONE.
C
      IF(0.0-R(I,J1)) 601,601,602
  601 GO TO 605
  602 PASL1=PASL1-EPS
      GO TO 500
  605 Z(I,J1)=(DIAM/2.-R(I,J1))*DTAN(BETA)
      A1=DSIN(FI)*(R(I,J1)-R(I-1,J1))
      A2=(1.-DSIN(FI))*(Z(I,J1)-Z(I-1,J1))
      A=A1-DTAN(FI)*A2
      C=GAMA*(Z(I,J1)-Z(I-1,J1)-DTAN(FI)*(R(I,J1)-R(I-1,J1)))
      SIGMA(I,J1)=SIGMA(I-1,J1)+SIGMA(I-1,J1)*(THETA(I,J1)-
     1THETA(I-1,J1))
     1*DTAN(FI)+C-SIGMA(I-1,J1)*A/R(I-1,J1)
      JJ=J1+1
      JJJ=JL+1
      IF(JJ.EQ.JJJ) GO TO 705
C
C        CALCULATION OF THE POINTS INSIDE THE ACTIVE ZONE
C        ------------------------
C
      DO 70 J=JJ,JL
      ALFA1=DTAN(THETA(I,J-1)+EMU)
      ALFA2=DTAN(THETA(I-1,J)-EMU)
      R(I,J)=(Z(I-1,J)-Z(I,J-1)+ALFA1*R(I,J-1)-ALFA2*R(I-1,J))/
     1(ALFA1-ALFA2)
C
C       CHECK THE VALUE OF R-CORD INSIDE THE ACTVE ZONE. IF +VE CONTINUE,
C       IF -VE DECREASE THE LENGTH OF THE PASSIVE ZONE
C
      IF(0.0-R(I,J)) 701,701,702
  701 GO TO 800
  702 PASL1=PASL1-EPS
      GO TO 500
  800 Z(I,J)=Z(I,J-1)+ALFA1*(R(I,J)-R(I,J-1))
      A1=DSIN(FI)*(R(I,J)-R(I-1,J))
      A2=(1.-DSIN(FI))*(Z(I,J)-Z(I-1,J))
      A=A1-DTAN(FI)*A2
      B1=DSIN(FI)*(R(I,J)-R(I,J-1))
      B22=1.-DSIN(FI)
      B3=Z(I,J)-Z(I,J-1)
      B2=B22*B3
      B=B1+DTAN(FI)*B2
      C=GAMA*(Z(I,J)-Z(I-1,J)-DTAN(FI)*(R(I,J)-R(I-1,J)))
      D=GAMA*(Z(I,J)-Z(I,J-1)+DTAN(FI)*(R(I,J)-R(I,J-1)))
      T1=SIGMA(I-1,J)*THETA(I-1,J)+SIGMA(I,J-1)*THETA(I,J-1)
      T2=SIGMA(I-1,J)/R(I-1,J)
      T3=SIGMA(I,J-1)/R(I,J-1)
```

```
      T4=2.*DTAN(FI)*(SIGMA(I-1,J)+SIGMA(I,J-1))
      THETA(I,J)=(SIGMA(I,J-1)-SIGMA(I-1,J)+2.*DTAN(FI)*T1-C+D+T2*A-T3*B
     1)/T4
      S1=2.*SIGMA(I-1,J)*SIGMA(I,J-1)
      S2=THETA(I-1,J)-THETA(I,J-1)
      S22=1.-DTAN(FI)*S2
      S3=SIGMA(I-1,J)*SIGMA(I,J-1)
      S4=A/R(I-1,J)+B/R(I,J-1)
      S5=SIGMA(I,J-1)+SIGMA(I-1,J)
      SIGMA(I,J)=(S1*S22+C*SIGMA(I,J-1)+D*SIGMA(I-1,J)-S3*S4)/S5
   70 CONTINUE
   61 CONTINUE
C
C     ITERATION AND CHECK THE CONVERGENCE.
C     -------------------------------------------
C
  705 IF(ALFA.EQ.PI) GO TO 3009
      IF(R(IL,JL).LE.0.0001) GO TO 305
      GO TO 3002
 3009 IF(R(IL,JL).LE.DIAM/2.) GO TO 305
 3002 CHECK(IET)=R(IL,JL)
      IF(IET.GE.2) GO TO 306
      PASL1=PASL1-EPS
      IET=IET+1
      GO TO 500
  306 IF(CHECK(IET)-CHECK(IET-1)) 801,802,803
  801 PASL1=PASL1-EPS
      IET=IET+1
      GO TO 500
  802 PASL1=PASL1-EPS/2.
      IET=IET+1
      IF(IET.EQ.50) GO TO 305
      GO TO 500
  803 GO TO 305
C
C     PRINT R-CORD, Z-CORD, THETA AND THE STRESSES AT ALL POINTS.
C     ================================================================
C
C
  305 WRITE(6,21)
   21 FORMAT(7X,'PRESCRIBED VALUEA AT THE BOUNDARY OF THE PASSIVE ZONE.'
     U,/,7X,55(1H=),//)
      DO 2000 J=1,JL
      I=JL-J+1
      PRINT 22,I,J,R(I,J),Z(I,J),THETA(I,J),SIGMA(I,J)
   22 FORMAT(7X,I5,7X,I5,5X,F16.8,5X,F16.8,5X,F16.8,5X,F16.8)
 2000 CONTINUE
      WRITE(6,8)
    8 FORMAT(7X,'VALUES OF THE PASSIVE ZONE',/,7X,30(1H=),//)
      DO 3000 K=1,N1
      K1=K+1
      DO 3001 J=K1,JL
      I=JL-J+K
      PRINT 81,I,J,R(I,J),Z(I,J),THETA(I,J),SIGMA(I,J)
   81 FORMAT(7X,I5,7X,I5,5X,F16.8,5X,F16.8,5X,F16.8,5X,F16.8)
 3001 CONTINUE
 3000 CONTINUE
      JLR=JL+1
      WRITE(6,39)
   39 FORMAT(7X,'TRANSITIONAL VALUES FROM PASSIVE TO ACTIVE ZONE.',/,
     U7X,50(1H=),//)
```

```
      DO 4000 I=ISP,IFR
      J=1
      PRINT 390,I,J,R(I,J),Z(I,J),THETA(I,J),SIGMA(I,J)
  390 FORMAT(7X,I5,7X,I5,5X,F16.8,5X,F16.8,5X,F16.8,5X,F16.8)
 4000 CONTINUE
      WRITE(6,37)
   37 FORMAT(7X,'VALUES OF THE RADIAL SHEAR ZONE.',/,7X,35(1H=),//)
      DO 5000 J=2,JL
      DO 5001 I=ISR,IFR
      PRINT 370,I,J,R(I,J),Z(I,J),THETA(I,J),SIGMA(I,J)
  370 FORMAT(7X,I5,7X,I5,5X,F16.8,5X,F16.8,5X,F16.8,5X,F16.8)
 5001 CONTINUE
 5000 CONTINUE
      WRITE(6,47)
   47 FORMAT(7X,'VALUES AT THE ACTIVE ZONE',/,7X,40(1H-),//)
      DO 6000 J1=2,JL
      I=ISA+J1-2
      PRINT 470,I,J1,R(I,J1),Z(I,J1),THETA(I,J1),SIGMA(I,J1)
  470 FORMAT(7X,I5,7X,I5,5X,F16.8,5X,F16.8,5X,F16.8,5X,F16.8)
      JJ=J1+1
      JJJ=JL+1
      IF(JJ.EQ.JJJ) GO TO 350
      DO 7000 J=JJ,JL
      PRINT 9, I,J,R(I,J),Z(I,J),THETA(I,J),SIGMA(I,J)
    9 FORMAT(7X,I5,7X,I5,5X,F16.8,5X,F16.8,5X,F16.8,5X,F16.8)
 7000 CONTINUE
 6000 CONTINUE
C
C       CALCULATION OF THE PENETRATION RESISTANCE
C       -----------------------------------------
C
  350 EPSI=COHES*DCOTAN(FI)
      F=0.0
      DO 80 J=1,JL
      I=ISA+J-2
      IF(J.EQ.1) GO TO 120
      IF(J.EQ.JL) GO TO 125
      ALENG=(R(I-1,J-1)-R(I,J))/2.+(R(I,J)-R(I+1,J+1))/2.
      PER=ALENG/DCOS(BETA)
      GO TO 121
  125 PER=((R(I-1,J-1)-R(I,J))/2.)/DCOS(BETA)
      GO TO 121
  120 PER=((R(I,J)-R(I+1,J+1))/2.)/DCOS(BETA)
  121 AREA=2.*PI*R(I,J)*PER
      SIGMA(I,J)=SIGMA(I,J)*DCOS(DELTA)
      P(J)=(SIGMA(I,J)*DSIN(ALFA/2.)+SIGMA(I,J)*DCOS(ALFA/2.)*DTAN
     1(DELTA)+EPSI*DCOS(ALFA/2.)*DTAN(DELTA))*AREA
      F=F+P(J)
   80 CONTINUE
      F=F/(PI*DIAM**2/4.)
      PRINT 11,F,PASL1,IET
   11 FORMAT(///5X,'UNIT PENETRATION RESISTANCE-----=',D15.8,
     U//,5X,'LENGTH OF PASSIVE ZONE=',D15.8,//,5X,'ITERATION NO=',I5,//)
   98 CONTINUE
   99 CONTINUE
      STOP
      END
```

APPENDIX C

A COMPUTER PROGRAM FOR THE DETERMINATION OF BEARING CAPACITY FACTORS OF CONES

This computer program is originally written by Durgunoglu and Mitchell (1973) to calculate the bearing capacity factors N_c and $N_{\gamma q}$ of wedges and cones at friction angle intervales of 5^o. In the present study the program was modified to calculate the unit penetration resistance of cones and obtain the output as a function of depth and relative depth.

The program consists of a main program N_c or $N_{\gamma q}$ and one subroutine (ANG). This subroutine calculates angle (γ). Programs (N_c) and ($N_{\gamma q}$) calculate the unit penetration resistance. Angle β is calculated in the main routine and Equation [15] was used for the shape factors. The at-rest earth pressure coefficient was assumed to be ($1 - \sin\phi$).

<u>Data Input</u>

Control Card (2I10)

Columns	1 - 10	Number of data sets to be calculated.
	11 - 20	Number of depths at which the above data sets are to be used.

N-cards each (4F10)

Columns	1 - 10	Semi-apex angle of the cone (α - ALFA)
	11 - 20	Roughness of the penetrometer (δ/ϕ - FAS)
	21 - 30	Unit weight of soil (γ_s -GAMA)
	31 - 40	Diameter of the penetrometer (B - DIA)

M-cards each (2F10)

Columns 1 - 10 Penetration depth (DEPTH)

11 - 20 Friction angle (ϕ - FI)

Program Output

The final output consists of unit penetration resistance, N_c and $N_{\gamma q}$ factors as functions of depth and relative depth.

Deducing of Angle of Internal Friction (ϕ) from the Above Computer Program:

It was previously demonstrated in Chapter IV that the angle of internal friction ϕ can be deduced from the results of cone penetration resistance using a procedure such that described by Durgunoglu and Mitchell (1973). This computer program can also determine ϕ if the cone apex angle, penetrometer roughness, and relative depth are known. Figures C.1 and C.2 show the relations between $N_{\gamma q}$ and ϕ for different relative depths obtained from the computer program. From the results of penetration resistance, q_f is known from which $N_{\gamma q}$ can be calculated ($N_{\gamma q} = q_f/\gamma_s B$). From the known value of the relative depth, the corresponding angle of internal friction can be determined using Figs. C.1 and C.2.

C

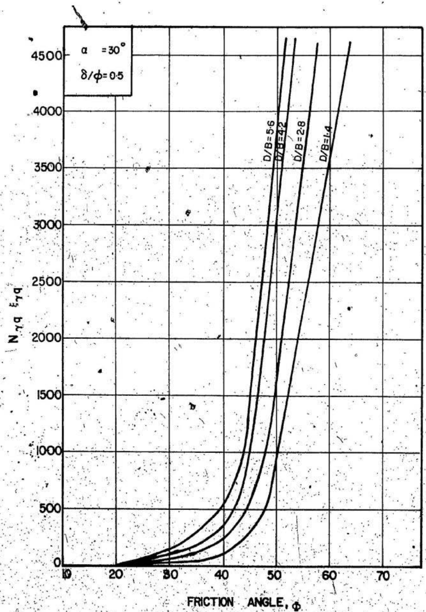

FIG. C.1 DETERMINATION OF THE ANGLE φ USING THE THEORY OF DURGUNOGLU AND MITCHELL (SMALL RELATIVE DEPTHS)

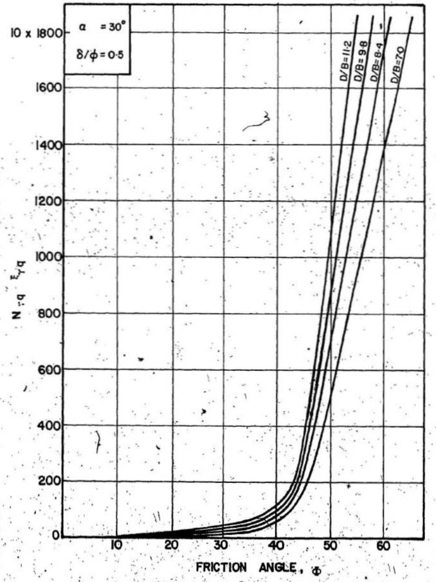

FIG. C.2 DETERMINATION OF THE ANGLE φ USING THE THEORY OF DURGUNOGLU AND MITCHELL (LARGE RELATIVE DEPTHS)

LISTING OF THE COMPUTER PROGRAM FOR THE
DETERMINATION OF UNIT PENETRATION RESISTANCE
OF CONE PENETROMETERS

```
//E3014602 JOB (3014,602C,1,2),GAWAD,CLASS=C
// EXEC WATFIV,REGION.GO=129K
//GO.SYSIN DD *
$COMPILE        ,TIME=60,PAGES=100
C
C     ************************************************************************
C                    PROGRAM CONE RESISTANCE NC FACTORS
C     *                                                                      *
C     ************************************************************************
C
C     N     =NUMBER OF DATA SETS
C     ALFA  =HALF APEX ANGLE
C     FAS   =ROUGHNESS
C     DPT   =DEPTH TO DIAMETER RATIO
C     FI    =ANGLE OF INTERNAL FRICTION
C     ATAR  =SHAPE FACTOR
C     DELTA= PENETRATION TO SOIL FRICTION ANGLE
C     GAMAS= UNIT SOIL WEIGHT
C     DIAM. =DIAMETER OF THE CONE BASE
C     COH   = COHESION OF SOIL
C
C
C     ------------------------------------------------------------------------
      READ 1,N
    1 FORMAT(I10)
C              READ AND PRINT WEDGE ANGLE, ROUGHNESS, REL. DEPTH
C              -----------------------------------------------------W
      DO 30 K=1,N
      READ 10, ALFA,FAS,GAMA,DIAM,COH,FI
   10 FORMAT(5F10.0)
      PRINT 21,K,ALFA,FAS,GAMA,DIAM,COH,FI
   21 FORMAT(1H1,/,40X,'DATA SET NO',I5,/40X,17(1H*),//,5X,
     1'HALF APEX ANGLE-----------=',F5.2//5X,
     2'ROUGHNESS-----------------=',F5.2,//5X,
     3'UNIT SOIL WEIGHT----------=',F15.8//5X,
     4'DIAMETER OF THE CONE------=',F8.4//5X,
     5'AVERAGE COHESION----------=',F15.8//5X,
     6'AVERAGE FRICTION ANGLE----=',F8.4)
      ALFAR=ALFA/57.28
      PRINT 24
   24 FORMAT(///,/,5X,'DEPTH',8X,'RELATIVE DEPTH',16X,
     1'CONE FACTOR(NC)',5X,'UNIT PENETRATION RESISTANCE'/5X,'-----',
     28X,14(1H-),16X,18(1H-),5X,27(1H-))
      DEPTH=5.0
  300 DPT=DEPTH/DIAM
      FIR=FI/57.28
      ATAR=1.0+0.2+(TAN(FIR)**6)
C                   CALCULATION OF ANGLE GAMA
C                 ----------------------------
      CALL ANG(FI,FAS,GAMA)
      V6=SIN(FIR)/COS(FIR)
      DELTA=FAS*FI
      DELTAR=DELTA/57.28
      IF(FAS-1.0) 33,32,33
   32 FIS=45.-FI/2.
      IF(ALFA-FIS) 15,15,16
   16 PSI=FIS+FI
      GO TO 17
   15 CONTINUE
   33 PSI=90.-ALFA
   17 PSIR=PSI/57.28
```

```
C                         CALCULATE BETA BY ITERATION
C                        ----------------------------
      BETA=FI
      BETAR=BETA/57.28
      GAMAR=GAMA/57.28
      TETA=180.-PSI+BETA-GAMA
      TETAR=TETA/57.28
      DEDPT=0.5*(COS(GAMAR-FIR))*(SIN(BETAR))*EXP((TETAR*SIN(FIR))/
     UCOS(FIR))/(COS(FIR)*COS(PSIR))
      IF(DEDPT-DPT) 11,11,12
   12 ETA=180.-PSI-GAMA
      SOTA=0.
      ETAR=ETA/57.28
      T1=2.*DPT*COS(FIR)*COS(PSIR)/(COS(GAMAR-FIR)*(EXP(ETAR*V6)))
      BOR=ATAN(T1)
      BO=BOR*57.28
      IF(BO-FI) 310,310,311
  311 BO=FI
  310 CONTINUE
      DO 101 I=1,20
      T2=2.*DPT*COS(FIR)*COS(PSIR)/(COS(GAMAR-FIR)*(EXP(((180.-PSI
     1-GAMA+BO)/57.28)*V6)))
      T3=T2/(SQRT(1.-T2**2))
      BNR=ATAN(T3)
      BN=BNR*57.28
      IF(ABS(BN-BO)-0.1) 501,501,502
  501 GO TO 102
  502 BO=(BN+BO)/2.
  101 CONTINUE
  102 BETA=BN
      BETAR=BETA/57.28
C****  CALCULATE WEDGE AND CONE FACTORS              *********************
      TETA=180.-PSI+BETA-GAMA
      TETAR= TETA/57.28
      GO TO 70
   11 CONTINUE
      B1=(2.*COS(FIR)*COS(PSIR)*DPT)/(COS(GAMAR-FIR)*COS(BETAR)*EXP(TETA
     1R*V6))
      QSIR=ATAN(B1)
      QSI=QSIR*57.28
      SOTA=0.
   70 SOTAR=SOTA/57.28
      C1=SIN(FIR)
      C2=COS(FIR)
      C3=SIN(2.*GAMAR-FIR)
      C4=EXP(2.*TETAR*V6)
      C5=SIN(2.*SOTAR+FIR)
      C6=COS(2.*GAMAR-FIR)
      C7=SIN(PSIR)/COS(PSIR)
      C8=((1.+C1*C3)/(C1*C2))*C4+(((C5-C1)*(1.+C1*C2))/((C2**2)*(C2-V6*
     1(C5-C1))))*C4-1./V6+(C6*C7*C4)/C2
      C9=(V6*C7*C6*(C5-C1)*C4)/(C2*(C2-V6*(C5-C1)))
      ENC=C8+C9
      ENCO=ATAR*ENC
      QF=COH*ENCO
      PRINT 26,DEPTH,QPT,ENCO,QF
   26 FORMAT(//,5X,F8.4,8X,F10.5,17X,F12.5,13X,F12.5)
      DEPTH=DEPTH+5.0
      IF(DEPTH.GE.50.0) GO TO 30
      GO TO 300
   30 CONTINUE
```

```
      STOP
      END
C
C     ------------------------------------------------------------------------
      SUBROUTINE ANG(FI,FAS,QNEW)
C     ZALCULATE OF GAMA ANGLE
      DELTA=FAS*FI
      DELTAR=DELTA/57.28
      IF(FAS.EQ.1.) GO TO 2
      IF(FAS.EQ.0.) GO TO 3
      QSI= (1.-FAS)*(45.+FI/2.)
      QSIR=QSI/57.28
      FIR=FI/57.28
      VALO=(SIN(DELTAR)/COS(DELTAR))*(1.+SIN(FIR)*SIN(2.*QSIR-FIR))
     1-SIN(FIR)*COS(2.*QSIR-FIR)
      DO 81 K=1,150
      QSI=QSI+0.1
      QSIR=QSI/57.28
      VALN=(SIN(DELTAR)/COS(DELTAR))*(1.+SIN(FIR)*SIN(2.*QSIR-FIR))
     1-SIN(FIR)*COS(2.*QSIR-FIR)
      VAL=VALN*VALO
      IF(VAL) 12,13,11
   11 VALO=VALN
   81 CONTINUE
   13 QNEW=QSI
      GO TO 4
   12 DQSI=(VALN/(VALN-VALO))*0.1
      QNEW=QSI-DQSI
      GO TO 4
    3 QNEW=45.+FI/2.
      GO TO 4
    2 QNEW=3.
    4 CONTINUE
      RETURN
      END
$EXECUTE
      6
  15.0      0.5     0.001759     3.56      0.055     5.0
  30.0      0.5     0.001759     3.56      0.055     5.0
  90.0      0.5     0.001759     3.56      0.055     5.0
  15.0      0.5     0.001759     7.62      0.055     5.0
  30.0      0.5     0.001759     7.62      0.055     5.0
  90.0      0.5     0.001759     7.62      0.055     5.0
/*
//
```

```
//E3014602 JOB (3014,602C,1,2),GAWAD,CLASS=C
// EXEC WATFIV,REGION.GO=129K
//GO.SYSIN DD *
$COMPILE          ,TIME=60,PAGES=100
C
C      ****************************************************************
C               CONE AND WEDGE RESISTANCE NGQ FACTORS.
C      *                                                              *
C      ****************************************************************
C
C
C       N      =NUMBER OF DATA SETS
C       M.     =NUMBER OF GIVEN SETS OFDPT AND FI
C       ALFA   =HALF APEX ANGLE
C       FAS    =ROUGHNESS
C       DPT    =DEPTH TO DIAMETER RATIO
C       FI     =ANGLE OF INTERNAL FRICTION
C       ATAR   =SHAPE FACTOR
C       DELTA= PENETRATION TO SOIL FRICTION ANGLE
C       GAMAS=UNIT SOIL WEIGHT
C       DIAM =DIAMETER OF THE CONE BASE
C              ---------------------------
C
      READ 1,N,M
    1 FORMAT(2I10)
C              READ AND PRINT WEDGE ANGLE, ROUGHNESS, REL. DEPTH
C      ------------------------------------------------------------
      DO 30 K=1,N
      ALFAR=ALFA/57.28
      READ   10,ALFA,FAS,GAMAS,DIAM
   10 FORMAT(4F10.0)
      PRINT 21,K,ALFA,FAS,GAMAS,DIAM
   21 FORMAT(1H1,/,20X,'DATA SET NO',I5,/20X,17(1H*),//,5X,
     1       'HALF APEX ANGLE-----------=',F5.2//5X,
     2       'ROUGHNESS-----------------=',F5.2,//5X,
     3       'UNIT SOIL WEIGHT----------=',F15.8//5X,
     4       'DIAMETER OF THE CONE-----=',F8.4),
      PRINT 24
   24 FORMAT(///,/,5X,'DEPTH',8X,'RELATIVE DEPTH',5X,'ANGLE OF INTERNAL'
     1    ,'FRICTION',5X,'CONE FACTOR(NGAMAQ)',5X,'UNIT PENETRATION RES'
     2    ,'ISTANCE'/5X,'-----',8X,14(1H-),5X,26(1H-),5X,18(1H-),5X,
     3     27(1H-))
      DO 25 J=1,M
      READ 100,DEPTH,FI
  100 FORMAT(2F10.0)
      FIR=FI/57.28
      DPT=DEPTH/DIAM
      ALEM=0.6+(1.5/(1./DPT+(1.5/(0.6+(TAN(FIR)**6)))))
C                 CALCULATION OF ANGLE GAMA
C      ------------------------------------------
      CALL ANG(FI,FAS,GAMA)
      V6=SIN(FIR)/COS(FIR)
      DELTA=FAS*FI
      DELTAR=DELTA/57.28
      IF(FAS-1.0) 33,32,33
   32 FIS=45.-FI/2.
      IF(ALFA-FIS) 15,15,16
   16 PSI=FIS+FI
      GO TO 17
   15 CONTINUE
   33 PSI=90.-ALFA
   17 PSIR=PSI/57.28
```

```
C                    CALCULATE BETA BY ITERATION
C     ------------------------------------------------------------------
      BETA=FI
      BETAR=BETA/57.28
      GAMAR=GAMA/57.28
      TETA= 180.-PSI+BETA-GAMA
      TETAR=TETA/57.28
      DEDPT=(0.5*COS(GAMAR-FIR)*SIN(BETAR)*EXP(TETAR*V6))/(COS(FIR)*COS
     1(PSIR))
      IF(DEDPT-DPT) 11,11,12
   12 DEDPT=DPT
      ETA=180.-PSI-GAMA
      ETAR=ETA/57.28
      T1=2.*DPT*COS(FIR)*COS(PSIR)/(COS(GAMAR-FIR)*(EXP(ETAR*V6)))
      BOR=ATAN(T1)
      BO=BOR*57.28
      IF(BO-FI) 310,310,311
  311 BO=FI
  310 CONTINUE
      DO 101 I=1,20
      T2=2.*DPT*COS(FIR)*COS(PSIR)/(COS(GAMAR-FIR)*(EXP(((180.-PSI
     1-GAMA+BO)/57.28)*V6)))
      T3=T2/(SQRT(1.-T2**2))
      BNR=ATAN(T3)
      BN=BNR*57.28
      IF(ABS(BN-BO)-0.1) 501,501,502
  501 GO TO 102
  502 BO=(BN+BO)/2.
  101 CONTINUE
  102 BETA=BN
      BETAR=BETA/57.28
      TETA=180.-PSI+BETA-GAMA
      TETAR=TETA/57.28
   11 CONTINUE
      RADIS=DEDPT/TAN(BETAR)
C     ***** CALCULATION OF NGQ FACTORS                 **********************
      WEIGHT =SIN(PSIR)/(4.*COS(PSIR))
      IF (ALFA-90.) 13,14,13
   13 WEIGH= 0.
   14 CONTINUE
      V1=EXP(3.*TETAR*V6)
      V1=EXP(3.*TETAR*V6)
      V2=V1*COS(BETAR)-COS(TETAR-BETAR)
      V3=V1*SIN(BETAR)+SIN(TETAR-BETAR)
      V4=3.*V6*V2+V3
      V5=V4/(1.+9.*(V6**2))
      U1=COS(GAMAR-FIR)
      U2=COS(FIR)
      U3=COS(PSIR)
      U4=COS(BETAR)
      U5=(1./4.)*(U1**2)*V5/((U3**2)*(U2**2))
      U7=EXP(2.*TETAR*V6)
      U8=U1*(U4**2)/(U3*U2)
      U9=(3./4.)*U8*U7*(DPT-(2./3.)*DEDPT)
      D6=1.-SIN(FIR)
      D2=((D6*U3*U2)/(U1))*((DPT-DEDPT)**2)*(DPT+2.*DEDPT)
      D4=((D6*U3*U2)*(DPT**3))/U1
      P1=(U5+U9-D2+D4)*(COS(PSIR-DELTAR)/COS(DELTAR))
      P2=((1.+SIN(FIR)*SIN(2.*GAMAR-FIR))/(U2*U1))*P1
      ENGAQ=P2-WEIGH
      ENGAC=ALEM*ENGAQ
```

```
      SURCHG=GAMAS*DIAM
      QF=SURCHG*ENGAC
      PRINT 26,DEPTH,DPT,FI,ENGAC,QF
   26 FORMAT(//,5X,F8.4,8X,F10.5,15X,F10.5,17X,F12.5,13X,F12.5)
   25 CONTINUE
   30 CONTINUE
      STOP
      END
C
C     ------------------------------------------------------------------
      SUBROUTINE ANG(FI,FAS,QNEW)
C     CALCULATE OF GAMA ANGLE
      DELTA=FAS*FI
      DELTAR=DELTA/57.28
      IF(FAS.EQ.1.) GO TO 2
      IF(FAS.EQ.0.) GO TO 3
      QSI= (1.-FAS)*(45.+FI/2.)
      QSIR=QSI/57.28
      FIR=FI/57.28
      VALO=(SIN(DELTAR)/COS(DELTAR))*(1.+SIN(FIR)*SIN(2.*QSIR-FIR))
     1-SIN(FIR)*COS(2.*QSIR-FIR)
      DO 81 K=1,150
      QSI=QSI+0.1
      QSIR=QSI/57.28
      VALN=(SIN(DELTAR)/COS(DELTAR))*(1.+SIN(FIR)*SIN(2.*QSIR-FIR))
     1-SIN(FIR)*COS(2.*QSIR-FIR)
      VAL=VALN*VALO
      IF(VAL) 12,13,11
   11 VALO=VALN
   81 CONTINUE
   13 QNEW=QSI
      GO TO 4
   12 DQSI=(VALN/(VALN-VALO))*0.1
      QNEW=QSI-DQSI
      GO TO 4
    3 QNEW=45.+FI/2.
      GO TO 4
    2 QNEW=3.
    4 CONTINUE
      RETURN
      END
$EXECUTE
          6                    8
   15.0          0.5      0.001759      3.56
    5.0          5.0
   10.0          5.0
   15.0          5.0
   20.0          5.0
   25.0          5.0
   30.0          5.0
   35.0          5.0
   40.0          5.0
   30.0          0.5      0.001759      3.56
    5.0          5.0
   10.0          5.0
   15.0          5.0
   20.0          5.0
   25.0          5.0
   30.0          5.0
   35.0          5.0
   40.0          5.0
```